論文 / 著書情報
Article / Book Information

題目(和文)	腐食した鉄筋コンクリート部材のひび割れ挙動と付着劣化
Title(English)	Cracking Behavior and Bond Splitting Degradation of Corroded Reinforced Concrete Members
著者(和文)	AryantoAris
Author(English)	aris aryanto
出典(和文)	学位:博士(工学), 学位授与機関:東京工業大学, 報告番号:甲第9512号, 授与年月日:2014年3月26日, 学位の種別:課程博士, 審査員:篠原　保二,坂田　弘安,河野　進,山田　哲,三上　貴正
Citation(English)	Degree:Doctor (Engineering), Conferring organization: Tokyo Institute of Technology, Report number:甲第9512号, Conferred date:2014/3/26, Degree Type:Course doctor, Examiner:,,,,
学位種別(和文)	博士論文
Type(English)	Doctoral Thesis

TOKYO INSTITUTE OF TECHNOLOGY

Cracking Behavior and Bond Splitting Degradation of Corroded Reinforced Concrete Members

by

Aris Aryanto

Supervisor: Prof. Yasuji Shinohara

A dissertation submitted in partial fulfillment of the requirements for the Doctor of Engineering Degree

ABSTRACT

The influence of corrosion of reinforcement on reinforced concrete members has been investigated in the following steps. First, tensile tests were conducted on RC cylindrical specimens with a corroded reinforcement to evaluate corrosion-induced cracking behaviors, bond and concrete tensile strength degradations and tension stiffening deteriorations with the aid of analysis. Second, bond behaviors of corroded reinforcement with various confinements were investigated through pullout tests using a beam type specimen to examine the residual bond splitting strength, bond-slip relationship and corrosion-induced transverse bar stress. In the last part, the mechanical properties of reinforcement, concrete and bond deterioration obtained from experiment and analysis are integrated in the numerical analysis using nonlinear finite element approach for assessing load-carrying capacity of corroded reinforced concrete members. The procedure developed in this study could be used as one of methods for the assessment of corrosion-damaged concrete structures from cover cracking behaviors.

ACKNOWLEDGEMENTS

First of all, I would like to express my sincere appreciation and deep gratitude to my supervisor Prof. Yasuji Shinohara for his continuous advice supporting my research and his invaluable guidance during my study at Tokyo Institute of Technology.

I would like to express my deep appreciation to the examiners of my dissertation, Prof. Hiroyasu Sakata, Prof. Susumu (Sam) Kono, Prof. Satoshi Yamada, and Prof. Takamasa Mikami for taking time from their busy schedule to read and give constructive feedback to my thesis.

I would like to thank to JICA-ITB for their scholarship and I also would like to thank to ASIASeed staff that support me from the first time came to Japan until going back to my country.

My special thanks to Prof. Iswandi Imran and Prof. Dradjat Hoedajanto who always encourage and support me and also introduce me to the research world.

Thanks to fellow students and friends at Shinohara Laboratory, Hayashi Laboratory and Kono Laboratory who helped me and support me during my research work especially during experimental work and who provide a pleasant atmosphere in the Labs. I greatly appreciate what all those people have done for me.

My sincerest gratitude goes out to my family, especially my parents, who always put me in their Doa during their prayers. Last but not least, I dedicate this work to my wife Dayu Puspasary and my daughter Marsya for their endless love, support and patience.

Aris Aryanto

Tokyo, February 2014

List of Publications

Journal Papers

*Aryanto, A.***,** and Shinohara, Y., Influence of bond-slip relationship and tensile strength on bond behavior between corroded steel bar and concrete, *Journal of Structural and Construction Engineering (Transactions of AIJ)*. Vol.78, No.685, pp. 559-567, 2013.

*Aryanto, A.***,** and Shinohara, Y., Effect of confinement and concrete strength upon crack behaviors induced by corrosion-product expansion for reinforced concrete members, *Journal of Structural and Construction Engineering (Transactions of AIJ)*. Vol.79, No.696 , pp.305-313, 2014.

Conference Papers

Aryanto, A., and Shinohara, Y., Bond splitting capacity of corroded bars confined by various stirrups ratio, *6th Civil Engineering Conference in Asian Region (CECAR)*, August 20-22, 2013, Jakarta, Indonesia.

Aryanto, A., and Shinohara, Y., Bond behavior between steel and concrete in low level corrosion of reinforcing steel, *15WCEE Conference*, September 24-28, Lisbon, Portugal, 2012.

Aryanto, A., and Shinohara, Y., Experimental study on bond behavior of steel bars in concrete in low level corrosion, *Proceedings of the Japan Concrete Institute*, Vol.34, No.2, pp. 571-576, JCI Annual Conference, 2012, July 4-6, 2012, Hiroshima, Japan.

Aryanto, A., and Shinohara, Y., Investigation of bond-slip parameter on corroded reinforced concrete tension member, *AIJ Annual Conference 2012*, September 12-14, 2012, Nagoya, Japan.

Aryanto, A., and Shinohara, Y., Cover crack-width propagation of reinforced concrete members induced by corrosion, *Proceedings of the Japan Concrete Institute*, Vol.35, No.1, pp. 1123-1128, JCI Annual Conference 2013, July 9-11, 2013, Nagoya, Japan.

Aryanto, A., Gakuhari, Y., and Shinohara, Y., Corrosion-induced cover crack propagation of reinforced concrete member, Part I: experimental study, *AIJ Annual Conference 2013*, August 30-31, 2013, Hokkaido, Japan.

Aryanto, A., Gakuhari, Y., and Shinohara, Y., Corrosion-induced cover crack propagation of reinforced concrete member, Part II: numerical study, *AIJ Annual Conference 2013*, August 30-31, 2013, Hokkaido, Japan.

篠原　保二，*Aryanto, A.,* 鉄筋の腐食膨張による RC 部材のひび割れ進展挙動，日本コンクリート工学会，鉄筋腐食したコンクリート構造物の構造・耐久性能評価の体系化シンポジウム　論文集，pp. 271-280, 2013.11

Contents

List of Figures

List of Tables

Notations

Roman upper case letters

A	crosssectional area
A_c	area of concrete
A_s	area of steel bar
E	elastic modulus
F	Faraday's constant
F_τ	tension force carried by concrete through bond
F_c	tensile strength of concrete to provoke cracking
K	stiffness
K_{cor}	stiffness of corrosion product
L_t	transmission length
M_{Fe}	atomic mass of iron
S	slip

Roman lower case letters

a	radius of free increase of corrosion rust
c	cover thickness
d	bar diameter
f_{ct}	average concrete tensile strength
i_{corr}	corrosion current density
k_c	correction factor related to confinement factor
k_R	correction factor for rate of loading
m	empirical constant
n	valence of iron
p_i	internal or expansion pressure
p_w	transverse bar ratio
r_{crack}	rate of crack propagation
t	time periods
t_{crack}	time from corrosion initiation to crack initiation
t_{prop}	time from crack initiation to crack width limit
u_{cor}	actual radius of corrosion expansion
w_{cor}	corrosion weight loss of corner bar
w_{mid}	corrosion weight loss of middle bar
w_{lim}	limit crack width
w_{crack}	critical mass of corrosion product per unit surface area of steel bar
x	corrosion depth penetration
x_{crack}	corrosion depth penetration at cover crack initiation

x_{cor} corrosion penetration of corner bar
x_{mid} corrosion penetration of middle bar

Greek letters

ΔA_{steel} part of bar area consumed by corrosion
$\Delta A_{steel.crack}$ part of bar area consumed by corrosion at crack initiation
Δx interval length of strain gauges
Σw_{exp} total crack width of experiment
Σw_{FEM} total crack width of finite element
α, β, γ empirical constant
ϕ_s steel bar perimeter
ε_{cor} strain of corrosion product layer
ε^{cr}_{max} maximum crack strain of concrete
σ_B compressive strength of concrete
σ_s stress of steel bar
$\sigma_{s,max}$ maximum stress of transverse bar
σ_t tensile strength of concrete
σ_y yield strength of steel
τ bond stress
τ_b local bond stress over the specified length
τ_m average bond stress over the transmission length
τ_{max} maximum bond stress
ρ_{Fe} specific weight density of iron
ν volumetric expansion ratio of corrosion products
ψ concrete cracking parameter

- blank page -

Chapter One

INTRODUCTION

Chapter 1
INTRODUCTION

1.1 BACKGROUND

Recently, a great attention has been given on durability and service-life prediction of reinforced concrete (RC) structures as an increasing number of deteriorated structures due to corrosion of reinforcement [1]. Corrosion of reinforcement becomes a problem on RC structures because it may induce cracking or spalling of concrete cover as well as bond deterioration between steel reinforcement and concrete. As a result, some issues that needed to be concerned in term of safety aspects are falling of concrete cover and degradation of load-carrying capacity that may leads to collapse of RC structures. Thus the knowledge of how material deteriorated and the effects to the structural behavior including the procedure to determine the load-carrying capacity of corroded RC structures becomes an important issue that needs to be considered. In addition, as growing number of deteriorated structures due to corrosion, the rehabilitation has also become an important issue.

In many cases of corroded RC structures, before structures showing a significant damage such as spalling of concrete cover, it preceded by sign of rust staining and cracking of concrete cover. This implies that an action is required to restore the condition of structures. In order to decide whether a structure has a sufficient remaining capacity or can fulfill the remaining service life, an estimate is required. However, the methodology for assessing these conditions has not been developed adequately. One of the key components for assessing the corroded RC structures is to know the level of corrosion in reinforcement. While direct measurement of corrosion loss without removing the reinforcement from the structure is difficult and costly, as an alternative way it may be estimated indirectly using the relation between cover crack width and corrosion loss. Thus, the knowledge of cracking behavior i.e. crack initiation and crack propagation and its corresponding corrosion loss became important due to serviceability requirement.

Moreover, bond behavior of corroded reinforcement still becomes an intriguing issue since number influencing factors on the bond behavior of corroded reinforcement that still need to be verified properly such as the influence of ratio of transverse bars and their configurations, bar positions, casting direction and concrete strength. Although

numerous research works have been conducted to evaluate the bond behavior of corroded steel bar in concrete, however, some aspects regarding the effects of corrosion on transverse bars and the presence of stress in transverse bars which develops during corrosion crack propagation need further study.

1.2 OBJECTIVE AND SCOPE

This research program aimed to investigate the effects of corrosion of reinforcement on cracking behavior and bond splitting behavior of corroded reinforced concrete members. This study encompasses both experimental and analytical studies including the evaluation of influencing factors such as effect of transverse bars, concrete strength and bar position on corrosion cracking and bond behavior of corroded RC members. To assess the cracking behavior of corroded reinforcement, an accelerated corrosion test of tension members and beam was performed. Moreover, the experiments of tension and pullout test were conducted to evaluate the bond characteristics and bond splitting behavior of corroded reinforced concrete members. The numerical study using non-linear finite element analysis was also undertaken to give a better understanding on the cracking behavior induced by corrosion product expansion. Finally, the knowledge obtained through accelerated corrosion and bond test was implemented in finite element simulations which can be used in the assessment of corroded RC members.

The main objectives of this research are

1. Develop rational prediction of corrosion loss through the evaluation of cover crack-width induced by corrosion product expansion.
2. Study the bond behavior and the bond splitting capacity of corroded RC members with different level of confinement, and develop bond stress-slip model for corroded RC members.
3. Evaluate the structural performance of corroded RC members and develop the procedure for assessing corroded RC members using the critical parameters of material deterioration of concrete and reinforcement and bond degradation.

So, broadly, the purpose of the study is to develop prediction of the structural performance of corroded RC members from the crack width evaluation.

1.3 OUTLINE

The content of this thesis is summarized in Fig. 1-1 and divided into six chapters as follows:

Chapter 1 briefly reviews background and objectives of current research. The outline of the present thesis is also described in this chapter.

Chapter 2 contains an evaluation of cracking behavior induced by corrosion product expansion. A series of accelerated corrosion test on beams specimens was conducted to investigate the cracking behavior of reinforced concrete structures due to corrosion products expansion. The experimental study was conducted to explore the influence of confinement from surrounding concrete (i.e. concrete strength) and transverse bar (i.e. transverse bar ratio and configurations) on cover crack behaviors i.e. crack initiation and crack propagation induced by corrosion product expansion. A numerical model through finite element analysis was also developed to simulate the crack behavior due to corrosion product expansion. In order to validate the numerical model, it was then compared with the experimental results.

Chapter 3 tries to evaluate bond characteristics of between corroded steel and concrete. A series of tension test on corroded RC tensile members was performed to evaluate corrosion-induced bond degradation which is reflected in the tension stiffness deterioration of corroded RC members. The effect of various corrosion levels was investigated. The cracking behavior i.e. crack spacing of corroded RC members under uniaxial tensile loading was also investigated. Moreover, the mechanical performance of cracked concrete due to corrosion was also evaluated through analysis of experimental results. In addition, a non-linear finite element analysis was performed to simulate the tension stiffening behavior of corroded RC tensile members and to reproduce the cracking behavior under tensile loading.

Chapter 4 covers the pullout testing of beam specimens. This test was dedicated to evaluate the effect of different transverse bar ratios and configurations of bar location on beams and its position to casting direction on bond splitting behavior of corroded RC members and also to investigate the residual bond splitting capacity, the mode of failure and the bond stress-slip relationships. As for the experimental database, the test results may help in establishing the bond deterioration model of corroded reinforcement with various confinement levels as well as in formulation of bond-slip model for assessing the structural behavior of corroded structures. Test results show a significant contribution of transverse bars on residual bond splitting capacity of corroded members. Moreover, different bond-slip relationship between healthy and corroded reinforcement was also identified. Suggestions were then made for bond splitting capacity and bond-slip relationship based on the current experimental results.

Chapter 5 presents a guideline for the method of evaluating the effect of corrosion on structural performance of reinforced concrete members. In this chapter, the key parameters of materials properties of structural element such as concrete, reinforcement and bond on the basis of corrosion deterioration as described in Chapter 2 to Chapter 4 are integrated to simulate the behavior of corroded RC columns. A non-linear finite element analysis were used to evaluate reinforced concrete members with a corroded rebar estimated from the observed crack widths.

Finally **Chapter 6** summarizes the main results and conclusions obtained from this research with the recommendations for further research.

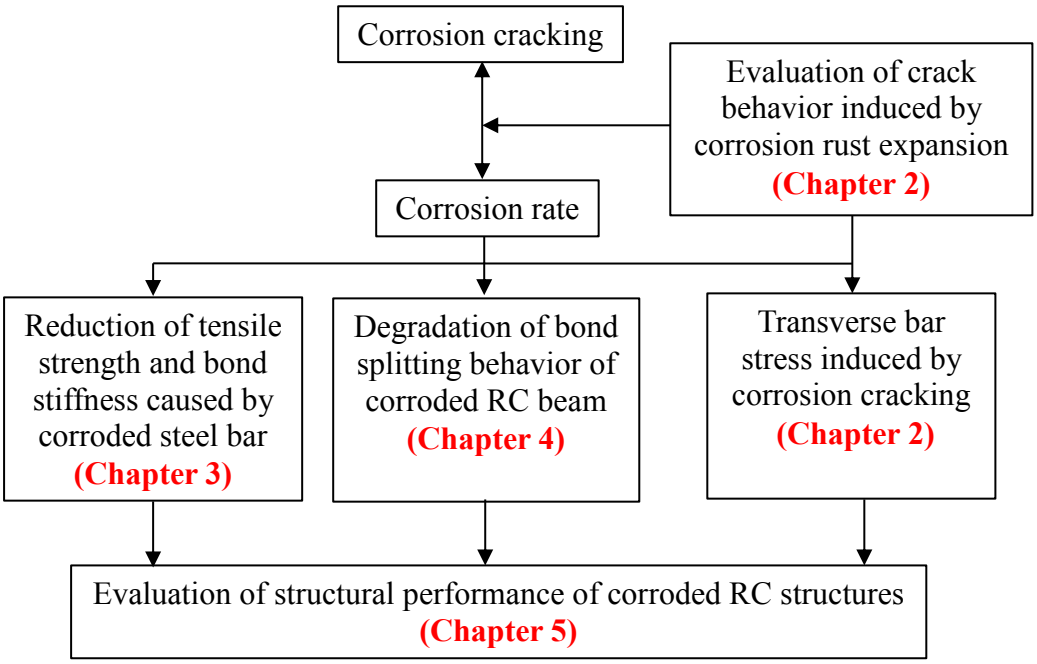

Fig. 1-1 Outline of the thesis

- blank page -

Chapter Two

EVALUATION OF CRACK BEHAVIORS INDUCED BY CORROSION-PRODUCT EXPANSION

Chapter 2
EVALUATION OF CRACK BEHAVIORS INDUCED BY CORROSION-PRODUCT EXPANSION

2.1 INTRODUCTION

Corrosion of reinforced concrete can be identified from rust staining and cracking of concrete cover. Cracking of concrete cover is also the main factor in determining durability performance and service life of RC structures. Usually, cracking of concrete cover began before corrosion has any significant effect on the structural performance. However, it may lead to acceleration of corrosion process because it may allow the oxygen and the water from the environment, which is required in the corrosion process, easily to penetrate and reach the embedded steel bar in concrete. As a result, the corrosion-induced cracking of the concrete cover is an essential parameter to determine the serviceability limit state and the time when actions required for structural repair or rehabilitation.

The prediction of corrosion-induced cover cracking has also become a main concern among researchers [2–5] because it can be used as an alternative ways for in situ assessments to predict reinforcement cross-section loss or corrosion rate of corroded RC members while direct measurement of corrosion loss without removing the reinforcement from the structure is difficult and costly. Reinforcement cross-section loss is also the main input parameter in the model that allows us to predict the structural performance of the corroded RC structures. To this purpose, it is important to be able to predict corrosion rate from observed crack width with sufficient accuracy.

In general, the stage of crack growth due to corrosion product expansion can be described in two stages [4] as presented in Fig. 2-1. First stage, crack initiation is the time when first cracking appeared on the concrete cover. It is usually a hairline crack with crack width of 0.05 mm. The next stage is crack propagation which the time for crack to develop from crack initiation to a limit crack width. For durability limit state, Andrade, et al.[6] suggest the crack width limit between 0.3 and 0.4 mm. ACI Committee 224 [7] and CEB Model code [8] suggested crack width limit between 0.15 and 0.4 mm depend on the exposure condition for durability and aesthetic concerns. On the other hand, Sakai et al. [9] recommended that a limit crack width of 0.8 mm is appropriate for serviceability

and aesthetic requirements. The definition of crack width limit varies among practitioners. It greatly depends on the individual engineering judgments and owner policies in the maintenance strategy of existing RC structures.

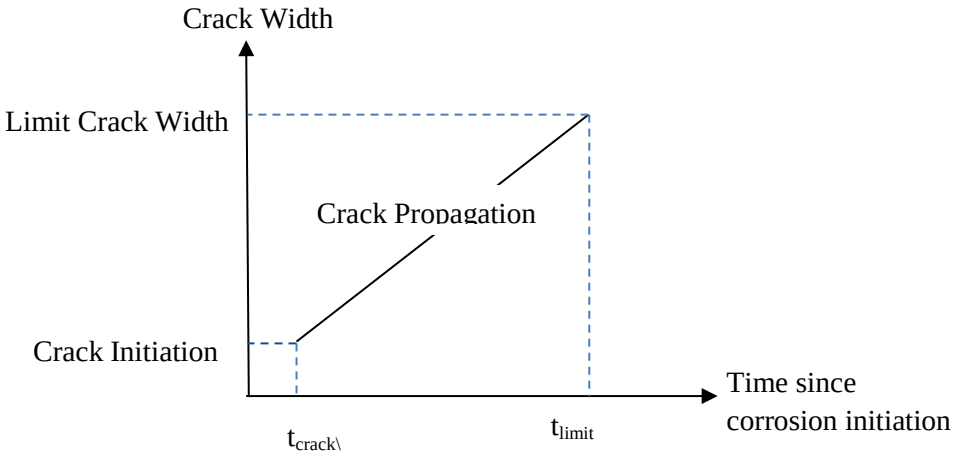

Fig. 2-1 Crack initiation and propagation [4]

A comprehensive study is required to obtain an accurate prediction on corrosion-induce cover cracking considering many factors influencing the corrosion of reinforced concrete. Numbers of experimental studies evaluating the cracking behavior e.g. crack initiation and crack propagation under corrosion of reinforcement have been undertaken for past years [4,5,10,11]. However, most of studies used a single bar in concrete prism or cylinder with absence of transverse bars which may not represent the real boundary conditions of reinforced concrete structures. Hence, the present experimental test tries to investigate the influence of transverse bar confinement, bar diameter, concrete strength on the cover crack initiation and crack propagation.

In addition, the corrosion of steel do not only induces cracking of concrete cover, but also it may generate stressing on the transverse bar that need to be taken into account in analysis which may reduce the residual shear capacity of RC structures and this has not been widely explored in the previous studies. Therefore, this study also investigate the effect of corrosion-induce transverse bar stress.

2.2 CURRENT EVALUATION OF CORROSION-INDUCED COVER CRACKING

2.2.1 Corrosion-induced cover crack initiation

The formula related to the critical amount of corrosion product required to cause cracking or the time to cover cracking empirically has been proposed based on the analysis of the experimental results. The formula was mostly derived from regression

analysis relating mechanical and geometrical properties such as cover thickness *c*, bar diameter *d*, and concrete properties. Andrade et al. [6] suggested that the critical amount of corrosion in term of corrosion depth penetration to cause cover cracking for c/d < 2 is x_{crack} = 20 μm. A linear relationship between corrosion depth penetration x_{crack} in μm and c/d ratio was proposed by Alonso et al. [10] as follows

$$x_{crack} = 7.53 + 9.32\frac{c}{d} \tag{2-1}$$

Another formula proposed by Morinaga [12] which make a relation between critical mass of corrosion product per unit surface area of steel bar, w_{crack}, and c/d ratio is given as

$$w_{.crack} = 0.6\times10^{-4} d\left(1+2\frac{c}{d}\right)^{0.85} \tag{2-2}$$

where $w_{rust.crack}$ in gr/cm^2 and *c* and *d* in mm. According to Rodriguez et al. [13] the critical corrosion product causing cover cracking also depends on the properties of concrete i.e. tensile strength of concrete σ_t , in N/mm^2

$$x_{crack} = 83.8 + 7.4\frac{c}{d} - 22.6\sigma_t \tag{2-3}$$

Using the Faraday's law and if the rate of corrosion is constant or assumed to be constant, the time from corrosion initiation to crack initiation, t_{crack} in year, can be estimated as

$$t_{crack} = \frac{x_{crack}}{11.6 i_{corr}} \tag{2-4}$$

where i_{corr} is corrosion current density in μA/cm^2.

2.2.2 Corrosion-induced crack propagation

For further crack opening or crack propagation, the crack propagation due to corrosion in terms of crack width has been investigated in a number of experimental studies[4, 13,14]. Most of the experiments using accelerated corrosion test with impressed current to give a reasonable test period. Based on those experimental results, numbers of empirical formulas were also developed. A linear relationship to predict the cover crack width *w* in mm due to corrosion products was proposed by Rodriguez et al. [13].

$$w = 0.05 + \gamma[x - x_{crack}] \tag{2-5}$$

where *x* are corrosion penetration in mm, x_{crack} is calculated by using equation (2-3) or at crack width 0.05 mm. γ was the slope of curve depending on bar location: 0.01 and

0.0125 for bar located at top and bottom in casting, respectively. A lower value for bar at top casting reflects higher porosity of concrete around top bar allows more diffusion of corrosion products.

Vidal et al. [14] proposed a relationship between the amount of corrosion and the crack width obtained from corroded beams on natural corrosion process for 14 and 17 years.

$$w = 0.0575[\Delta A_{steel} - \Delta A_{steel.crack}] \tag{2-6}$$

where ΔA_{steel} is part of bar area consumed by corrosion in mm^2 and $\Delta A_{steel.crack}$ is part of bar area consumed by corrosion at crack initiation in mm^2. ΔA_{steel} is determined by

$$\Delta A_{steel} = \frac{\pi}{4} \nu x(2d - \nu x) \tag{2-7}$$

where ν is the volumetric expansion ratio of corrosion products and $\Delta A_{steel.crack}$ is calculated by

$$\Delta A_{steel.crack} = A_s \left[1 - \left(1 - 0.001\nu \frac{7.53 + 9.32 c/d}{d} \right)^2 \right] \tag{2-8}$$

where A_s is original cross-section area of steel bar in mm^2.

Another empirical models proposed by Vu et al. [4] directly relates crack width with the time needed to reach a certain crack width. The model distinguish the time from corrosion initiation to cover cracking t_{crack} (crack initiation) and the time form crack initiation until the crack width reach crack width limit (crack propagation).

$$t_w = t_{crack} + t_{prop} \tag{2-9}$$

where t_{crack} can be estimated using a model for prediction of crack initiation. A nonlinear relationship for predicting t_{prop} was developed by Vu et al. [4] depending on the ratio between cover and w/c ratio. The time for crack propagation can be described as

$$t_{prop} = \alpha \left(\frac{c}{w/c} \right)^{\beta} \tag{2-10}$$

where α and β are constants depends on for given crack width 0.3, 0.5 and 1.0 mm. The formula was then developed by Mullard et al. [5] by involving rate of loading (rate of the impressed current, i_{corr}) and cover cracking parameters e.g. cover thickness, bar diameter, concrete tensile strength. Hence, the time for a crack to a limit crack width from first cracking can be described as

$$t_{prop} = k_R \frac{w_{\lim} - 0.05}{k_c r_{crack}} \left(\frac{i_{corr(\exp)}}{i_{corr(real)}} \right) \quad (2\text{-}11)$$

Where w_{lim} is limit crack width in mm, k_c is correction factor related to confinement factor (k_c = 1 for bar in an internal location), k_R is correction factor for rate of loading and empirically determined as

$$k_R \approx 0.95 \left[\exp\left(\frac{0.3 i_{corr(\exp)}}{i_{corr(real)}} \right) - \frac{i_{corr(\exp)}}{2500 i_{corr(real)}} + 0.3 \right] \geq 0.25 \quad (2\text{-}12)$$

where $i_{corr(exp)}$ is accelerated corrosion rate, and $i_{corr(real)}$ is actual or real corrosion rate typically less than 5μA/cm^2. r_{crack} is rate of crack propagation in mm/hour determined as

$$r_{crack} = 0.0008 e^{-1.7\psi} \quad (2\text{-}13)$$

where ψ is concrete cracking parameter, $\psi = c/(d\, f_{ct})$.

The existing empirical models aforementioned are derived based on the experimental test mostly conducted using a single bar in concrete prism or cylinder which may not represent the real boundary conditions of RC structures such as location of corroding bars in a RC members and presence of transverse bars. Because of that, the present experimental test discussed in section 2.3 is to investigate the influence of corrosion on cracking behavior on actual RC member i.e. corroded beam. The comparison between the empirical formula for crack initiation and crack propagation will be discussed in chapter 2.4.

2.3 ACCELERATED CORROSION TEST FOR EVALUATION OF CORROSION-INDUCED COVER CRACKING

2.3.1 Objectives

The present experimental test is intended to investigate the influence of actual confinement provided by surrounding concrete and transverse bar on the cover crack behaviors induced by corrosion product expansion of steel bar in order to obtain a general relationship between corrosion level and crack propagation (crack width growth) and to obtain the relation between corrosion rate and crack propagation (crack width) including the stress behavior of the transverse bars. Moreover, the test results may also help to develop FEM approach on prediction of corrosion loss of reinforcement from observed cover crack width. Broadly, the main objective is to estimate the corrosion rate of corroded reinforcement in concrete from observed cover crack width which can be easily determined through in situ assessment in order to assess structural performance of corroded RC members.

2.3.2 Detail of specimens

A series of accelerated corrosion test was conducted to investigate the cracking behavior of reinforced concrete structures due to corrosion products expansion. The mixture proportion of concrete and measured material properties used in the experiment are summarized in Table 2-1 and Table 2-2. The preheated high strength of steel bar that used here was to avoid the yielding before bond splitting failure in the pullout test (Chapter 4).

Table 2-1 Mixture proportions

Test No.	w/c (%)	Cement (kg/m^3)	Water (kg/m^3)	Fine aggregate (kg/m^3)	Coarse aggregate (kg/m^3)	Admixture (kg/m^3)
1-5	74	257	190	830	979	0.2
6	46	392	180	807	979	0.3

Table 2-2 Measured material properties

Material parameter	Concrete		Steel		
			D19	D22	U6.4
Compressive strength, (N/mm^2)	22	49	-	-	-
Tensile strength, (N/mm^2)	1.9	2.8	1128	1031	1490
Yield strength, (N/mm^2)	-	-	1053	980	1414
Modulus elasticity , ($x10^5$ N/mm^2)	0.23	0.3	1.87	1.85	2.0

Table 2-3 Test variables

No.	Specimens	Concrete strength (N/mm^2)	Longitudinal bar	Transverse bar
1	4LT-∞S-NC	22	4D19	No (p_w=0%)
2	4L2T-200S-NC		4D19	U6.4@200 (p_w=0.15%)
3	4L2T-100S-NC		4D19	U6.4@100 (p_w=0.3%)
4	4L4T-200S-NC		4D19	2-U6.4@200 (p_w=0.3%)
5	3L2T-100S-NC		3D22	U6.4@100 (p_w=0.3%)
6	4L2T-100S-HC	49	4D19	U6.4@100 (p_w=0.3%)

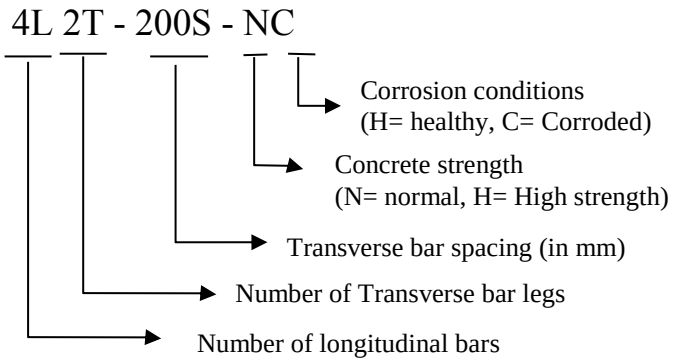

The test variables included transverse bars ratio and its configuration, diameter of longitudinal bar and concrete strength (Table 2-3). To consider the effect of confinement, transverse bar ratio of 0%, 0.15% and 0.3% were applied. To maintain the transverse bar area or constant confinement level during accelerated corrosion of longitudinal bar and to protect transverse bar gages, uncorroded transverse bars were used insulated by vinyl tape. Typical specimen configurations and gage locations are shown in Fig. 2-2. The specimens were cured for 28 days before accelerated corrosion test was conducted.

2.3.3 Accelerated corrosion setup and crack monitoring

During the accelerated corrosion test the specimens were placed above two supports and the tank containing 3% of NaCl solution was put below them and NaCl solution penetrated to the concrete through water sponge as shown in Fig. 2-3(a). Moreover, a constant 10 Volt was given and the current was monitored and recorded using data logger. The longitudinal bars were corroded up to approximately 6% of weight loss where cover crack width estimated larger than serviceability limit e.g. ACI's crack width limit of 0.15-0.5mm. Surface cracks of cover were visually observed and the crack width at certain locations was frequently measured using digital microscope having resolution of 0.01mm to monitor the crack width increment as shown in Fig. 2-3 (b). To measure the strain development in transverse bar due to corrosion cracking, three gages were installed at each transverse bar (Fig. 2-2)**.** The strain in transverse bar was recorded by data logger at each 60 minutes increment.

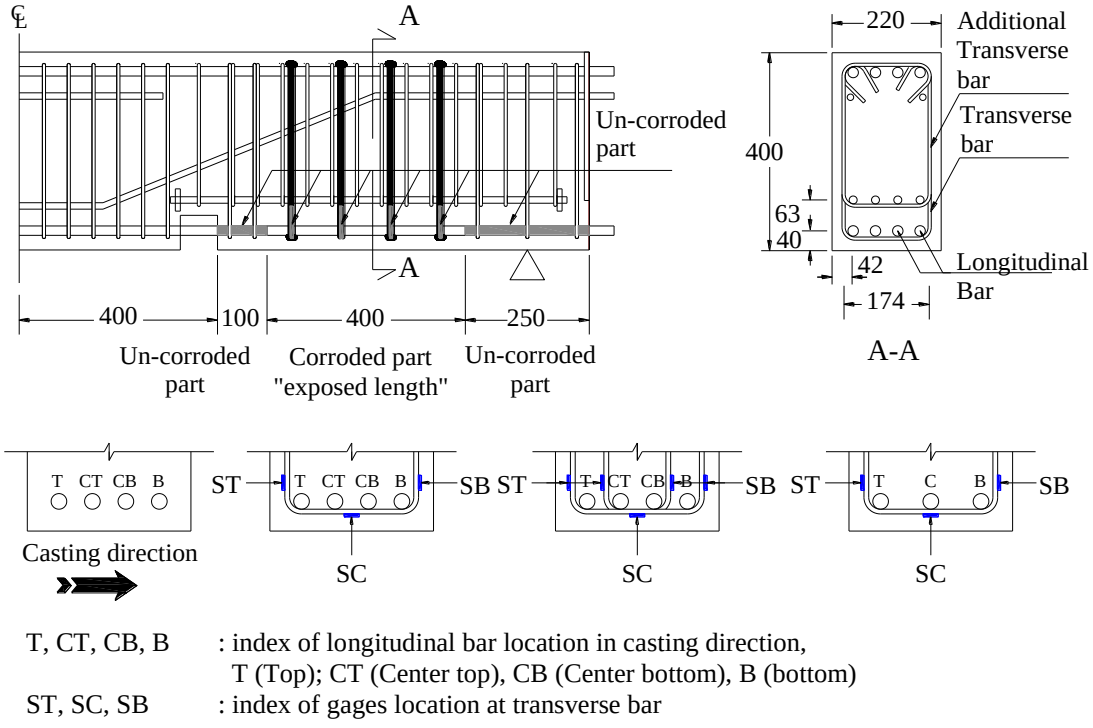

Fig. 2-2 Typical specimen configuration and gage attachment

(a)

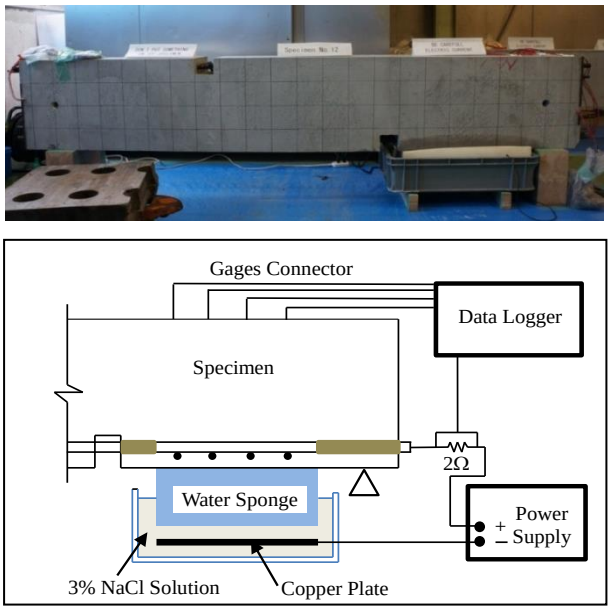

(b)

Fig. 2-3 (a) Overview of accelerated corrosion test (b) digital microscope measurement

After the testing, the longitudinal bars were removed from their concrete beams and the corrosion rust was chemically cleaned by 10% diammonium hydrogen citrate solution, and then mechanically removed using a steel wire brush after that the weight of reinforcement was measured to determine the weight loss due to corrosion (Fig. 2.4). The cleaning procedure of the rust and the measurement of weight loss are conformed to JCI-SC[15].

Fig. 2-4 Overview of corrosion weight loss measurement

2.4 EXPERIMENTAL RESULTS

2.4.1 Measured corrosion weight loss

Table 2-4 shows measured corrosion loss of individual longitudinal bar for each specimen. A different corrosion loss of each longitudinal bar i.e. T, CT, CB and B was observed although the measured output current of each longitudinal bar was relatively similar. Higher corrosion loss was obtained from the longitudinal bars located at corner

beam (T and B) which have two directional surfaces and corrosion cracking. The largest corrosion loss was obtained for bar located at top in casting (T). This can be attributed to the following: (a) the bar located at top of concrete casting tends to have higher porosity than at bottom casting due to settlement of fresh concrete [16]; (b) the cover crack initially occur at corner bar, thus it allows water and oxygen to penetrate to the bar easily and accelerates the corrosion process. However, for higher concrete strength of No.6 tends to have similar corrosion loss. If the average measured corrosion loss of longitudinal bar in one beam compared with estimated corrosion loss by Faraday's law, the difference between the two methods is approximately 10%.

Table 2-4 Measured corrosion in weight loss (%)

No.	Bar Location				Average		$i_{corr\ (predicted)}$
	T	CT	CB	B			mA.hr/cm^2
1	10.6	4.7	3.8	5.6	6.2	(222)	210
2	8.9	4.9	4.4	4.9	5.8	(207)	210
3	8.2	4.4	5.4	6.3	6.1	(218)	210
4	7.4	4.5	4.6	5.2	5.4	(195)	210
5	7.4	3.9		6.3	5.8	(243)	262
6	6.6	4.0	6.0	6.1	5.7	(205)	210

Note: number in the parenthesis shows the equivalent of accumulative current density estimated by Faraday's Law in mA.hr/cm^2

2.4.2 Measured crack initiation and crack propagation

The first crack, crack initiation, in the concrete surface was visually observed within a few days after accelerated corrosion being started for all specimens. The crack was initiated at bottom side of beams and mostly located near beam edge or corner bar. For further corrosion process, crack then propagated and formed a continuous crack approximately parallel to the longitudinal bars. The crack patterns and crack width at average corrosion loss of 6% are shown in Fig. 2-5. Generally, two major cracks were formed at the bottom cover of beams parallel to longitudinal bar. A relatively close spacing of longitudinal bars seems to promote the corrosion crack among bars to propagate horizontally connecting each longitudinal bar (See Appendix C). This can be seen from the stain in the concrete after removing the bottom cover as shown in Fig. 2-6. In addition, only specimen No.6 develops a side crack and a bottom crack perpendicular to the longitudinal bars direction. This side crack has a similar mechanism with the splitting crack parallel to longitudinal bar at bottom beam. Meanwhile, the transverse crack at bottom beam may develop from two adjacent longitudinal cracks which tend to propagate at the weak point in the concrete section.

Specimen No.6 which has higher concrete strength and lower w/c ratio (Table 2-1 and Table 2-3) may have lower porosity. Therefore, it can generate higher expansion pressure and become more easy to develop a new splitting/radial crack e.g. side crack for high strength concrete than normal concrete as shown in Fig. 2-5.

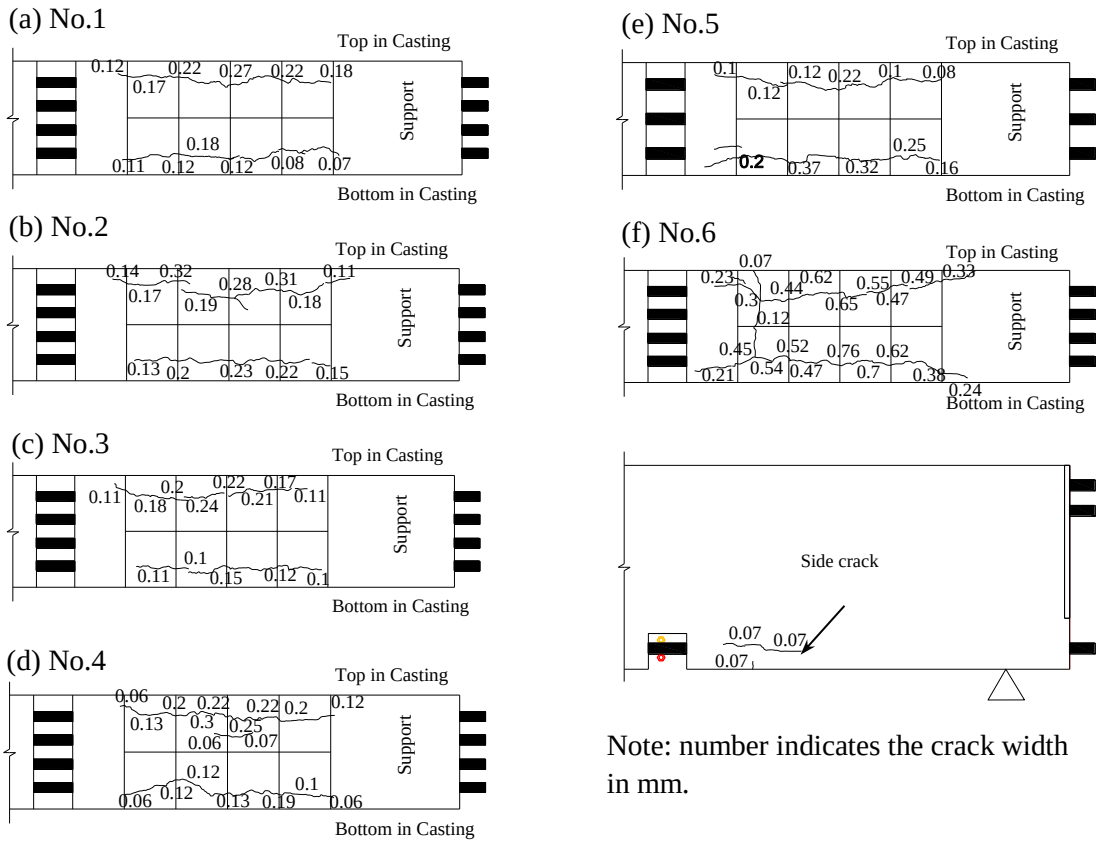

Fig. 2-5 Crack pattern at average corrosion loss of 6%

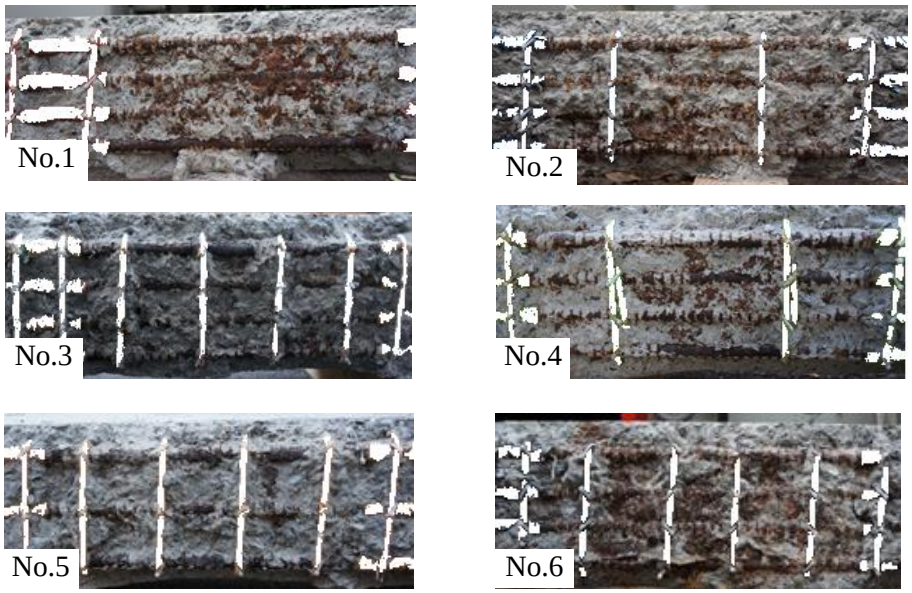

Fig. 2-6 Rust staining on concrete surface after removing cover

Fig. 2-7 presents the relations between observed maximum crack width along the exposed length and average corrosion penetration. The average corrosion penetration

was determined from means value of corrosion depth penetration for all longitudinal bars in one specimen or one beam. Corrosion depth penetration was estimated from the relationship of accumulative current density and corrosion cross-sectional loss and calibrated with the measured corrosion weight loss (Table 2-4). According to Faraday's law, corrosion depth penetration *x* can be expressed as

$$x = \frac{M_{Fe} i_{corr} t}{\rho_{Fe} n F} \tag{2-14}$$

where M_{Fe} is atomic mass of iron (56.10^{-3} kg/mol), ρ_{Fe} is specific weight density of iron (7800kg/m^3), n is valence of iron (n = 2), F is Faraday's constant (96500 ^{o}C/mol), i_{corr} is corrosion current density (mA/cm^2), and t is test period (s).

As shown in Fig. 2-7, the corrosion penetration at first concrete cracking (crack initiation) is around 30-60 micrometers. All specimens produce relatively same corrosion penetration at crack initiation. This indicates that the presence of transverse bars do not significantly influence the level of corrosion to generate crack initiation.

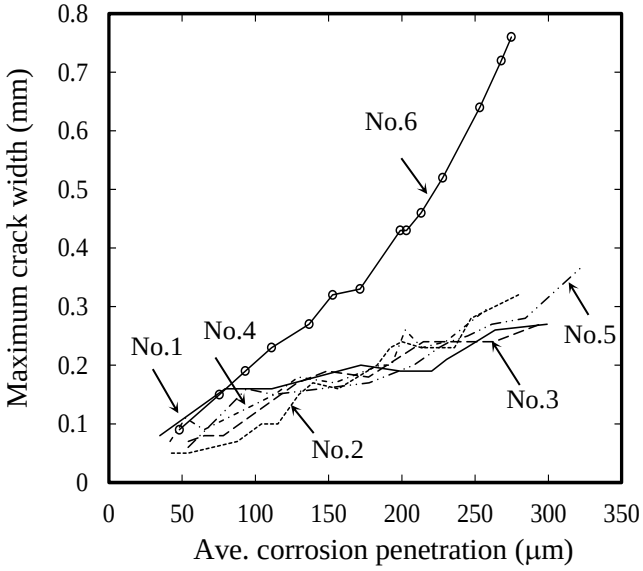

Fig. 2-7 Maximum crack width vs. average corrosion penetration

Specimen No.6, with high strength concrete, clearly showed that larger crack width growth compared to specimens with normal concrete strength. This can be attributed to lots of corrosion products accumulated around bars in high strength concrete which prevented the corrosion product to penetrate or to diffuse within the pores of hardened cement paste (Fig. 2-8). As reported by Tanaka [17], the porosity of hardened cement paste increase with an increase of w/c ratio. For example, the porosity of hardened cement paste at 28 days for w/c ratio of 0.45 and 0.6 are 15% and 25%, respectively (Fig. 2-9). Moreover, the amount of pores greater than 1 μm^2 is also increased for

higher w/c ratio. Because of that, the corrosion product may be difficult to penetrate or to diffuse in the cement paste for high strength concrete. It should be noted that the use of high strength concrete may delay the corrosion initiation time or chloride diffusion due to the lower porosity [18], although higher concrete strength produced faster crack width growth as shown in Fig. 2-7.

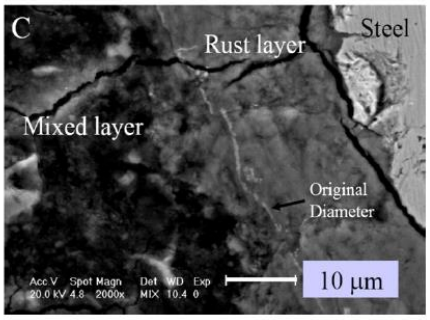

Fig. 2-8 Microstructure of corrosion around bar surface [18]

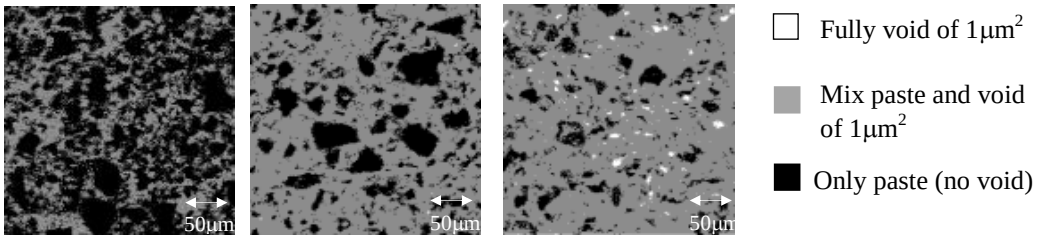

w/c =0.3 w/c =0.45 w/c =0.6

Fig. 2-9 Effect w/c ratio on pore structure of hardened cement paste [17]

The effect of transverse bar seems insignificant on the crack propagation. It is shown in Fig. 2-7 the crack widths of specimen with various transverse bars (No.2-No.5) are relatively close as well as with specimen without transverse bar (No.1). This can be attributed to the use of vinyl taping that may reduce the bond between transverse bars and concrete so that the crack are more concentrated at corner bars and may increase the crack width.

Fig. 2-10 shows comparison of current experimental results of crack propagation with the empirical model as mentioned in section 2.2. Two typical specimens having different concrete strengths (No.3 and No.6) are compared in Fig. 2-10. The empirical models of Rodriguez et al., Vu et al. and Vidal et al. models showed that an overestimated prediction of crack width for both cases (see Appendix A). This comparison illustrates the limitations of the empirical models because of their dependency on limited test data. Therefore, a numerical models using finite element analysis simulation were investigated in this present study.

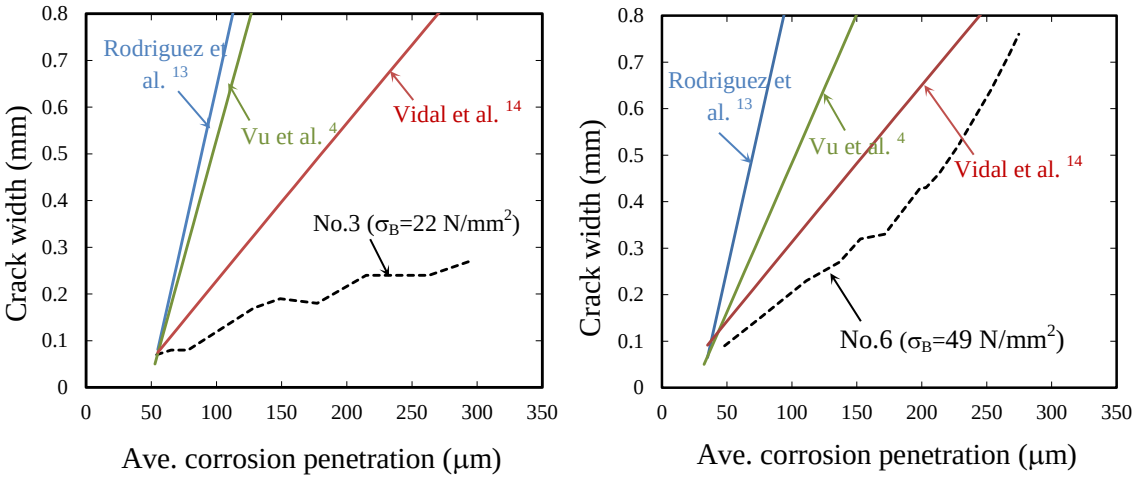

Fig. 2-10 Crack width vs. average corrosion penetration relations

2.4.3 Measure of transverse bar stress

It is well known that the presence of transverse bars increase the confinement level around longitudinal bar. When corrosion occurs at longitudinal bar, it may induce internal expansion pressure to the surrounding concrete. As a response to the concrete cracking around corroded bar, the transverse bar will deform and generate strain/stress. The deformation of transverse bar will greatly depends on cracking behavior due to corrosion expansion and bond interaction between transverse bar and surrounding concrete.

Fig. 2-11 shows the relation between corrosion penetration in longitudinal bars and measured strain of transverse bar at the middle of bottom leg of transverse bar (SC). For specimens with normal concrete strength and with transverse bars ratio of 0.15-0.3% (No.2-No.5), the strain observed on the transverse bar is relatively small and less than 200μm or equivalent with 40N/mm^2 as shown in Fig. 2-11(a)-(d). However, a higher strain at transverse bar was observed for the specimen with high strength concrete (No.6). Maximum strain generated at SC for No.6 is 700μm (140 N/mm^2) or only 10% of its yields stress (σ_y =1450 N/mm^2). However, if using normal strength of transverse bars e.g. σ_y = 295 N/mm^2, it then will reduce to almost 50% of its capacity. Therefore, it may significantly reduce the residual shear capacity of RC structures under service loading or seismic loading. Higher stress on the transverse bar was due to larger crack width (Fig. 2-7) and higher adhesion between high strength concrete and bar. The strain at the bottom leg (SC) tends to have larger tensile strain than at the side leg (ST and SB) because the majority of cracks were propagated crossing the bottom leg of transverse bars. A higher strain of side leg is shown when the crack propagated at side of beams for specimen No.6 (Fig. 2-11(f)).

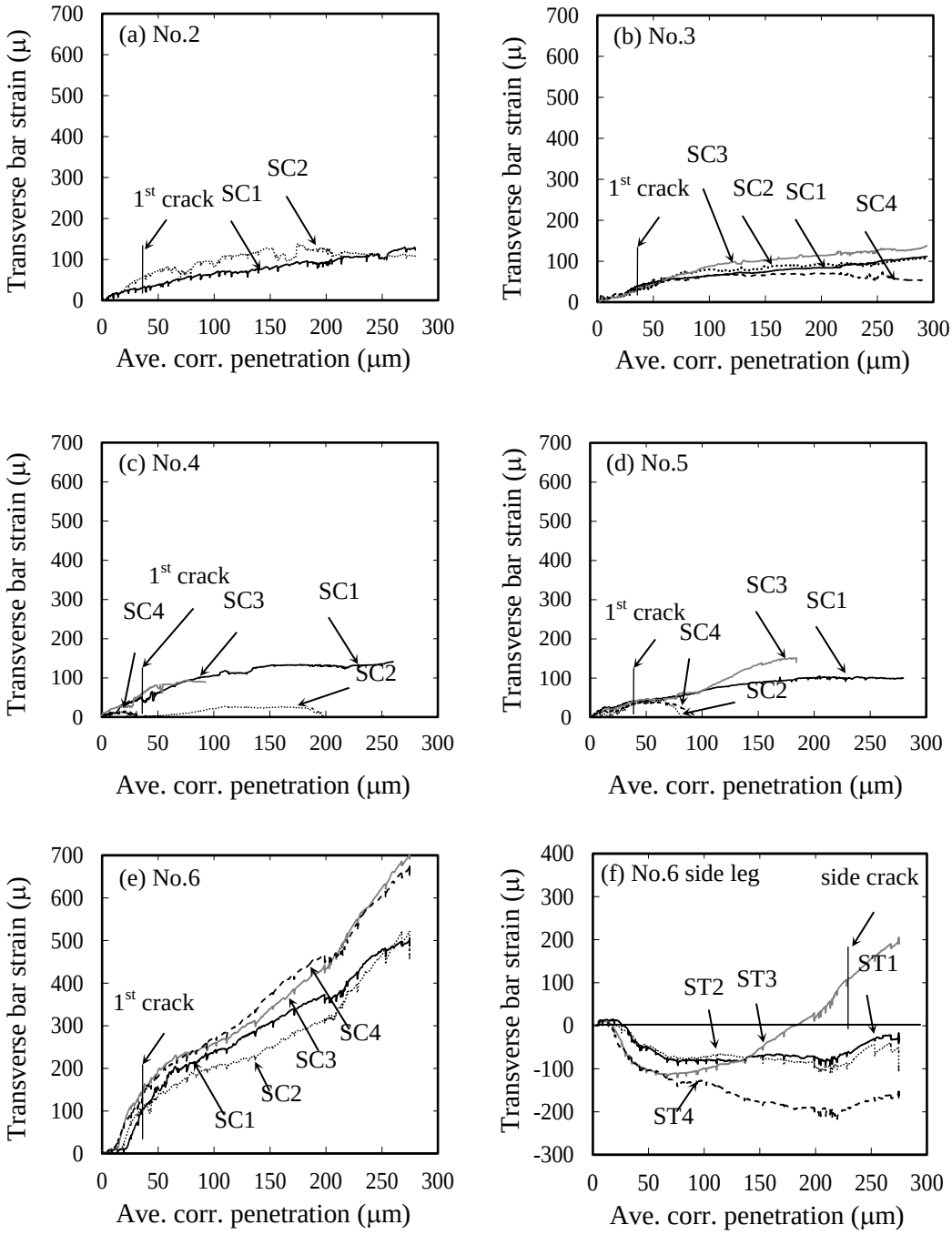

Fig. 2-11 (a)-(e) Measured strain of transverse bar at middle of bottom leg (SC), (f) at side leg (ST) of transverse bar for Test No.6

Assuming a perfect bond between concrete and transverse bar, the strain on the transverse bar can roughly be estimated as the total crack width over the selected length of transverse bar divided by selected length of transverse bar. For example, for specimen No.3, the strain at bottom leg of transverse bar is approximately equal to the total crack width at bottom face divided by the total length of bottom leg of 0.39mm/174mm = 2300μm and for specimen No.6 is about 1.4mm/174mm = 8000μm.

The observed transverse bar strain rate from tests for both specimens is not so large compared to above estimation. It can be due to the bond between steel bars and concrete that is not perfect due to vinyl taping.

2.5 EVALUATION OF CORROSION-INDUCED COVER CRACKING THROUGH FINITE ELEMENT ANALYSIS

2.5.1 Deformation induced by corrosion products

A relative volume increase of the corrosion products compared with original steel volume generates an expansion pressure to the surrounding concrete. Arising pressure from corrosion products expansion may induce tensile stress or ring tension in surrounding concrete (Fig. 2-12(b)). Further increase of tensile stress will provoke concrete cracking around corroded steel bar. The crack will propagate radially until reaching the surface of concrete cover or connect with another crack for further expansion process. Therefore, the knowledge on the relationship between the amount of corrosion of steel bar and the expansion pressure generated from corrosion is required when evaluating cracking behavior of concrete due to steel corrosion.

Fig. 2-12 illustrates deformation around steel due to corrosion expansion. Generally, there are two types of displacement radius, i.e. free-increase radius (free swelling) and actual increase radius. When the corrosion product can expand to free-increase radius a, so there is no expansion pressure will be generated. However, considering the compaction effect of corrosion product due to confinement of surrounding concrete as mentioned by Lundgren [19], the free-increase radius will reduce to the actual radius u_{cor}.

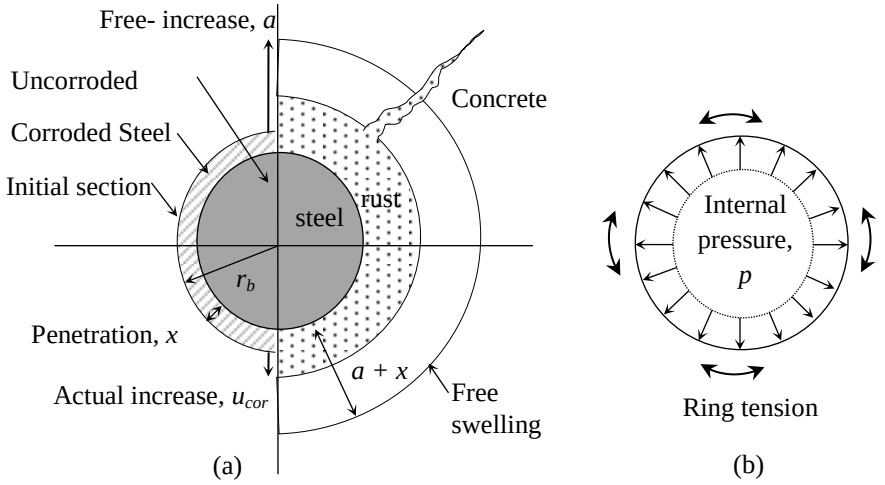

Fig. 2-12 (a) Deformation around corroded bar due to corrosion expansion, (b) internal expansion pressure

By assuming the corrosion penetration, x, and the volume of the rust relative to corroded steel, v, the radius of free increase, a, can be expressed as follows [19]

$$a = -r_b + \sqrt{r_b^{\,2} + (v-1)(2r_b x - x^2)} \tag{2-15}$$

The value of relative volume of the rust to corroded steel, v, greatly depends on corrosion product formation [3]. Common value used in analysis were taken between 2.0 (Andrade et.al [2]) and 4.0 (Liu & Meyers [3]). The strain of corrosion product layer, ε_{cor}, due to compaction effect is defined as follows [19]

$$\varepsilon_{cor} = \frac{u_{cor} - a}{x + a} \tag{2-16}$$

Evaluating the deformability of corrosion products around corroded bar, a nonlinear relation has been proposed between internal pressures, p developing around bar and corresponding strain of corrosion product layer, $\varepsilon_{cor,}$ in radial direction may be expressed as [19]

$$p = K_{cor}\,\varepsilon_{cor}^{\,m} \tag{2-17}$$

where K_{cor} and m represent the stiffness of corrosion product and empirical constant, respectively. The value of K_{cor} = 7000 N/mm^2 and m =7.0 were chosen in the present analysis to give reasonable agreement with the results from the analysis of the test.

2.5.2 Modeling approach

Finite element (FE) analysis was performed to analyze the crack propagation induced by corrosion of longitudinal bars. For the sake of simplicity, two-dimensional (2D) analysis with plane stress elements having a thickness of exposed length were used to model the concrete and only a half of beam sections were modeled. The longitudinal bars were modeled as holes and the transverse bars were modeled using truss elements where the center line as shown in Fig. 2-13. The truss element plays a role to resist the internal expansion pressure from corroded longitudinal bars together with surrounding concrete. In the actual condition, almost perimeter of longitudinal bars is fully attached to concrete. The mechanical properties of concrete and transverse steel are presented in Fig. 2-14.

The concrete behavior under compression was assumed to be linearly elastic since the concrete behavior in this analysis is dominantly governed by tensile cracking at low levels of compressive stresses. Concrete crack initiated when its maximum tensile stress reaches the tensile strength, or Rankine criterion. A multidirectional smeared crack model that takes 60 degrees as threshold value was used. After cracking, bi-linear tension softening model [20] was adopted. The transverse steel used a bi-linear model without strain hardening.

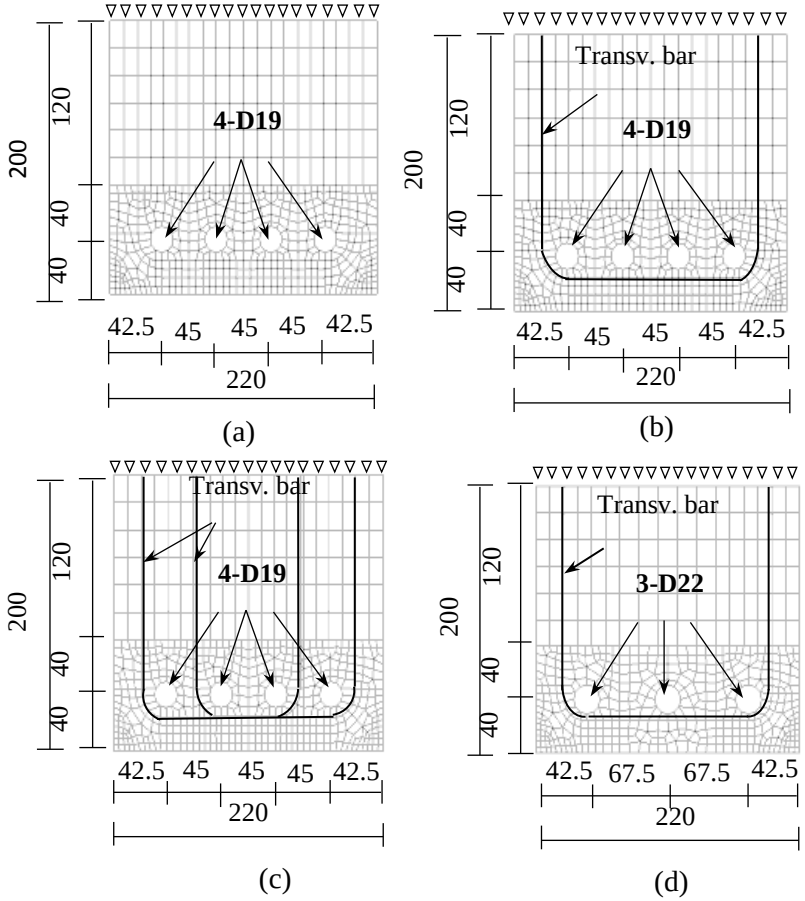

Fig. 2-13 Typical finite element model

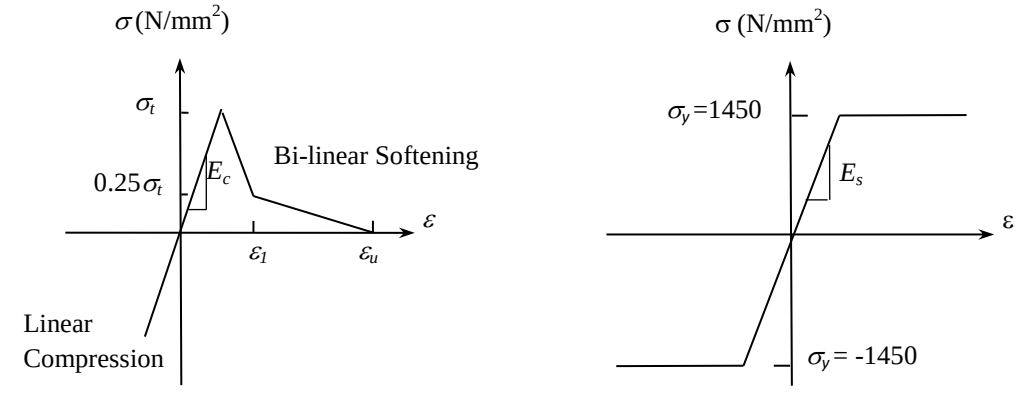

(1) Concrete

Thickness	400 mm
Elastic modulus, E_c	23000 N/mm^2 33000 N/mm^2
Poisson's ratio, v	0.2
Tensile strength, σ_t	1.9; 2.8 N/mm^2

(2) Transverse reinforcement

Sectional area	0, 60, 120 mm^2
Elastic modulus, E_c	200000 N/mm^2
Yield strength, σ_y	1450 N/mm^2

Fig. 2-14 Mechanical properties for concrete and reinforcement

To simulate corrosion attack associated with corrosion-product expansion, the expansion pressure around corroded bar was applied by internal pressure normal to bar perimeter as shown in Fig. 2-12(b). The relation between the internal pressure and strain of corrosion products is expressed in equation 2-17, where the internal pressure greatly depends on the expansion of corrosion product including compaction effect given by surrounding concrete as mentioned in equation 2-16. Although internal pressure is not always parallel to corrosion ratio, the internal pressure of corner bars, which were more severely corroded, were assumed to be two times of that of middle bars in order to obtain a crack pattern from tests. Therefore, two types of internal pressure control were applied

a) uniform distributed loading (UL), and
b) non-uniform distributed loading (NL).

For uniform loading (UL) a similar pressure was applied on all bars i.e. corner and middle bars and for non-uniform loading (NL) the internal pressure of corner bar was two times of that of middle bars. The basic increment of internal pressure was set at $0.05N/mm^2$. The following assumptions were also adopted in this FE analysis:

a) corrosion was assumed to be uniformly distributed along the longitudinal bar direction and over the perimeter of bar,
b) absorption of corrosion product into concrete pores and cracks was not considered.

The mechanical interaction between transverse bar and concrete is necessary to consider when evaluating the influence of confinement provided by transverse bars. The finite element program DIANA [21] provides some features to model mechanical interaction of steel reinforcement and concrete in the plane stress using interface element where the interaction of both elements is expressed by bond-slip relationship. The bond slip relationship was assumed as a bi-linear model [22] as shown in Fig. 2-15. Because no available test data on bond-slip relationship for transverse bar covered by taping, the maximum bond stress and slip at maximum bond stress were determined according to CEB-FIP Model code [8] assumed as plain bars. Therefore, the maximum bond stress and slip at maximum bond stress were $0.3\sigma_B^{1/2}$ and 0.1 mm, respectively.

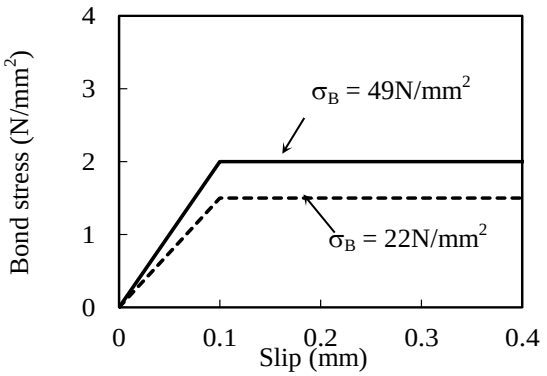

Fig. 2-15 Bond-slip relationship of transverse bar

The corrosion depth penetration x, and the corrosion weight loss w, were estimated based on the average radial deformation of hole (longitudinal bar) assumed that the corrosion products occupied the deformation space and the relative volume of the rust to corroded steel, v = 2, which depends on the rust formation. The procedure to obtained corrosion depth penetration is described in Fig. 2.16.

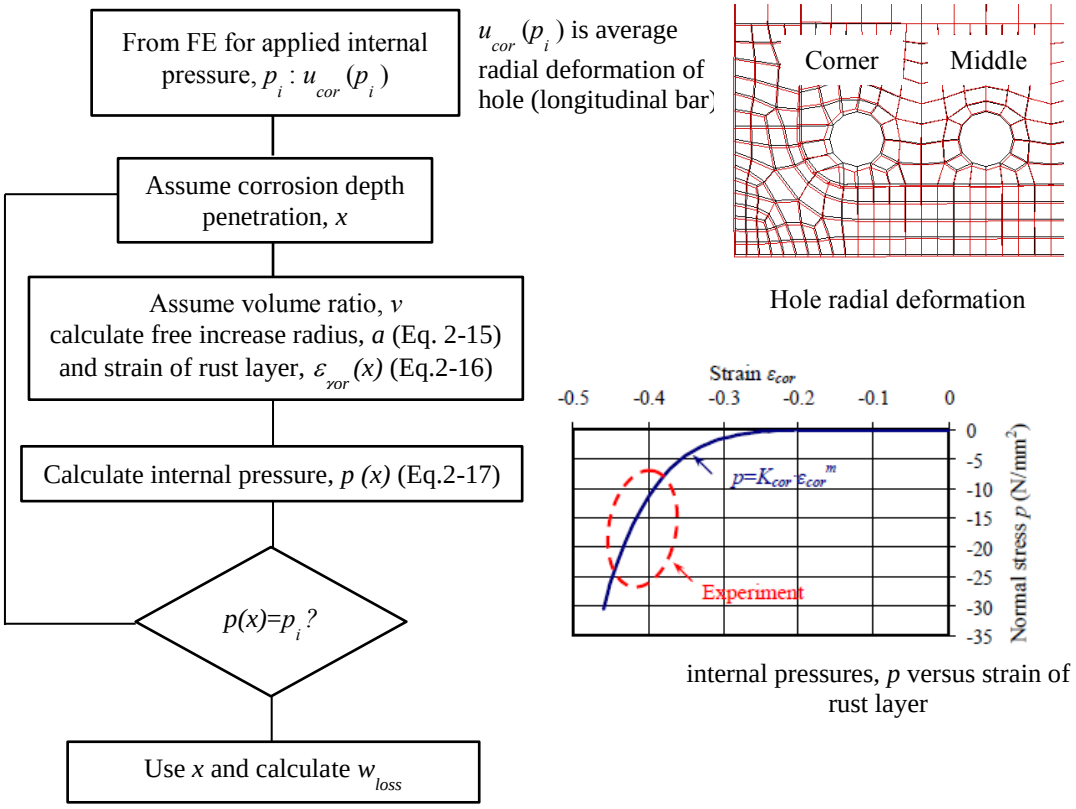

Fig. 2-16 Flowchart to determine corrosion penetration

2.6 COMPARISON OF CORROSION-INDUCED COVER CRACKING FROM EXPERIMENTAL AND FINITE ELEMENT ANALYSIS

2.6.1 Comparison of crack initiation and crack propagation

Fig. 2-17 and Fig. 2-18 shows crack strain behaviors and deformation obtained from FE analysis at cracking of cover concrete using two loading patterns, i.e. uniform (UL) and non-uniform (NL) load increments. The internal pressure p, maximum crack strain ε^{cr}_{max}, and maximum transverse bar stress $\sigma_{s,max}$, are also provided in the figure.

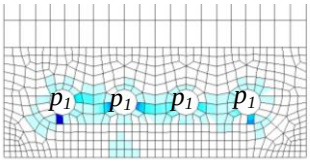

p_1 = 2.45 N/mm^2
ε^{cr}_{max} = 7.8×10^{-3}
$\sigma_{s,max}$ = N/A
x_{cor}; x_{mid} =32; 21 μm
w_{cor}; w_{mid} = 0.67; 0.43 %
(a) No.1

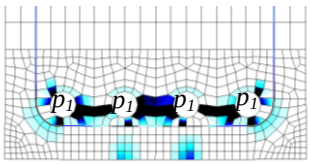

p_1 = 2.35 N/mm^2
ε^{cr}_{max} = 8.28×10^{-3}
$\sigma_{s,max}$= 58.2 N/mm^2
x_{cor}; x_{mid} = 35; 41 μm
w_{cor}; w_{mid}= 0.72; 0.86 %
(b) No.2

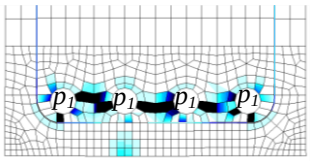

p_1 = 2.5 N/mm^2
ε^{cr}_{max} = 7.2×10^{-3}
$\sigma_{s,max}$= 29.5 N/mm^2
x_{cor}; x_{mid} = 32; 25 μm
w_{cor}; w_{mid}= 0.67;0.53 %
(c) No.3

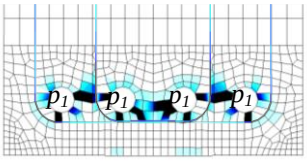

p_1 = 2.3 N/mm^2
ε^{cr}_{max}= 1.06×10^{-2}
$\sigma_{s,max}$= 137 N/mm^2
x_{cor}; x_{mid} = 26; 41 μm
w_{cor}; w_{mid}= 0.55;0.86 %
(d) No.4

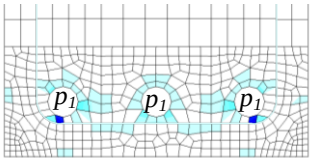

p_1 =3.1 N/mm^2
ε^{cr}_{max}= 7.36×10^{-3}
$\sigma_{s,max}$= 24.9 N/mm^2
x_{cor}; x_{mid} = 41; 16 μm
w_{cor}; w_{mid}= 0.74; 0.3%
(e) No.5

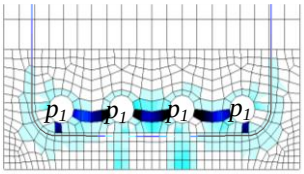

p_1 = 3.6 N/mm^2
ε^{cr}_{max}= 1.73×10^{-2}
$\sigma_{s,max}$= 94.9 N/mm^2
x_{cor}; x_{mid} = 54; 90 μm
w_{cor}; w_{mid}= 1.14; 1.89%
(f) No.6

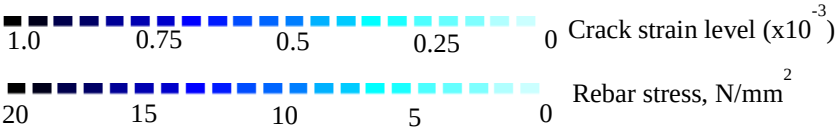

Note: p_1, p_2: internal pressure (p_2 = 2 p_1) ; ε^{cr}_{max}: max. crack strain ; $\sigma_{s,max}$: max. transverse bar stress ; x_{cor}; x_{mid}: corrosion penetration of corner bar and middle bar ; w_{cor}; w_{mid}: corrosion weight loss of corner bar and middle bar

Fig. 2-17 Crack strain, internal pressure, transverse bar stress and corrosion rate at first cracking of cover (uniform loading – UL)

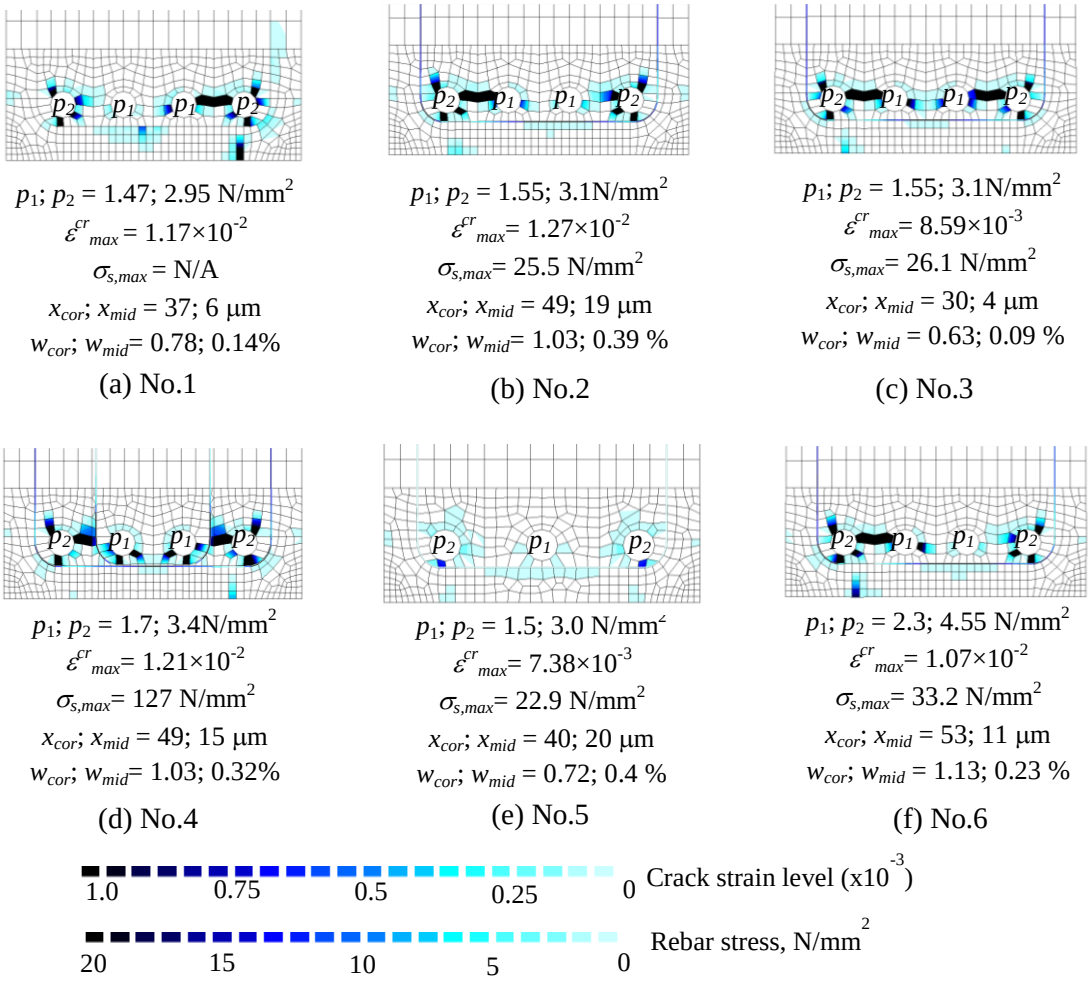

Note: p_1, p_2: internal pressure (p_2 = 2 p_1) ; ε^{cr}_{max}: max. crack strain ; $\sigma_{s,max}$: max. transverse bar stress ; x_{cor}; x_{mid}: corrosion penetration of corner bar and middle bar ; w_{cor}; w_{mid}: corrosion weight loss of corner bar and middle bar

Fig. 2-18 Crack strain, transverse bar stress and corrosion rate at first cracking of cover (non-uniform loading – NL)

As shown in Fig. 2-17 and Fig. 2-18 the crack initially tends to form a horizontal crack pattern connecting each longitudinal bar. This can be attributed to the small distance of bar spacing. For uniform loading (UL), cracks tend to propagate to the concrete surface at the middle of beam. Meanwhile, for non-uniform loading increment (NL), cracks mostly propagated to concrete surface near the corner beam indicated by higher crack strain. The crack pattern produced by NL loading showed a good agreement with the experimental results where cracks mostly located near corner bars (Fig. 2-18). This also indicates the influence of corrosion loss distribution associated with expansion pressure distribution among bars on crack propagation.

From the analytical results for non-uniform loading (NL) and when the cracks reach the concrete surface, the corrosion penetration is around 30 to 53 micrometers or corrosion weight loss of steel bars is 0.63% to 1.13%. This shows that the corrosion penetration that induces cracking on concrete surface is relatively low. This is also reported by other researchers [23]. The analytical results reasonably agree with experimental results where the corrosion penetration at first cracking of concrete cover was around 30-60 micrometers.

To evaluate the relation between crack width and corrosion levels, here, the comparison between the test and the analytical results was performed using total crack width of concrete surface at certain section of beams. The total crack width from the experimental data was determined as the summation of crack width at one section along the exposed length as illustrated in Fig. 2-19(a)-(b). Therefore, the total crack width from test data can be expressed as

$$\sum w_{small} = w_1 + w_2 \tag{2-18}$$

where w_1 and w_2 are crack width of individual splitting crack on concrete surface at one section along exposed length. In this study, the total crack width was determined at three locations, i.e. sections (*1*), (*2*), and (*3*) as shown in Fig. 2-19(b).

The total crack width from FE analysis was determined by the total of relative nodal displacement of two corner beam section from its original position as shown in Fig. 2-19(c) which still reliable for cracks that relatively small and using continuum crack model [20] because concrete tensile strain is generally negligible. Thus, the total crack width from the analysis can be expressed as follows:

$$\sum w_{FE} = \Delta_1 + \Delta_2 \tag{2-19}$$

where Δ_1 and Δ_2 are relative nodal displacement of two corner beam sections.

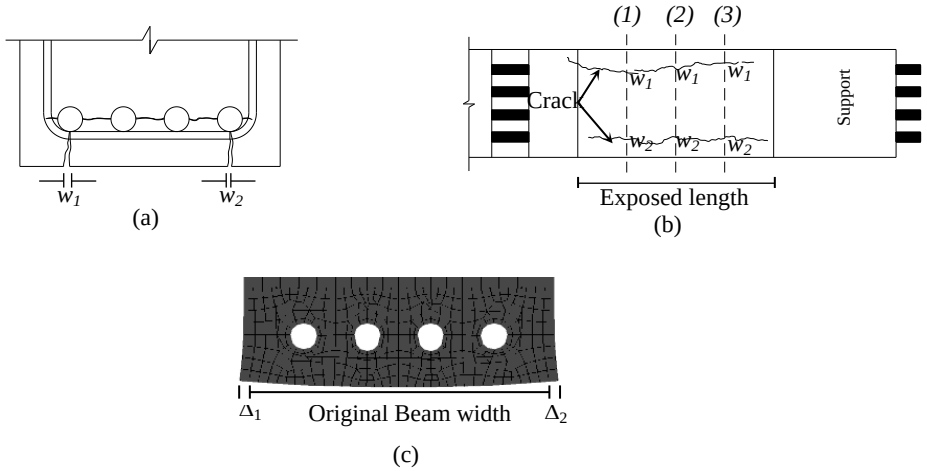

Fig. 2-19 Determination of total crack width of surface cracking from (a) experiment (b) observed sections (c) FE analysis

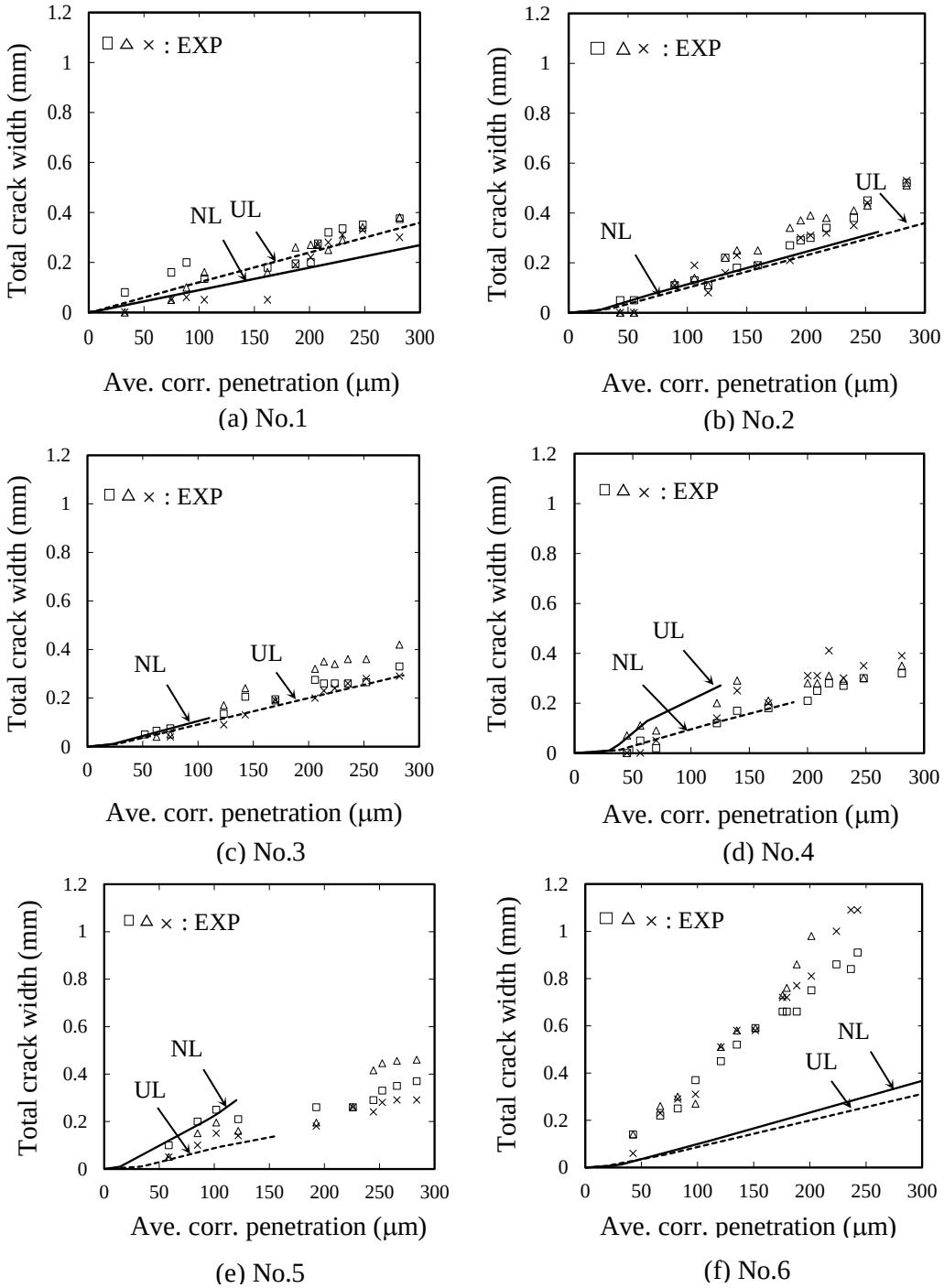

Fig. 2-20 Corrosion penetration and total crack width relationship
(Ratio volume increase, v = 2)

Fig. 2-20 presents the comparison between test and analysis results on the total crack width and average corrosion penetration with different loading distribution using ratio of volume increase v = 2. For specimens with normal concrete strength (Fig. 2-20(a-c)), the analytical result shows a good agreement of crack width with the experimental result for both uniform loading (UL) and non-uniform loading (NL). Both loading patterns generate a slightly different value. However, for specimens No.6 as shown in Fig. 2-20(d), it generates an underestimate prediction compared to experimental results for both UL and NL. This indicates that a different expansion is required for high strength concrete because only a small amount of corrosion products can penetrate to the concrete pore due to lower porosity. Therefore, the volume increase ratio, v need to be increased for high strength concrete. As shown in Fig. 2-21, based on simulation for different value ratio volume increase, the ratio volume increase of v = 3 gives a good agreement with test results for Test No.6.

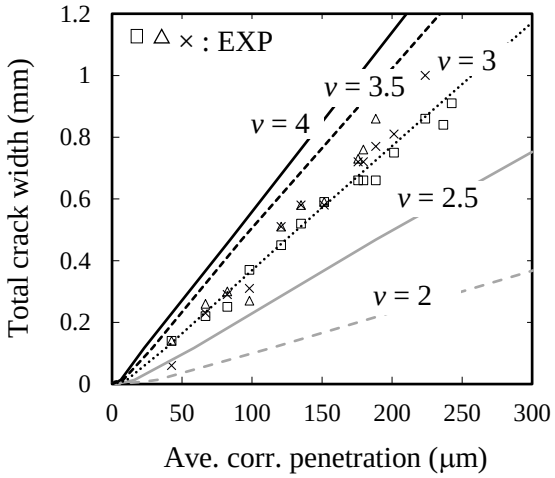

Fig. 2-21 Effect of ratio volume increase, v on total crack width of high strength concrete (No.6) for NL

2.6.2 Comparison of transverse bar stress

Fig. 2-22 presents the typical transverse bar stress at the middle of bottom leg of transverse bar where the strain gages were installed at this location. The analytical results generally show an overestimated prediction for test No.2 and No.3 particularly for larger corrosion penetration as shown in Fig. 2-22(a)-(b). However, a lower transverse bar stress compared to test result was produced for test No.6 when using ratio volume increase, v = 2 for both UL and NL loading types (Fig. 2-22(c)). When ratio volume increase of corrosion product was increased to v =3, it showed an overestimate value for larger corrosion penetration (Fig. 2-22(d)) like the specimen with normal concrete strength. This indicates that the bond-slip relationship of transverse bar should be changed according to cracking due to corrosion and further investigation need to be conducted.

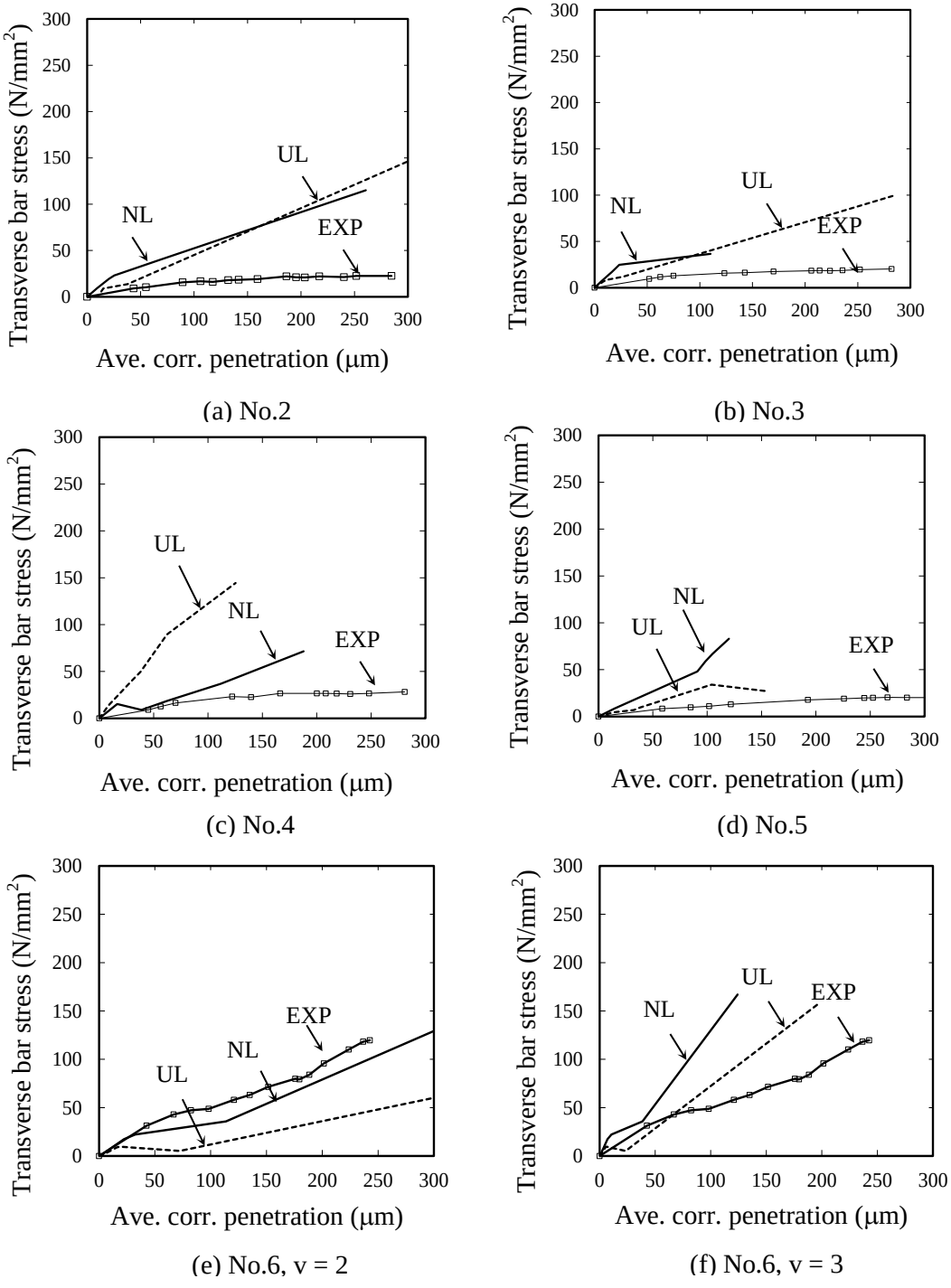

Fig. 2-22 Transverse bar stress at the middle of bottom leg (SC)

2.7 SUMMARY OF CHAPTER TWO

A series of accelerated corrosion test was conducted to investigate the cracking behavior of reinforced concrete structures due to corrosion products expansion. The experimental study was conducted to explore the influence of confinement from surrounding concrete i.e. concrete strength and transverse bar i.e. transverse bar ratio and configurations on cover crack behaviors i.e. crack initiation and crack propagation induced by corrosion product expansion. A numerical model through finite element analysis was also developed to simulate the crack behavior due to corrosion product expansion. In order to validate the numerical model, it was then compared with the experimental results. Based on both experimental and numerical analysis several conclusions can be drawn as follows:

a) Test data showed that corrosion rate is not uniformly distributed among longitudinal bars and over perimeter of longitudinal bars caused by the different of bar location in casting direction and in chloride diffusion direction and the different of water and oxygen availability.
b) The influence of concrete strength significantly governs the crack width growth due to corrosion product expansion. Meanwhile, the presence of confinement up to 0.3% of transverse bar ratio showed an insignificant effect on the crack width growth. This significant effect of concrete strength on crack propagation can be attributed to lower porosity of concrete which prevent corrosion product to penetrate to the surrounding concrete and generate larger expansion. Larger transverse bar stress was also generated in specimen with high strength concrete corresponding with larger crack opening. This transverse bar stress may reduce the residual shear capacity of RC structure, particularly when using normal strength of transverse bars e.g. σ_y = 295 N/mm^2.
c) Both experimental and analytical results indicated that crack initiates in concrete surface occur in small amount of corrosion penetration around 30 to 53 micrometers. The numerical model has a reasonable agreement with the experimental results. A larger volume increase ratio of corrosion product is required in the model when evaluating member with high strength concrete since the diffusion of corrosion products into concrete pores and cracks was not considered in the analysis.
d) The present study showed that the distribution of internal pressure among longitudinal bars or loading pattern, to simulate uneven corrosion distribution among longitudinal bars, influence the cracking pattern but it does not influence the crack width so much if the average corrosion rate is considered. The bond–slip relationship between transverse bars and concrete seems affect the stress development on the transverse bars.

Next chapter try to evaluate the effect of applied accelerated corrosion on bond behavior of reinforcement.

Chapter Three

BOND CHARACTERISTICS BETWEEN CORRODED STEEL AND CONCRETE THROUGH TENSION TEST

Chapter 3
BOND CHARACTERISTICS BETWEEN CORRODED STEEL AND CONCRETE THROUGH TENSION TEST

3.1 INTRODUCTION

Corrosion of reinforcement adversely influences the performance of structure in the form of cracking of concrete cover induced by expansion of corrosion product, decreasing of bond strength caused by changing in the concrete-steel interface, and reducing in the steel bar cross-section. The effect of corrosion on RC members as mentioned above also may lead to the stiffness degradation which may influence the structural performance concerning the serviceability.

Number of studies has been conducted to investigate the bond degradation of corroded RC members and its effect on the tension stiffening. For example, a tensile test was conducted by Amleh et al.[24] on corroded reinforcing bars with various corrosion levels. However, most of their specimens were experiencing severe corrosion, more than 4% of corrosion rate in mass, and having longitudinal cracks before the loading test. Nevertheless, a little attention is given on the bond behavior in low level corrosion. Although, there is not significant change on steel cross-section, but high expansion pressure and cover cracking are known began in early corrosion process of corroded RC members. Motivated by the need of comprehensive assessment at any level of corrosion, the experimental tensile test of corroded tension member were performed and evaluated in this chapter. The main purpose is to explore the bond characteristics of corroded RC tension members i.e. bond stress, bond stiffness, bond softening and to gain more knowledge on bond behavior of corroded steel bar especially in low level corrosion.

As mentioned above, basically, there are three important factors causing the degradation of structural performance of corroded RC members as follows (1) losses in mechanical performance of steel bar due to the reduction in cross-sectional area consumed during corrosion process; (2) losses in the effective area of concrete due to cover cracking or spalling induced by expansion of corrosion product; and (3) losses in bond performance between concrete and steel bar. In this chapter, the evaluation of effective area of concrete due to corrosion cracking in term of concrete tensile strength deterioration is discussed through the analysis of experimental results of tension members. Moreover,

the bond degradation of corroded reinforcement is investigated through evaluation of stiffness degradation of corroded RC members and cracking behavior.

3.2 TENSION TEST FOR THE EVALUATION OF BOND BEHAVIOR OF CORRODED STEEL BAR

3.2.1 Objectives

A series of tension test on corroded RC tensile members was performed with an emphasis to evaluate corrosion-induced bond degradation which is reflected in decreasing of the tension stiffness of corroded RC members. The crack behavior i.e. crack spacing of corroded RC members under uniaxial tensile loading was also investigated. The parametric study of experimental test was effect of various corrosion levels on bond behavior of corroded RC tensile members. In addition, the mechanical performance of cracked concrete due to corrosion was also evaluated through analysis of experimental results.

3.2.2 Details of specimens

Seven specimens of tension test were prepared and tested. As shown in Fig. 3-1, for each specimen, a deformed bar of 19 mm was installed in the center of a 125 mm diameter concrete cylinder. Strain gauges were attached along the bar at interval of 100 mm to measure steel strain distribution. This gauge interval seemed to be reasonable to study the bond behavior for common RC structural members and without considering the shape of bar such as rib geometry. For placing strain gauges in the steel bar, a machine groove cutting of 3 mm in width, 3 mm in depth, and 840 mm in length were made. This grooving was made to avoid damage in strain gauges during accelerated corrosion process and during concrete placing and to prevent the alteration on the actual bond behavior. Before and after grooving, the weight of steel bars was measured to estimate a reduction rate of sectional area by grooving. After attaching strain gauges on grooving, the grooving was filled by waterproofing material. At top and bottom of the specimens, a 50 mm of bond insulation was installed around steel bar to avoid cone damage.

The specified compressive concrete strength of 28 days was 48 N/mm^2 with concrete mix proportion presented in Table 3-1. The steel bars have the specified yield strength of 390 N/mm^2 (SD390) and the average yield strength and the modulus elasticity of reinforcing bar from tests were 435 N/mm^2 and 1.85×10^5 N/mm^2, respectively.

Table 3-1 Concrete Mixing (unit: kg/m^3)

w/c	Water	Cement	Fine Aggregate	Coarse Aggregate	Air entraining and water reducing
0.50	175	350	780	968	0.80%

3.2.3 Accelerated corrosion and loading method

An accelerated corrosion using the electrochemical process was performed after curing for 4 weeks. During electrochemical process specimens were placed in the tank filled with 3% NaCl solution. The electrochemical set up was arranged so that the steel bar acted as anode and the copperplate acted as cathode (Fig. 3-2). Furthermore, a constant of 200mA current was applied and monitored using data logger. A load-controlled tensile test was performed using an Amsler UTM with capacity of 2000kN (Fig. 3-3). The applied load and the displacement were recorded.

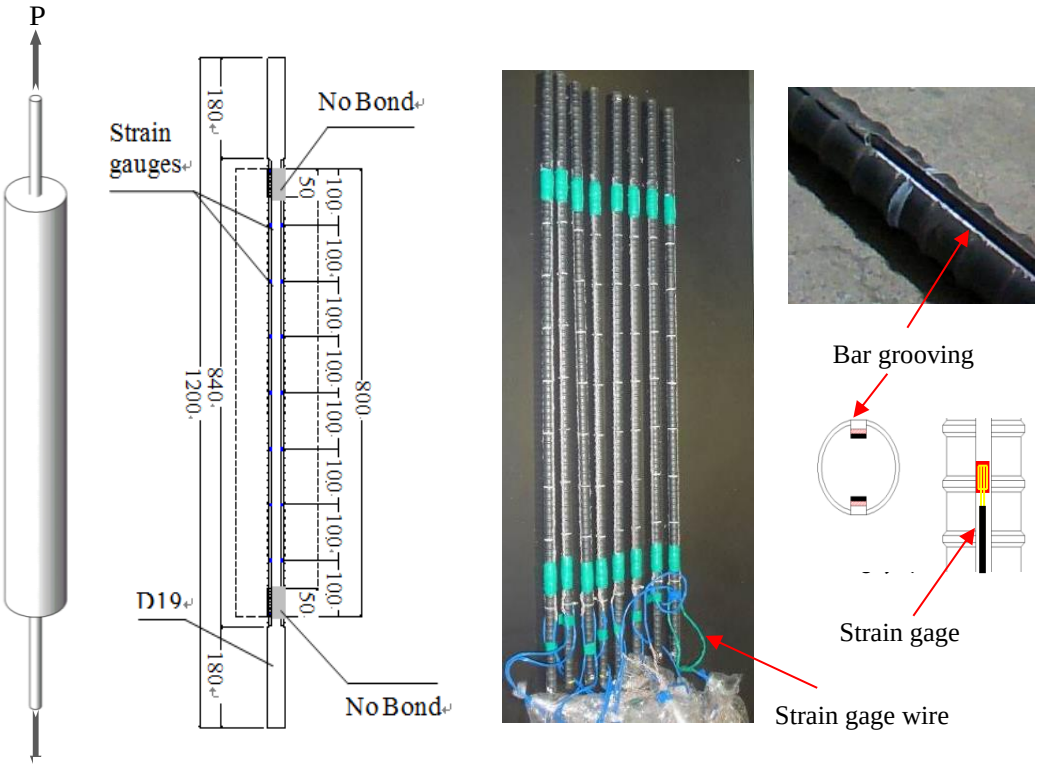

(a) (b) (c)

Fig. 3-1 (a) Typical specimens (b) Strain gauges location (c) bar grooving

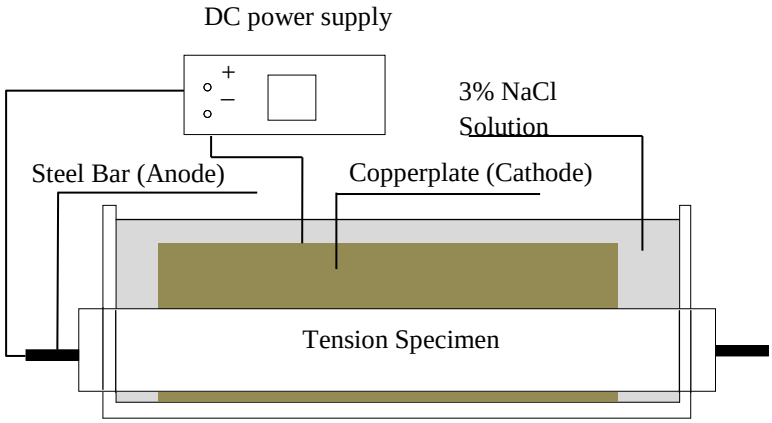

Fig. 3-2 Overview of Electrochemical Corrosion Setup

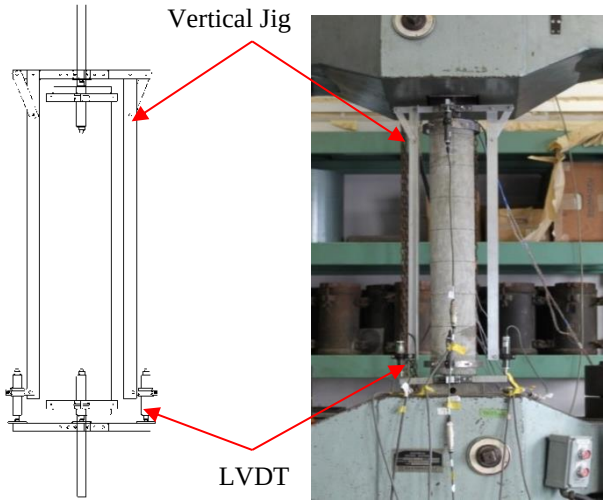

Fig. 3-3 Loading test setup and vertical jig

3.3 EXPERIMENTAL RESULTS

3.3.1 Measured corrosion loss

To measure the corrosion loss, a corrosion section of 700mm was taken out to measure the corrosion level by a weight measurement. The corrosion level was measured as weight loss of steel bar divided by the original weight. The corrosion level was also estimated using Faraday's law of electrolysis from the electric current measurement. The corrosion target was set to have 0 - 7%. The cover crack may initiate in only small corrosion level, however, for architectural buildings such as houses and apartment, the small crack appears on the surface of structural element may become an aesthetic and safety problem for the owner or the occupants. From Table 3-2, the corrosion efficiency by the electrolytic corrosion considerably varies from 30% to 60% from the weight measurement, except for specimen No.2. This phenomenon has also been reported by Auyeung et al.[25]. Based on the measured corrosion loss, specimens can be classified into seven corrosion levels as shown in Table 3-2.

Table 3-2 Corrosion level in weight loss in g (number in parenthesis in percentage)

Specimens	Estimated by Faraday's law (g)	Determined by weight measurement (g)
No.1	-	-
No.2	9.54 (0.72)	9.60 (0.72)
No.3	30.18 (2.26)	11.70 (0.88)
No.4	39.74 (2.97)	14.00 (1.05)
No.5	50.36 (3.77)	14.90 (1.12)
No.6	73.37 (5.49)	36.30 (2.27)
No.7	90.94 (6.78)	52.90 (3.95)

3.3.2 Crack pattern and steel strain distribution

The specimen's crack pattern and steel strain distribution are presented in Fig. 3-4. The number inside the circle indicates the order of crack occurrence due to tensile loading. Amount of transverse cracks from specimen No.1 to specimen No.7 tend to increase with an increase of corrosion level unlike Amleh's test [24]. A longitudinal crack due to corrosion product expansion only appeared at specimens No.6 and No.7 as shown in Fig. 3-5. As a result, the transverse crack generated from tensile force can easily develop at specimen No.6 and No.7 from the corrosion crack and the apparent tensile strength can be reduced. From Fig. 3-4, it obviously shown that the strain/stress of the steel bar varies along the bar. Clearly, when crack was formed in the specimen, the steel strain/stress at crack location becomes larger. This means that the steel carried most of the applied load. However, because more than a half of attached strain gauges were damage for specimen No.1 and No.6, the strain distribution cannot be presented in Fig. 3-4.

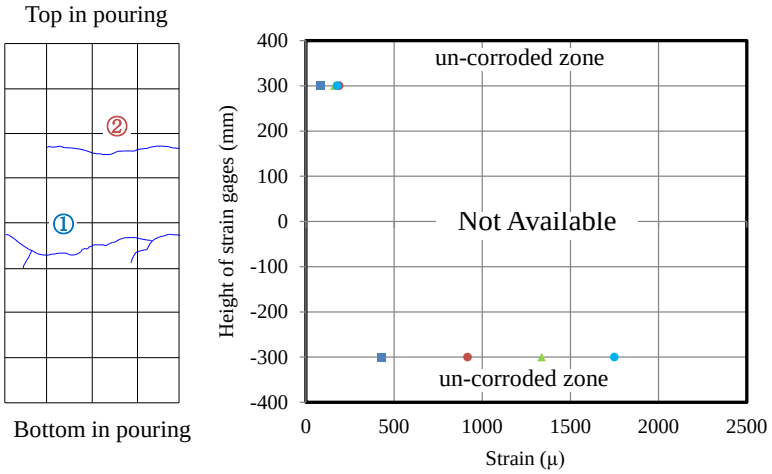

(a) No.1 (Corrosion = 0 %)

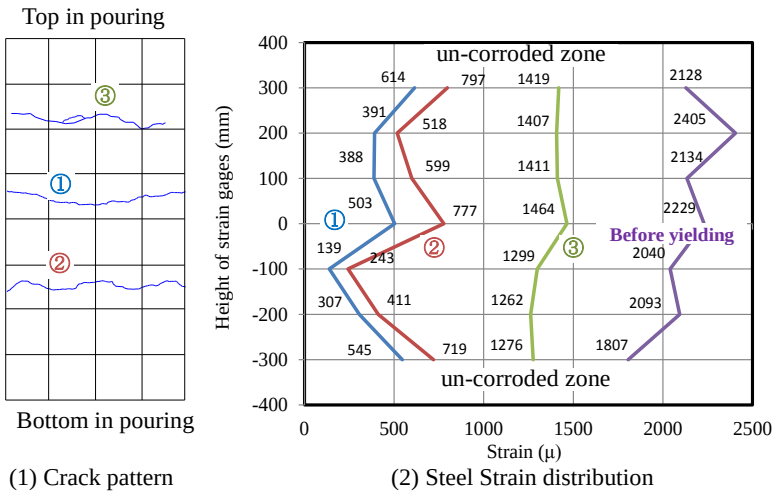

(b) No.2 (Corrosion = 0.72 %)

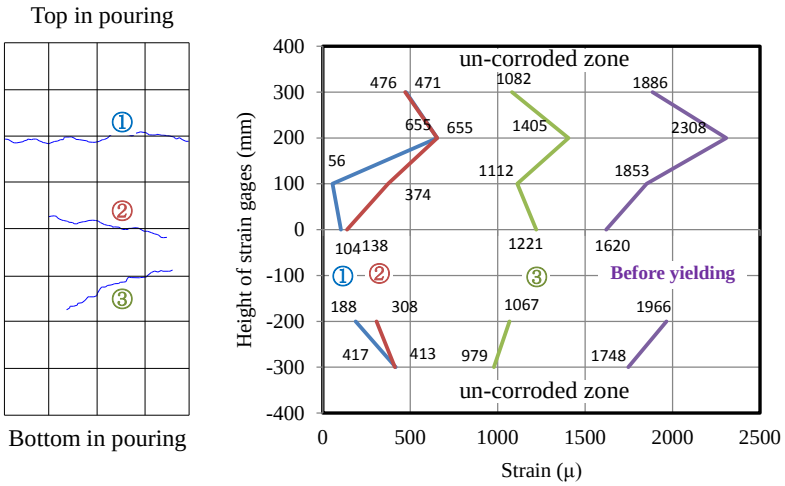

(1) Crack pattern (2) Steel Strain distribution

(c) No.3 (Corrosion = 0.88 %)

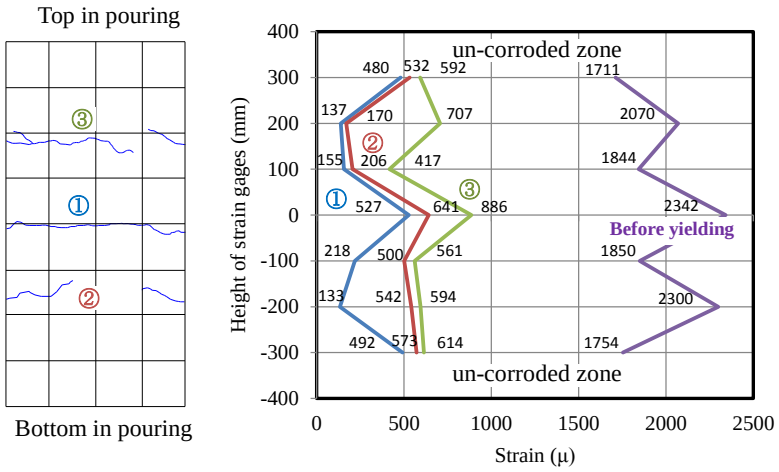

(1) Crack pattern (2) Steel Strain distribution

(d) No.4 (Corrosion = 1.05 %)

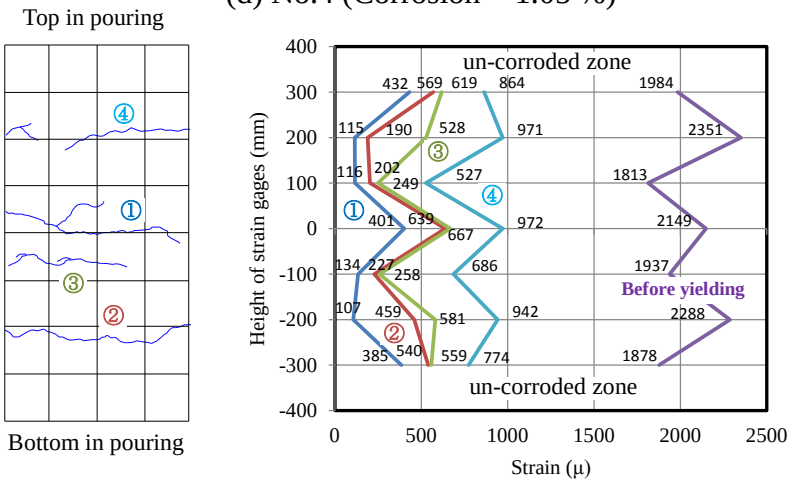

(1) Crack pattern (2) Steel Strain distribution

(e) No.5 (Corrosion = 1.12 %)

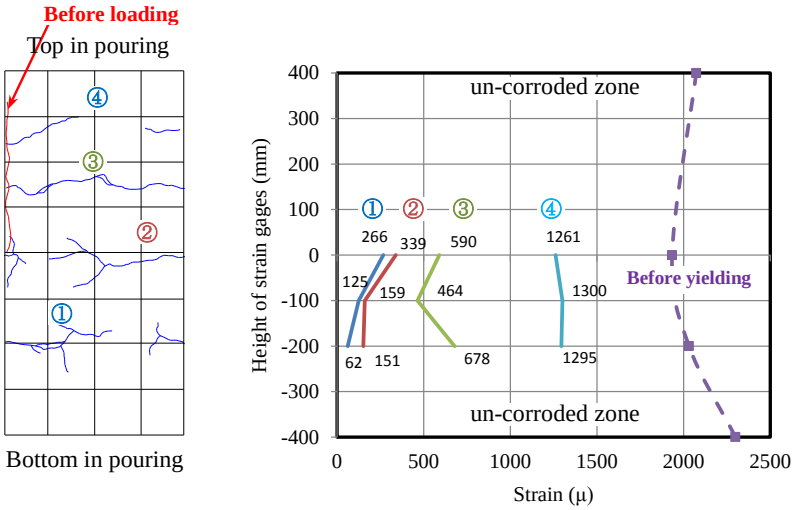

(1) Crack pattern (2) Steel Strain distribution

(f) No.6 (Corrosion = 2.27 %)

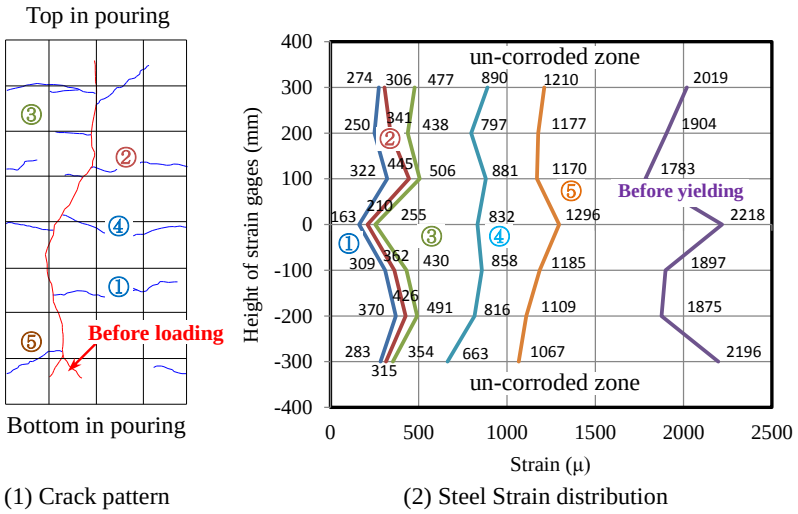

(1) Crack pattern (2) Steel Strain distribution

(g) No.7 (Corrosion = 3.95 %)

Fig. 3-4 Specimen's Crack Pattern and Steel Strain Distribution

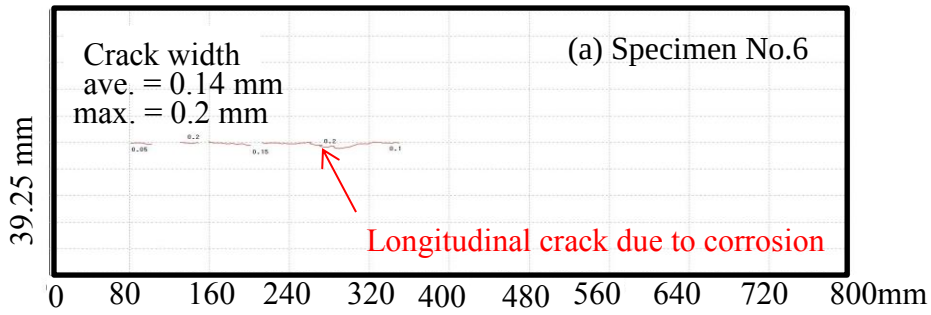

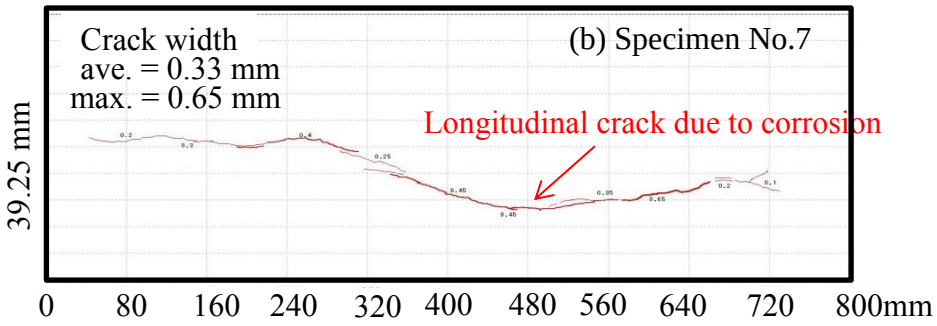

Fig. 3-5 Longitudinal crack pattern due to corrosion

In a typical RC tension member described in Fig. 3-6, at main crack, all loads are carried entirely by steel bar $\sigma_s=P/A_s$. Between adjacent cracks, a portion of tensile force was transmitted to the surrounding concrete by bond over the transmission length L_t causing stress distribution along the steel bar. The local bond stress along bar between two adjacent cracks is defined as steel stress variation at certain length Δx. The relationship between local bond stress and steel stress variation at certain length can be expressed as follows:

$$\tau_b = \frac{(\sigma_{s1}-\sigma_{s2})A_s}{\Delta x \phi_s} = \frac{(\sigma_{s1}-\sigma_{s2})}{\Delta x}\frac{d}{4} \tag{3-1}$$

where τ_b is local bond stress over the length Δx; σ_{s1} and σ_{s2} are steel stress between Δx, A_s is effective area of steel bar, ϕ_s is bar perimeter, d is bar diameter and Δx is specified length along the bar or in this study is interval length of strain gauges.

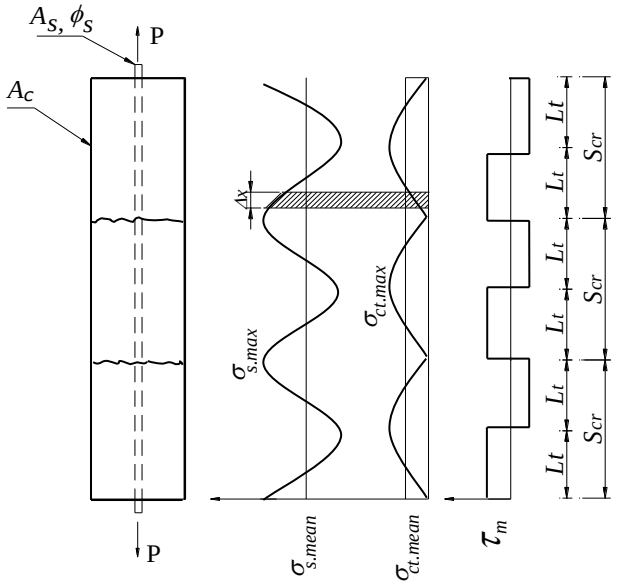

Fig. 3-6 Stress Distribution on RC Tension Member

The tension force carried by concrete along the transmission length, F_τ, can be described by

$$F_\tau = \tau_m \phi_s L_t \tag{3-2}$$

where τ_m is average bond stress over the transmission length L_t. The maximum tensile strength of concrete to provoke cracking is given by

$$F_c = f_{ct} A_c \tag{3-3}$$

where f_{ct} is mean value of concrete tensile strength when crack appeared in concrete and A_c is effective area of concrete. A transverse crack occurs on member when $F_\tau = F_c$. Therefore, from Eq. (3-2) and (3-3), the transmission length, L_t can be derived by

$$L_t = \frac{f_{ct} A_c}{\tau_m \phi_s} \tag{3-4}$$

From Eq. (3-4), the transmission length L_t will decrease if bond stress τ_m increases or concrete tensile strength f_{ct} decreases. Using Eq. (3-1) and the steel strain distribution as shown in Fig. 3-4, the local bond stresses are obtained for each gauge interval and only the absolute value of the local bond stress are compared to obtain the maximum bond stress for each specimen. Then, from Eq. (3-4) the average concrete tensile strength f_{ct} is assumed to be estimated using the maximum local bond stress and the corresponding of half crack spacing obtained in the tests. The results are summarized in Table 3-3.

Table 3-3 Maximum Local Bond Stress and Concrete Tensile Strength

Specimens	Corrosion rate (%)	Maximum local bond Stress (N/mm^2)	Concrete tensile strength, f_{ct} (N/mm^2)
No.1	0	N/A*	2.30**
No.2	0.72	4.15	2.04
No.3	0.88	4.65	2.33
No.4	1.05	3.64	1.73
No.5	1.12	3.44	1.72
No.6	2.72	N/A*	N/A*
No.7	3.95	1.89	1.34

Note:

* Specimen No.1 and No.6 is not available (N/A) caused by the damage of attached strain gauges

** Estimated based on AIJ code [26]

From Table 3-3, it is shown that for corrosion level up to 1 %, with increasing corrosion level, the local bond stress increased. One of the possible reasons for increasing bond stress is that corrosion product filled the interface between concrete and steel bar and then increased the mechanical properties of interface. The increase of bond strength has also been reported by Al-Musallam et al. [27], Al-Sulaimani et al. [28] and Auyeung et al.[25] from their experimentally pullout test on embedded corroded bar approximately up to 1 % of corrosion level. The change of roughness in steel interface due to corrosion leading to the increasing of mechanical interlocking or friction was also mentioned as mainly cause of increasing of bond strength. From Table 3-3, the local bond stress and average concrete tensile strength gradually decreased for larger corrosion level above 1%. The decrease in local bond stress and tensile strength can be mainly due to increasing local cracking around bar surface and widening of initial longitudinal crack caused by corrosion expansion product.

The average concrete tensile strength was plotted against corrosion rate and normalized to the average concrete tensile strength of healthy specimen, No.1, as shown in Fig. 3-7. The behavior of corroded RC member which relationship between corrosion rate and average concrete tensile strength representing the reduction of concrete confinement due to cover cracking. For simplicity, a bilinear relationship between the reduction factor of average concrete tensile strength and corrosion level based on the calculation aforementioned. A relative constant of reduction factor of effective concrete area due corrosion beyond 3% of corrosion loss was reported by Dai et al.[29].

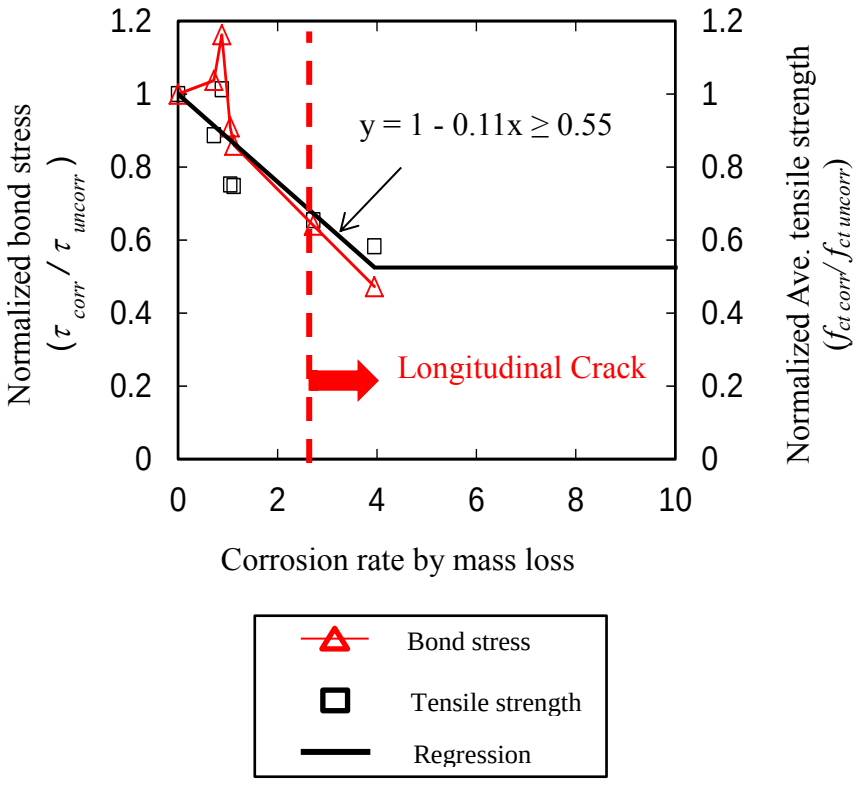

Fig. 3-7 Average concrete tensile strength correspond with corrosion rate

3.3.3 Crack spacing

Fig. 3-8 presents the relationship between average transverse crack spacing and corrosion rate of the present and the Amleh's work. A different trend between present work and Amleh et al.[24] is identified. In Amleh's work the average crack spacing increase with increase corrosion rate due to lower bond stress. In the present work for low corrosion without corrosion crack, average crack spacing tended to decrease due to high bond stress. Meanwhile, for larger corrosion with cover crack decreases average crack spacing because low bond stress and decrease in tensile strength. This result agreed with the analysis results as described in Fig. 3-7 and equation 3-8.

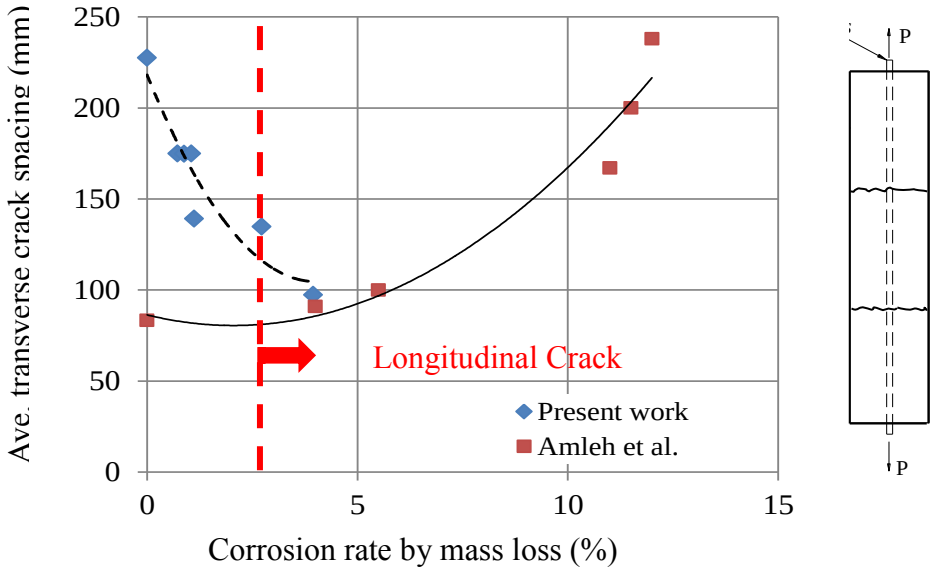

Fig. 3-8 Average transverse crack spacing

3.3.4 Tension stiffening

Because concrete shares some tensile force, the specimen's tensile load generates a larger value than the bare bar until yielding of the steel bar, which is called the tension stiffening. Fig. 3-9 shows the load-strain relationship of specimens No.1 to No.7 compared with the bare bar. The actual global elongation was measured over the length of 840 mm. However, in Fig. 3-9, the average strain was determined from the effective bond length of 700 mm. It is obtained from the actual global elongation reduced by the total elongation of 140 mm of un-corroded zone or the bare bar at both ends of specimens.

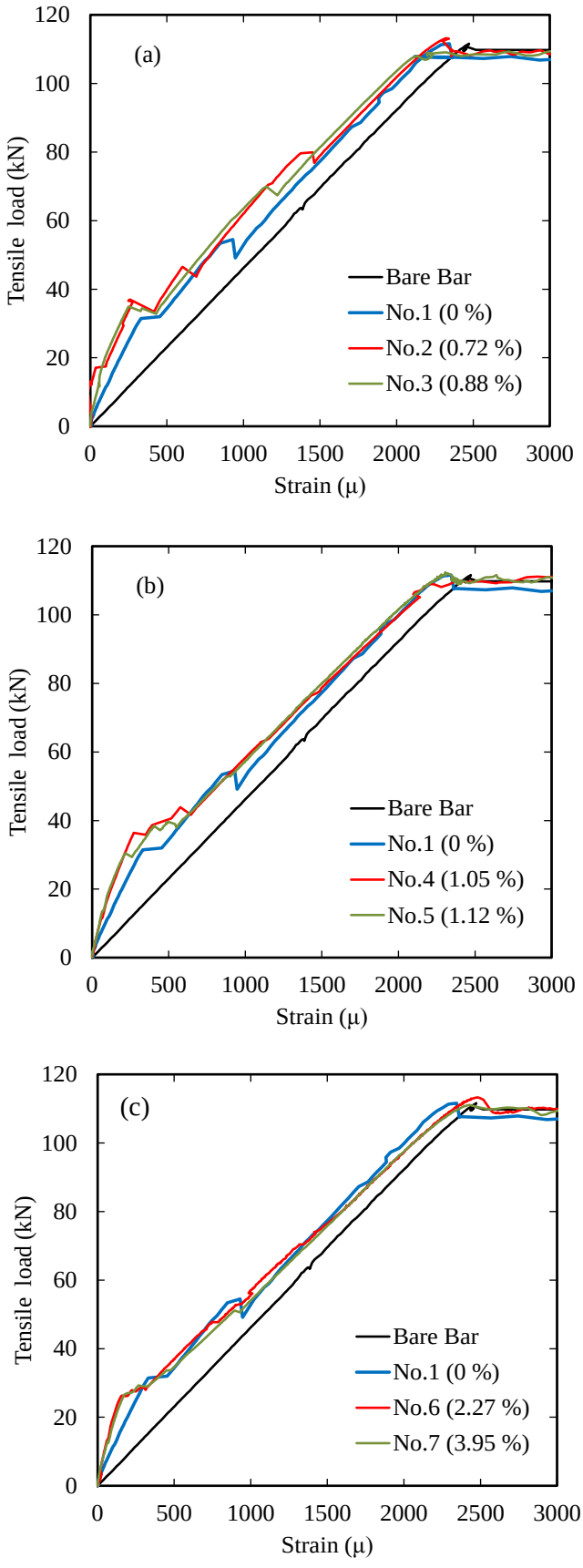

Fig. 3-9 Tensile load vs. average strain

If specimens No.2 and No.3 are compared with the healthy specimen of No.1, it slightly produced higher tension stiffening as shown in Fig. 3-9(a). For specimens No.4 and No.5, almost the same tension stiffening was produced as specimen No.1 (Fig. 3-9(b)). This indicates that there is no significant influence of corrosion in very low level before cover cracking occurred. However, as shown in Fig. 3-9(c) for specimens No.6 and No.7 where the longitudinal corrosion crack appeared before loading test, they generated slightly lower tension stiffening than specimen No.1. This indicates that corrosion influences tensile force transmission from steel bar to concrete through bond mechanism, and that longitudinal crack results in bond deterioration. Moreover, an increase in crack number for specimens No.6 and No.7 also indicated a decrease in concrete tensile strength that should be considered in analysis. The yielding load of tension specimen has only small different compared to yielding load of bare bar. This shows that the applied corrosion level is not significantly influence the yield strength of RC members.

3.4 EVALUATION OF CORROSION-INDUCED TENSION STIFFENING DETERIORATION TROUGH FINITE ELEMENT ANALYISIS

3.4.1 Objectives

A non-linear finite element analysis was performed to simulate the tension stiffening behavior of corroded RC tensile members. The purposes are to reproduce cracking behavior under tensile loading and to clarify the effect corrosion that influences bond-slip relationship and tension stiffening behavior.

3.4.2 Finite element model

An axisymmetric 8-node element for concrete was used in FE analysis as shown in Fig. 3-10(a). The concrete was modeled using constitutive model based on non-linear fracture mechanics using smeared crack model. For concrete in tension, concrete behaves elastically up to the tensile strength and followed by tension softening as described in Fig. 3-10(b)-(c). The bilinear tension softening model was employed to the model [20]. The concrete tensile strength f_t was obtained from experimental analysis based on average concrete strength as shown in Table 3-3, except for specimen No. 1 and specimen No.6 determined based on AIJ code [26] and data interpolation, respectively. In addition, due to unavailable data from the experiment caused by gauges damage, the maximum local bond stress of both specimens was also obtained from the interpolation of available data. The values are 4.0 N/mm^2 and 2.56 N/mm^2, respectively. Because concrete behavior in this analysis is dominated by tensile cracking at low level of compressive stress, the concrete in the compressive zone can be assumed to behave in an elastic manner.

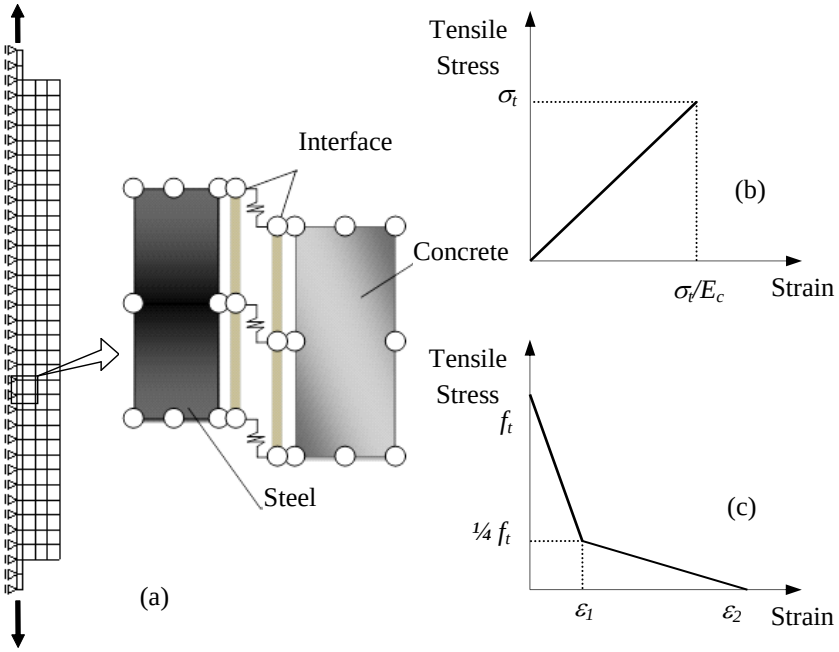

Fig. 3-10 Finite Element Model: (a) Typical Meshing and Element Model (b) & (c) Concrete Stress-strain in Tension

The axisymmetric model was also applied to specimen No.6 and No.7 having a longitudinal crack on modeling of tension members in order to obtain a general tendency on bond-slip relations due to corroded bars. Therefore, the maximum local bond stress and concrete tensile strength estimated from the test results were used in this analysis.

The steel bar was also modeled as an axisymmetric 8-node element. The linear elastic to yield point without hardening was assumed using Von Misses criterion. The effective diameter of steel bar should be adjusted due to corrosion and grooving loss. For convenience in modeling, to consider reduction of cross sectional area of steel bar, the modified modulus elasticity and yield strength of steel bar was employed to keep the steel bar cross-section remains constant in model. It was also assumed that the steel bar experiences uniform corrosion, so that only a uniform corrosion and material strength are considered in this analysis in order to discuss a general tendency on bond behaviors. Therefore, the properties of corroded steel bar is described as follows:

$$E_2 = \frac{A_2}{A_1} E_1 \tag{3-5}$$

$$f_{y2} = \frac{A_2}{A_1} f_{y1} \tag{3-6}$$

where E_1, f_{y1}, A_1 and E_2, f_{y2}, A_2 are elastic modulus, yield strength, and cross-sectional area of un-corroded and corroded steel bar, respectively. Because a small of corrosion

level as mentioned in section 3.3.1 the post yield effect of change rate of cross sectional area is neglected.

It was a common way to describe the interaction between steel and concrete by considering the relation between bond stress and slip, which is defined as relative displacement between steel bar and concrete. The concept was adopted in this analysis to describe the interaction between steel and concrete through the interface element. 6-node interface element was used for steel-concrete interface element. The parameter of interface element is given by bond-slip relationship model. Since, corrosion of steel bar influences the mechanical behavior of interface between concrete and steel, therefore it will influence the bond-slip relationship.

Bi-linear and tri-linear bond-slip models were applied to evaluate the sensitivity of input parameter of bond-slip relationship on modeling corroded RC tension members. In the bond-slip relationship models, there are many parameters that need to be considered such as maximum bond stress τ_{max}, bond stiffness K, and bond softening. In this case, the maximum bond stress τ_{max} was obtained from analysis of experimental results as discussed in Chapter 3.3. The influence of bond stiffness K and bond softening was evaluated and simulated trough three bond-slip models described hereafter.

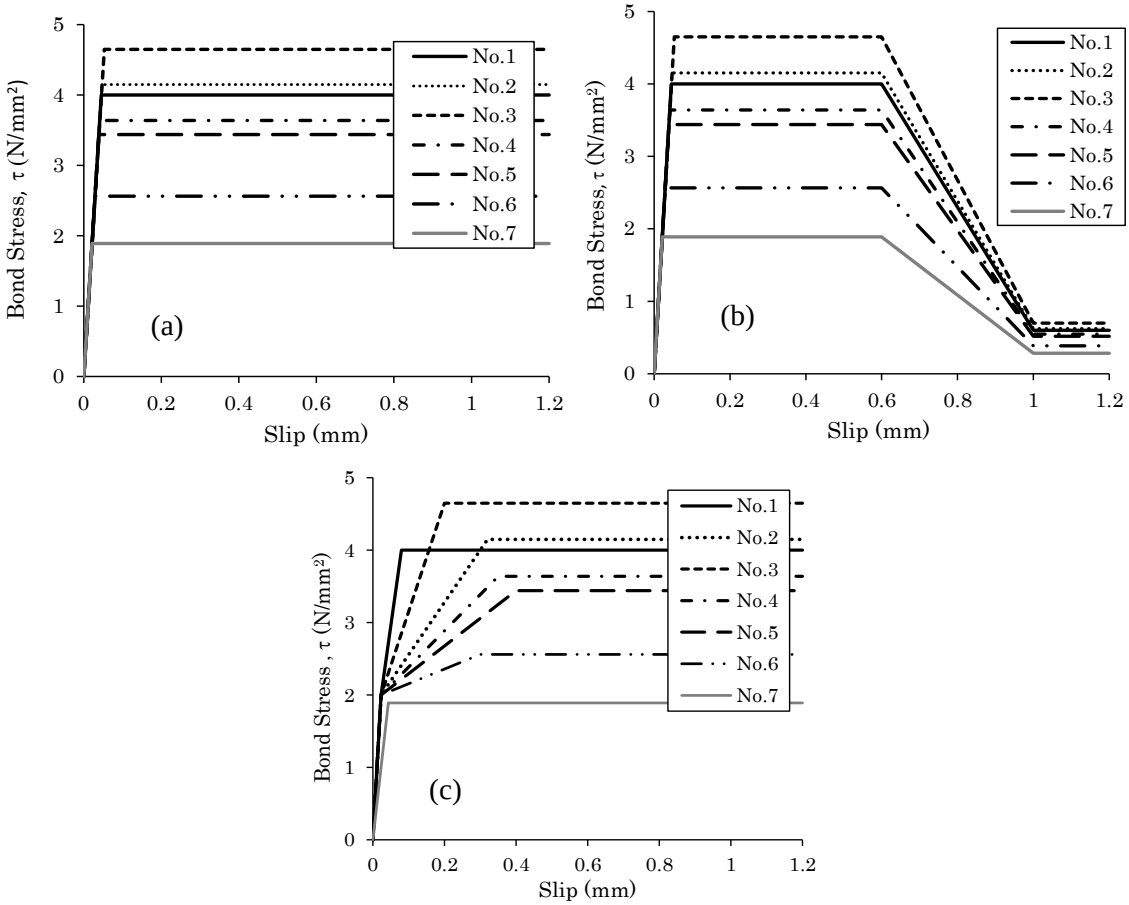

Fig. 3-11 Bond-slip Models: (a) Bi-linear (b) Bi-linear with Bond Softening (c) Tri-linear

A linear bond-slip model, until reaching maximum bond stress was proposed for Model 1 as shown in Fig. 3-11(a). When slip is greater than $S_1 = \tau_{max}/K_1$, the bond stress remains constant. Therefore, the slip at maximum bond stress greatly depends on assumed bond stiffness. The bond stiffness K_1 = 88.0 N/mm^3 was used in this case which is confirmed from the experimental test by Hayashi et al.[30] and from FE analysis by Shinohara [22] . In Model 1 for both un-corroded (healthy) and corroded specimen, the initial bond stiffness K_1 was assumed to be similar or without bond stiffness degradation. The corrosion-induced bond deterioration was only covered by decreasing maximum bond stress as shown in Table 3-3.

Model 2 was defined as a linear ascending curve up to τ_{max} and followed by plateau and descending curves (bond softening) as shown in Fig. 3-11(b). The bond softening was reported by Eligehausen et al. [31] and Harajli et al. [32] from the experimental tests and adopted in CEB-FIP model code [8]. The plateau curve is limited by the descending curve at S_2 or slip at end of plateau. The descending curve is linearly decreasing to the value $\tau = 0.15\tau_{max}$, which is known as minimum bond stress resistance that can be provided by friction until reaching S_3, slip at end of descending curve. In this case, S_2 = 0.6 mm and S_3 = 1.0 mm were used for all specimens adopted from CEB-FIP model code [8].

A bi-linear ascending curve was introduced in Model 3 as shown in Fig. 3-11(c) so that there are two bond stiffness values that need to be determined. A similar bond stiffness as used for Model 1 and Model 2 was selected for the first bond stiffness K_1. The first maximum bond stress τ_a = 2 N/mm^2 was determined for the first linear curve which is noted as maximum adhesion and friction resistance [33] . The second bond stiffness K_2 was adjusted so that the tension stiffening curve from FE analysis closely coincides with the experimentally tension stiffening curve. The second linear curve is limited by maximum bond stress τ_{max}. However, because the maximum local bond stress of specimen No.7 is less than τ_a = 2 N/mm^2, for specimen No.7 a bi-linear bond-slip model with lower bond stiffness of K = 44.0 N/mm^3 was used in Model 3. The summary of bond stiffness used for Model 3 is provided in Table 3-4.

Table 3-4 Bond Stiffness of Model 3 (N/mm^3)

Bond Stiffness	No.1	No.2	No.3	No.4	No.5	No.6	No.7
K_1	88						44
K_2	35	10	15	5	4	2	

3.4.3 Comparison of tension stiffening

Fig. 3-12 shows the tension stiffening for each specimen from FE analysis using three bond-slip models compared with the experimental results. For healthy specimen (No.1), all applied bond-slip models show a good agreement on overall tension stiffening behavior between experimental and analytical results as shown in Fig. 3-12(a).

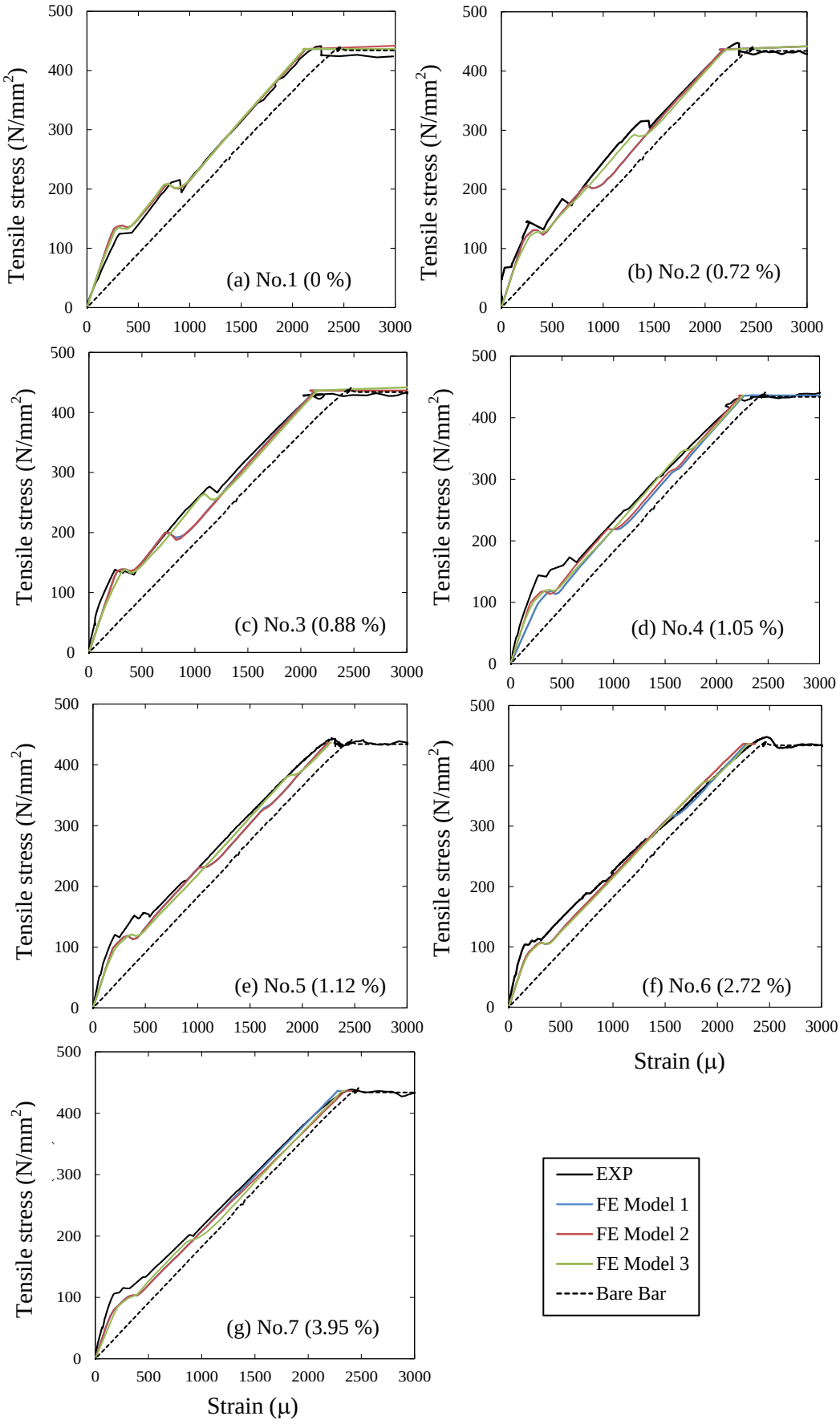

Fig. 3-12 Comparison of Tension Stiffening: Experiment and Analysis

Generally, all bond-slip models also provide reasonable results on predicting the first and second cracking load compared with experimental results. This indicates a proper input parameter of concrete tensile strength and maximum bond stress was made for healthy specimen.

Model 1, a bi-linear bond slip model without bond softening, produced a slightly underestimated tension stiffening for specimens No.2 to No.5 in compared with the experimental results particularly after the first crack until stabilized cracking as shown in Fig. 3-12(b)-(e). This is probably due to higher bond stiffness that generates different transverse crack patterns as mentioned later.

Model 2, a bi-linear bond-slip model with bond softening, closely exhibited similar results with Model 1. The bond softening gave insignificant effect on tension stiffening behavior in this case because the yielding of steel bar was reached for very small slip value approximately less than 0.3 mm, whereas the assumed bond softening in Model 2 is started at slip S_2=0.6 mm as shown in Fig. 3-11(b).

Model 3 using a tri-linear curve clearly produces a good agreement of tension stiffening curve between experimental and analytical results compared with Model 1 and Model 2 for all specimens, except for specimen No.7 where it exhibited slightly underestimated result.

If the stress-strain curves obtained from Models 1 and 2 is compared with Model 3 which has different bond stiffness, clearly, bond stiffness gives a significant contribution on predicting overall tension stiffening behavior. Bond stiffness influences the tension stiffening particularly on crack development or crack formation. The lower bond stiffness also can delay the crack occurrence as shown in Fig. 3-12. Moreover, as presented in Table 3-4, bond stiffness tends to decrease with an increase of corrosion levels. The tri-linear bond-slip model provides a good result on predicting tension behavior of corroded tension members.

3.4.4 Comparison of cracking behavior

Fig. 3-13 shows the crack patterns obtained from FE analysis at the same global elongation (2.7mm) and after steel bar reach its yield stress. The dark color in element mesh indicates crack location or higher crack strain level. The tensile force acted at both ends of specimen was transferred to the concrete over the surface of steel bar by bond until reaching its concrete tensile strength or crack occurred. Because the model is symmetric and uniform material was assumed, a transverse crack developed symmetrically and simultaneously at both sides of specimen i.e. top and bottom. The crack location and crack number will be greatly depending on the transfer length L_t and the available space/distance to develop a new crack.

As shown in Fig. 3-13, Model 1 and Model 2 exhibited a similar crack patterns for all specimens because both models have similar tension stiffening behavior due to similar maximum bond stress and bond stiffness. The applied bond softening in Model 2 also gave insignificant effect on the crack formation as well as on the tension stiffening.

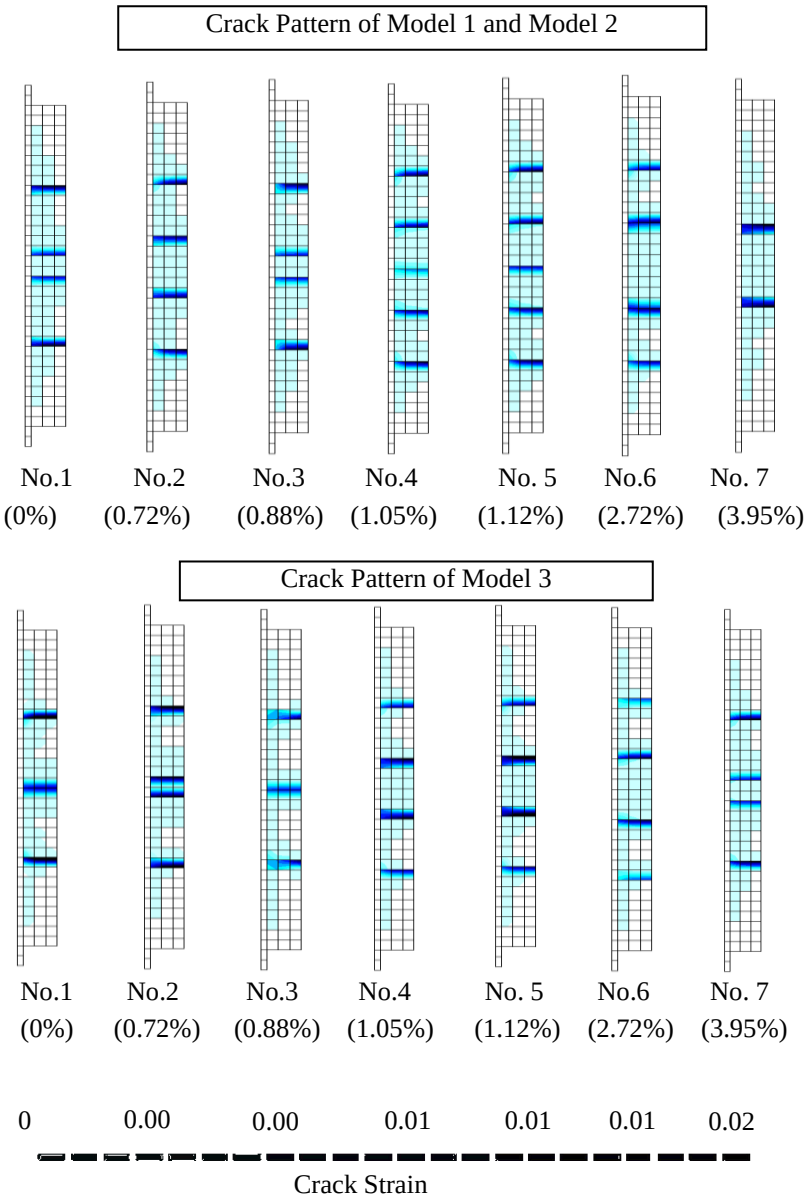

Fig. 3-13 Crack formations: Analysis Results

An increase of crack number is shown for Model 1 and Model 2 for corrosion level up to 1.12% (specimen No.5), and then is followed by decreasing of crack number for higher corrosion level. A different crack pattern is obtained using Model 3 which has different bond stiffness. For Model 3, the trend of crack number increased up to 4% of corrosion level. If the crack number and the crack formation are compared with the experimental results, Model 3 has a close prediction rather than Model 1 and Model 2.

In Fig. 3-13 two cracks appeared simultaneously and symmetrically around center of specimen No.7 for Model 3 and two more cracks formed with further loading. On the other hand, for Model 1 and Model 2, two cracks appear at a distance from the center and no more cracks appeared for further loading. The reason was that the space between two cracks or between the first two cracks and no bond zone is less than twice of transmission length therefore no more cracks will be generated. In detail for specimen No.7, if average concrete strength and bond stress from Table 3 are 1.34 and 1.89 N/mm^2, respectively, and effective concrete area A_c is 11 988 mm^2, by using Eq.(3-4) the transmission length L_t is 141 mm. Therefore, twice of transmission length or 282 mm is required to develop a new crack. As shown in Fig. 3-13 for Model 1 and 2 the available space between first crack and no bond region is only 250 mm, therefore a new crack cannot be developed.

In summary, concrete tensile strength, maximum bond stress and bond stiffness together provide substantial influence on predicting crack formation of corroded tension members. From FE analysis, it is shown that a good agreement crack number with the experiment may be obtained by considering both bond and tensile strength deteriorations. This analysis mostly could capture the general tendency of corroded RC member on tension stiffening behavior and crack formation. However, to produce an exactly similar crack pattern and the order of crack occurrence with experimental results, further study is required due to the sensitivity to concrete properties and corrosion level.

3.5 SUMMARY OF CHAPTER THREE

A series of tension test on corroded RC tensile members was performed to evaluate corrosion-induced bond degradation reflected in the tension stiffness deterioration of corroded RC members. The effect of various corrosion levels was investigated. The cracking behavior i.e. crack spacing of corroded RC members under uniaxial tensile loading was also investigated. Moreover, the mechanical performance of cracked concrete due to corrosion was also evaluated through analysis of experimental results. In addition, a non-linear finite element analysis was performed to simulate the tension stiffening behavior of corroded RC tensile members and to reproduce the cracking behavior under tensile loading.

The following conclusions can be drawn according to experimental and analytical results that were discussed in this chapter.

a) From the experimental test, the average crack spacing decreased with increasing of corrosion level up to 4% of corrosion level. This was mainly due to the increasing of bond stress for small corrosion level up to 1% and to the decreasing of concrete tensile strength induced by cracks around corroded bar for higher corrosion levels.

b) According to analysis of experimental results, the relation between the reduction factor of average concrete tensile strength and corrosion level was established.
c) From the numerical analysis, the maximum bond stress and bond stiffness are important parameters of bond-slip relationship model on predicting overall tension stiffening and crack behavior. The applied lower bond stiffness can delay the crack occurrence or increase the cracking load level particularly for the second cracking. The bond stiffness also generally decreased with increasing corrosion levels. However, bond softening showed an insignificant effect in the case where small slip occurred before steel bar reached its yield strength.
d) Compared to bi-linear bond-slip model, the tri-linear bond-slip relationship provided a good agreement with the experimental results on predicting tension stiffening and cracking behavior, because it provided a higher initial bond stiffness and a lower second bond stiffness for further loading due to growth of cracking. The second bond stiffness also decreased with increasing corrosion levels because of the soft layer of corrosion products.

In the next chapter the bond strength of corroded reinforcement under different confinement level i.e. different concrete strength and transverse bar ratio would be evaluated through experimentally pullout test. The bond-slip relationship between corroded bar and concrete would be also discussed.

Chapter Four

BOND SPLITTING BEHAVIOR OF CORRODED RC MEMBER THROUGH PULLOUT TEST

Chapter 4
BOND SPLITTING BEHAVIOR OF CORRODED RC MEMBER THROUGH PULLOUT TEST

4.1 INTRODUCTION

This chapter focuses on the evaluation of bond splitting behavior of corroded RC members through pullout test. A significant number of experimental studies devoted to evaluate the effect of corrosion of steel bar in concrete with various types of testing method. In spite of large scatter of test results, the test shows different trends of bond strength with an increasing of corrosion level. A slight increase of bond strength for corrosion levels at pre-cracking stage is followed by a decrease of bond strength because of splitting crack of cover at post-cracking stage [22, 25, 27]. A significant reduction of bond strength up to 70% has been observed for corroded of reinforcement without transverse bars as reported by Auyeung et al. [25] , Al-sulaimani et al.[28], and Mangat et al.[34]. Meanwhile, insignificant bond strength deterioration were observed around 20-30% reduction when the transverse bars have been introduced [28 13 35]. However, most of studies give a comparison between the presence and the absence of transverse bars and a little attention has been given for different of confinement levels. Therefore, in the present experiment, one of the main parameters is the different of confinement levels with various bars ratio and configurations.

In addition, in natural environment, not only longitudinal bars may experience corrosion, but also it may occur on transverse reinforcement. Corrosion of transverse bars may weaken the confinement of longitudinal bars caused by (1) reducing in transverse bars area, (2) provoking extensive cover cracking [36] and (3) diminishing of adhesion or interface friction between transverse bars and surrounding concrete. The combined effect of corrosion on longitudinal reinforcement and transverse bars has been investigated in a few studies [36]. In this study the effect of transverse bars is evaluated using non-corroded transverse bars insulated by vinyl taping. To simulate the reduction in transverse bars area, a small transverse bar ratio and with different of spacing and bar arrangements were taken into consideration of specimen parameters. The use of non-corroded transverse bars is intended to maintain the transverse bars area while corrosion of longitudinal bar is occurred. The used of vinyl taping on transverse bars may also simulate the reduction in adhesion and friction of interface between corroded transverse bars and concrete.

4.2 PULLOT TEST FOR EVALUATION OF BOND SPLITTING BEHAVIOR OF CORRODED RC MEMBERS

4.2.1 Objectives

Pullout tests using beam type were carried out to evaluate the bond behavior of corroded reinforcements. The effect of confinement condition by means of transverse bars with different ratios and configurations and the influence of bar position on beams i.e. corner and middle bars and bar position to casting direction i.e. top or bottom in casting were evaluated in this study to investigate the bond splitting capacity, the mode of failure and the bond stress-slip relationships between corroded steel bar and concrete. As the experimental database, the test results may help in establishing the bond deterioration model of corroded reinforcement with different confinement levels as well as in formulation of bond-slip model of corroded reinforcement in order to assess the structural performance of corroded RC members.

4.2.2 Specimens and materials

Six 220x400 mm rectangular beams were produced. Each beam had two test regions, the corroded and the healthy regions (as reference) having a similar bar arrangement. Therefore, a total of twelve specimens were tested. The specimen variables are summarized in Table 4-1. In this study only longitudinal bars located at bottom side of beams were subjected to corrosion which had 400 mm of embedment length as shown in Fig. 4-1. On the right and the left side of embedment length, the longitudinal bars were insulated using vinyl tape as non-corroded and un-bonded regions. The transverse bars were also covered by vinyl tape to protect transverse bar gages during concrete placing and accelerated corrosion process as shown in Fig. 4-2.

Two concrete strengths of 24 and 48 N/mm^2 were used representing normal and high strength concrete. The preheated high strength of steel bar was also selected for longitudinal bars to avoid the yielding before bond splitting failure. Two bar diameters of 19 mm and 22 mm were used for longitudinal bars. The average yield strength, tensile strength and elastic modulus were 1053, 1128 and 1.87×10^5 N/mm^2 for D19 and 980, 1031 and 1.85×10^5 N/mm^2 for D22, respectively. For transverse bars, high strength steel bar were also used having average yield strength, tensile strength and elastic modulus were 1414, 1490, and 2.0×10^5 N/mm^2, respectively.

The effect of corrosion attacks was investigated by performing accelerated electrochemical corrosion program to give a reasonable corrosion time periods. Before the accelerated corrosion test, all specimens were cured for 28 days in the laboratory environment. The procedure of accelerated corrosion test was described in detail in Chapter 2.3.3

Table 4-1 Specimens parameter

No.	Specimens	Concrete Strength (N/mm^2)	Longitudinal bar			Target Corrosion Rate (%)	Transverse bars	
			No. bar	dia. (mm)	Ratio		Bar	Ratio
1	4LT-∞S-NH	24	4	19	1.29%	0	0	0%
2	4LT-∞S-NC					6		
3	4L2T-200S-NH					0	2-U6@200	0.15%
4	4L2T-200S-NC					6		
5	4L2T-100S-NH					0	2-U6@100	0.29%
6	4L2T-100S-NC					6		
7	4L4T-200S-NH					0	4-U6@200	0.29%
8	4L4T-200S-NC					6		
9	3L2T-100S-NH		3	22	1.30%	0	2-U6@100	0.29%
10	3L2T-100S-NC					6		
11	4L2T-100S-NH	48	4	19	1.29%	0	2-U6@100	0.29%
12	4L2T-100S-NC					6		

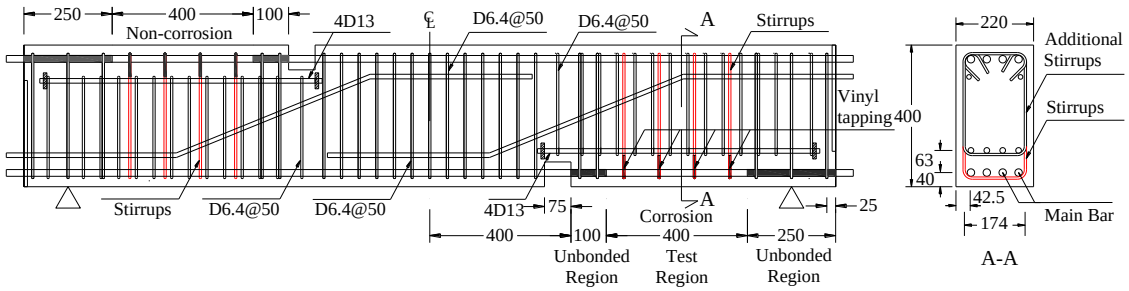

Fig. 4-1 Typical specimen configuration

Tranverse bars Taping Longitudinal bar Taping

Fig. 4-2 Longitudinal and transverse bars vinyl taping

4.2.3 Loading method

The specimens were tested in a simple three point loading. Because the beam had two test regions or specimens, corroded and healthy regions, so after loading test was finished for one region, it was then continued with another test region in the opposite loading directions by turning upside down. The outline of loading test set-up is described in Fig. 4-3(a). The loading was controlled by displacement with deformation rate 0.1 mm/min for loading stage and 0.5mm/min for unloading stage. The typical

loading cycle is demonstrated in Fig. 4-3(b). The peak of loading cycle was controlled by measured strain of longitudinal bar and the slip of each bar was measured using linear variable differential transformers (LVDT) at the end of beams and the total load was monitored using the load cell put at the middle of beam below the loading actuator.

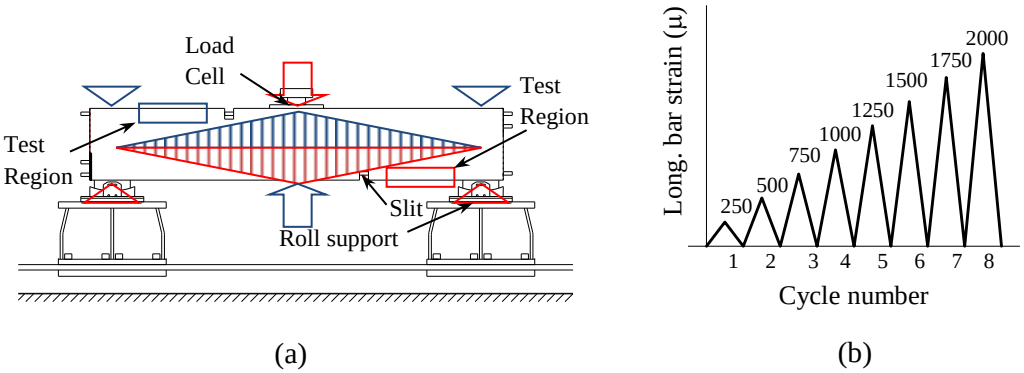

(a) (b)

Fig. 4-3 Schematic illustration of test setup and loading pattern

4.3 PULLOUT TEST RESULTS

4.3.1 Measured bond stress-slip relationships

Fig. 4-4 shows bond stress-slip relationship for each longitudinal bar distinguished by bar location in casting direction (T, CT, CB and B). The bond stress was calculated from the tensile load acting on each longitudinal bar measured by strain gages attached on the longitudinal bar at slit and at unbounded region divided by the surface area along the embedment length of 400 mm. Therefore, the results are the average bond stress along embedment length. The dash line and the solid line in Fig. 4-4 shows the history and the envelope curves of bond stress-slip relationship, respectively. The average bond stress-slip relationship for all longitudinal bars in one specimen is illustrated by the black line.

Without transverse bars

For specimen without transverse bars, specimen No.1 and No.2, as shown in Fig. 4-4(a)-(b) the maximum bond stress of both specimens are relatively small around 2 N/mm^2 and it occurred at lower end slip, less than 1 mm. Corroded specimen of No.2 has a slightly higher maximum bond stress than specimen No.1, the healthy specimen. This may be a possibility that the corrosion product filled the void at interface between reinforcement and concrete and enhanced the bond stress. However, after reaching maximum bond stress, the bond stress of specimen No.2 rapidly deteriorated due to influence of initial corrosion splitting crack. As reported by several researchers [27, 28], generally generate significant bond deterioration, however in a relatively low level corrosion an enhancement of bond properties may be occurred.

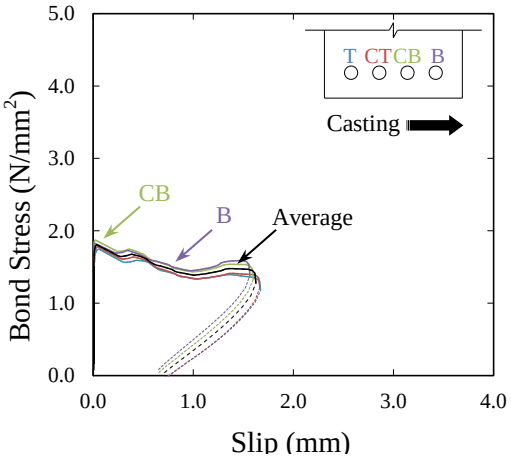

(a) No.1 (Ave. corrosion = 0 %)

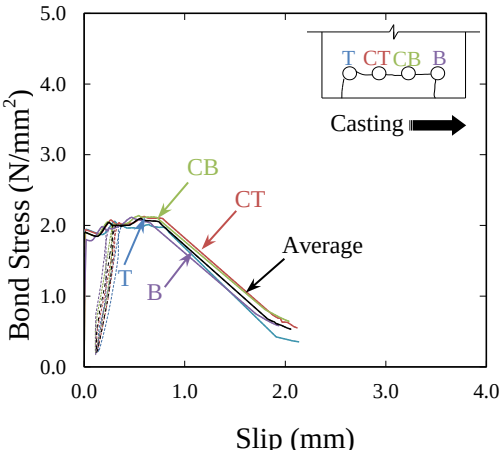

(b) No.2 (Ave. corrosion = 6.2 %)

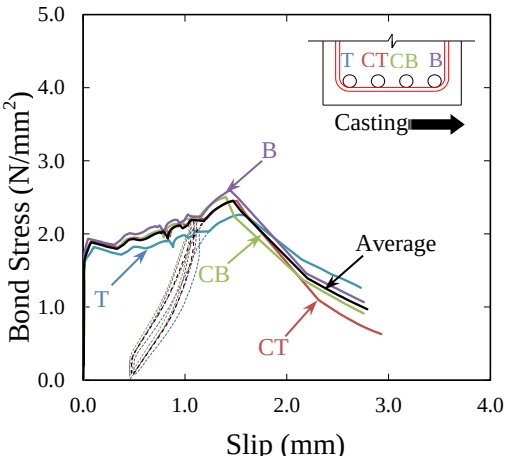

(c) No.3 (Ave. corrosion = 0 %)

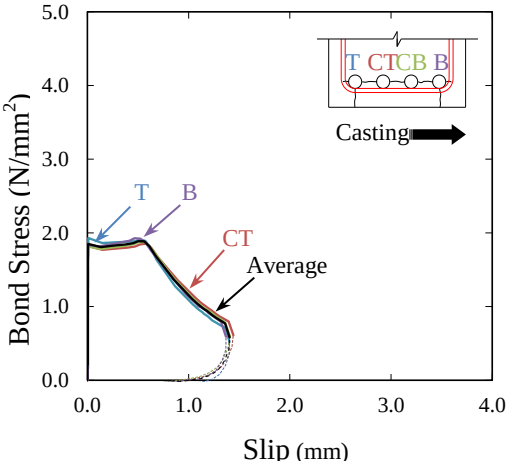

(d) No.4 (Ave. corrosion = 5.8 %)

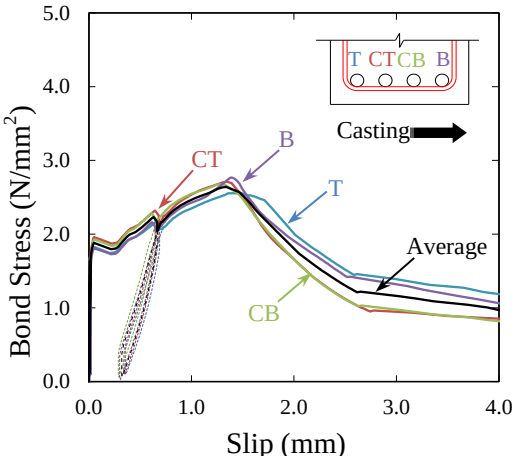

(e) No.5 (Ave. corrosion = 0 %)

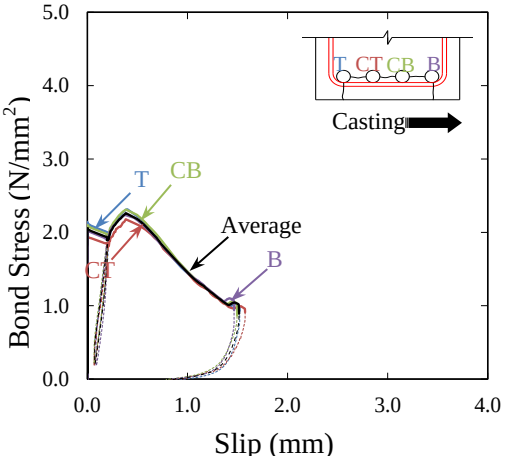

(f) No.6 (Ave. corrosion = 6.1 %)

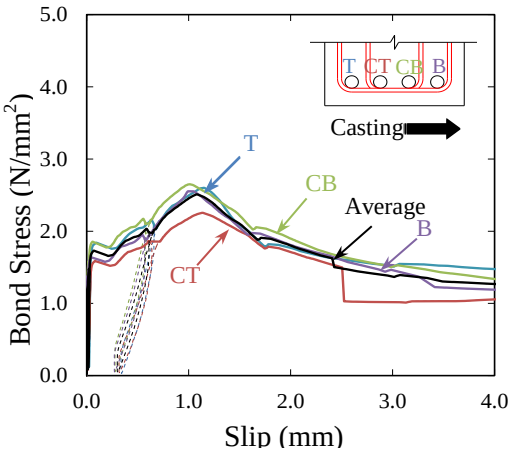

(g) No.7 (Ave. corrosion = 0 %)

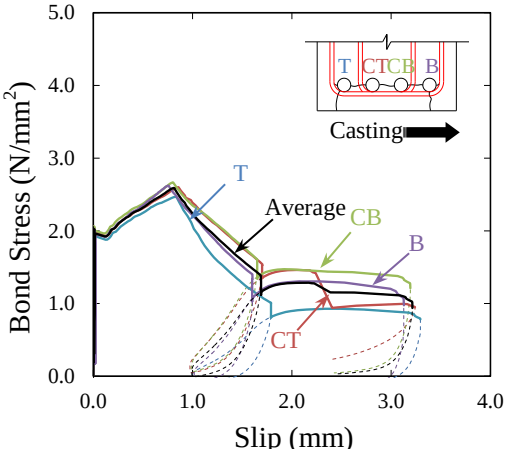

(h) No.1 (Ave. corrosion = 5.4 %)

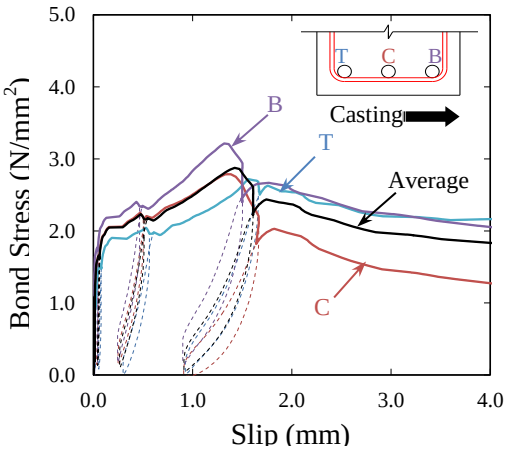

(i) No.9 (Ave. corrosion = 0 %)

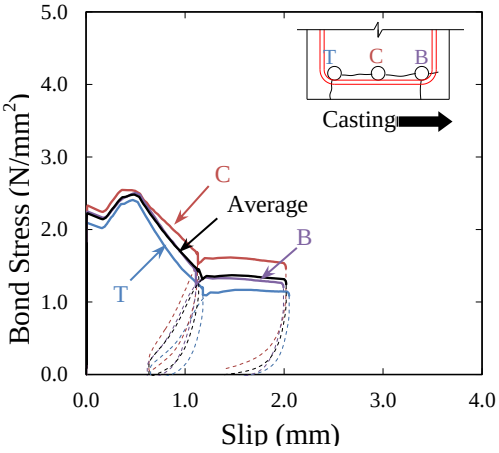

(j) No.1 (Ave. corrosion = 5.8 %)

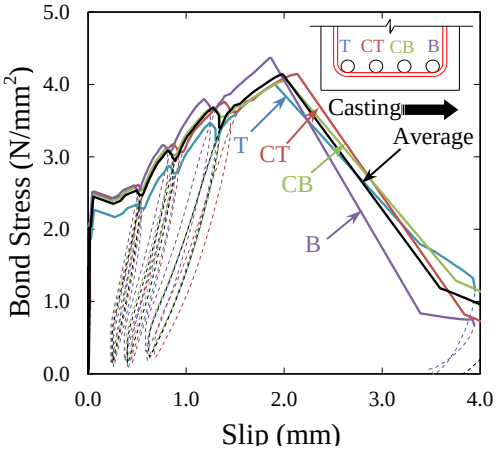

(k) No.11 (Ave. corrosion = 0 %)

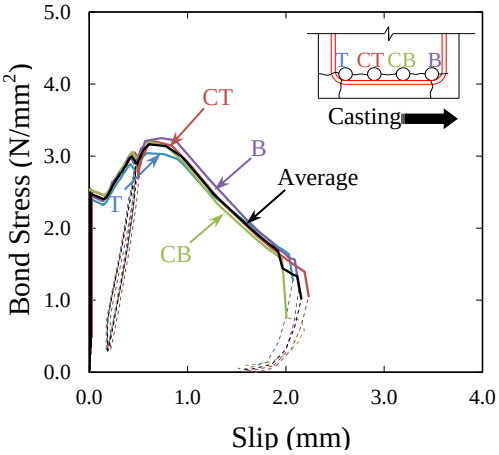

(l) No.12 (Ave. corrosion = 5.7 %)

Fig. 4-4 Measured bond stress-slip relationship

With transverse bars

For specimens with transverse bars, the bond stress-slip relationship of specimen No. 3 to No. 12 clearly demonstrated that corrosion reduces the bond splitting capacity when comparing the bond strength between the healthy and the corroded specimens. It also showed that maximum bond stress for healthy specimens mostly occurred at larger slip more than 1 mm meanwhile for corroded specimens occurred at lower slip smaller than 1 mm and after reaching its maximum bond value the bond stress rapidly decreases indicating the brittle of bond behavior of corroded reinforcement.

If compared to the specimen without transverse bars, as expected, the presence of transverse bars mostly increased the bond splitting capacity for uncorroded specimens. An increase in transverse bars ratio will increase the residual bond strength. Moreover, it is also shown that the presence of transverse bars enabled to maintain its bond stress after reaching maximum bond stress at least one third of maximum bond stress at larger slip as shown in Fig. 4-4. This indicates that the presence of transverse bars influence the bond stress-slip relationship for corroded RC members. Finally, the bond stress at the beginning of slip approximately at slip = 0.02 mm is about 2 N/mm^2 as reported by Aryanto et al. [22] .

With different bar location

If bond stress-slip relationship is compared among longitudinal bars with respect to bar location in casting direction, for healthy specimens the bond stress-slip relationship of bars located at top (T) in casting had slightly lower bond value compared to bar located at bottom (B) in casting as shown in Fig. 4-4. This can be due to larger porosity of concrete around bars located at top in casting. A large difference between bond behaviors among bar location is shown in Fig. 4-4(i) when spacing between longitudinal bars is relatively large and when large bar diameter are used. However, the effect of bars location on bond-slip relationships among corroded longitudinal bars seems insignificant. This can be attributed to some of corrosion product that may fill the concrete pore.

With high concrete strength

The bond-slip relationship for specimen with high concrete strength as shown in Fig. 4-4(k)-(l) had a larger maximum bond stress than for normal strength specimens. The average maximum bond stress for high concrete strength was 4.1 N/mm^2 and 3.2 N/mm^2 for healthy and corroded bars, respectively. This indicates the high contribution of concrete strength on bond capacity. Moreover, the slip at maximum bond stress was also larger than normal concrete strength. However, the bond stress decreased rapidly after the maximum bond stress to lead a brittle behavior.

4.3.2 Crack patterns

Typical crack patterns at failure of pullout specimens are described in Fig. 4-5. The crack patterns for all specimens are presented in Appendix D. Different types of crack patterns were observed from the test results depending of the presence or absence of corrosion and transverse bars. For healthy specimens without transverse bars a small number of inclined cracks formed starting from the bottom support observed from the side view of beam. As illustrated in Fig. 4-5(a) several transverse crack (flexural cracks) and inclined cracks (splitting cracks) were generated in the bottom of beam. The typical crack patterns for healthy specimens with transverse bars at the side of beam were dominated by inclined cracks which more uniformly distributed along longitudinal bars compared to specimen without transverse bars as shown in Fig. 4-5(b). At the bottom beam several transverse and inclined cracks were also observed and these bottom cracks were mostly connected with cracks at side of beams.

As shown in Fig. 4-5(c) typical crack patterns for corroded specimens at side beam were also dominated by inclined cracks, however the cracks tended to form parallel to longitudinal bars or to have a smaller slope. Some of the parallel cracks were extended from the existing corrosion cracks. A similar behaviour was observed at the bottom face which was mostly governed by parallel cracks from the extension of existing splitting cracks due to corrosion and only a few of transverse cracks were developed at bottom beams. According to the observed crack patterns on corroded specimens, the mode of failure for corroded specimens dominantly governed by splitting cracks parallel to longitudinal bars.

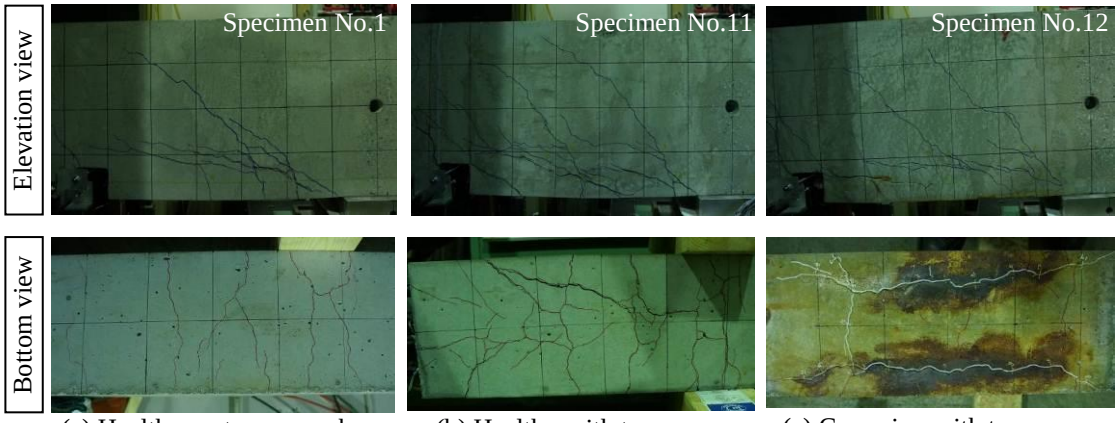

(a) Healthy-no transverse bars (b) Healthy-with transverse (c) Corrosion-with transverse

Fig. 4-5 Crack pattern at failure

4.3.3 Bond splitting strength

Fig. 4-6(a)-(f) summarizes the test results in term of normalized maximum bond stress of each longitudinal bar with respect to maximum bond stress of bars located at bottom in casting (B) plotted against corrosion (see also Appendix B). In general, for healthy bars the effect of bar location in term of casting direction slightly influence the bond

splitting capacity of bars. The difference of bond capacity between the bar located at bottom in casting (B) and top in casting (T) is approximately 5-15%. A small effect of bar location in casting direction on the residual bond capacity for corroded specimens was shown. This can be due to the concrete voids may be filled by corrosion products. As shown in Fig. 4-6(b)-(e) an increase in transverse bars ratio generated a lower bond splitting deterioration or higher residual bond splitting capacity. This showed substantial contribution of confinement provided by transverse bars in corroded specimens.

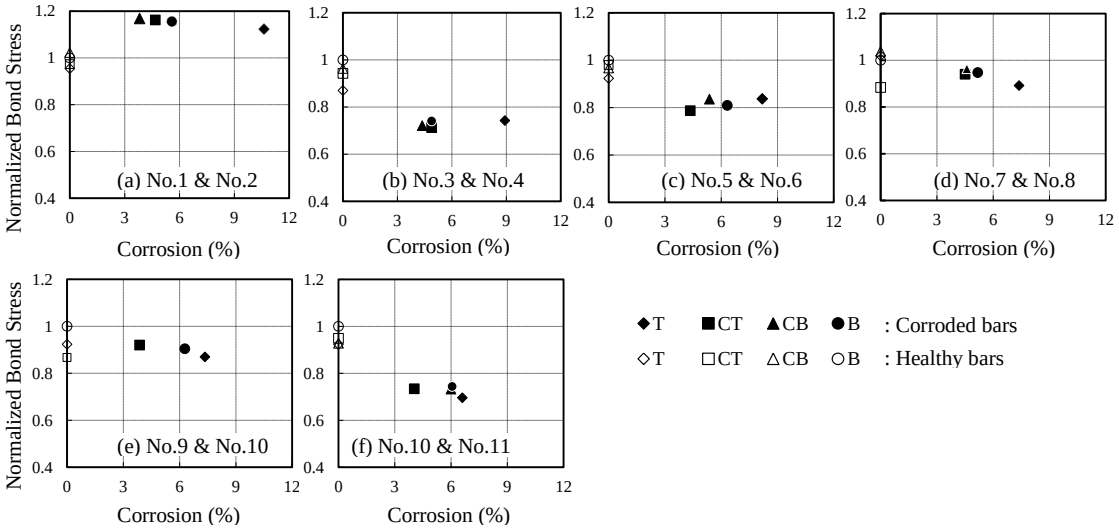

Fig. 4-6 Test results of bond splitting strength normalized with respect to that of the bar at bottom in casting (B) in uncorroded specimen

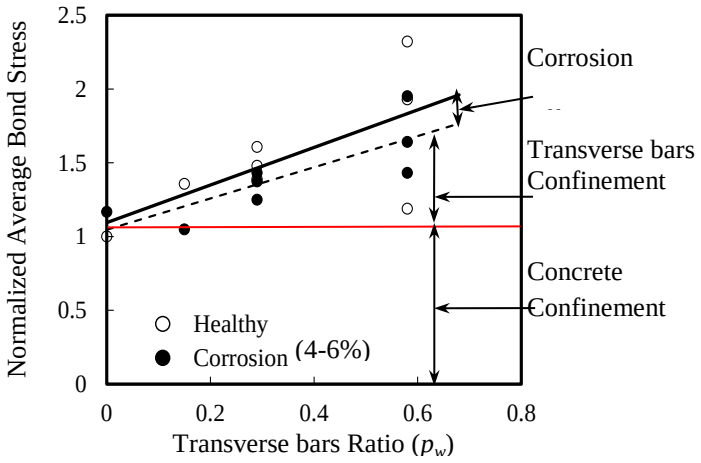

Fig. 4-7 Test results of bond splitting strength normalized with respect to that of the uncorroded specimen without transverse bars

The average maximum bond stress of each specimen normalized with respect to that of the healthy specimen without transverse bars (Specimen No.1) plotted against transverse bars ratio is shown in Fig. 4-7. In addition, the experimental test result conducted by Morita et al.[37] which had transverse bars ratio of 0.58% was added into the graph (Table 4-2 and Table 4-3). From the figure, for healthy specimens an increase

of bond splitting capacity was observed with the increasing transverse bars ratio as illustrated by linear regression curve, solid black line, indicating the significant contribution of transverse bars. However, as indicated by a linear regression of corroded specimens, dash line, the test results showed bond deterioration due to effect of corrosion attack

Table 4-2 Specimens parameter from Morita et al.[37]

No	Specimen	Longitudinal Bar			Measured Corrosion (%)	Transverse Bar	
		Bar	Dia. (mm)	Ratio		Bar	Ratio
13	4L2T-50S-NH	4	19	1.29 %	0	2-U6@50	0.58%
14	4L2T-50S-NC1				0.5		
15	4L2T-50S-NC2				5	2-U6@50	
16	4L2T-50S-NC3				6		
17	4L4T-100S-NH				0	4-U6@100	
18	4L4T-100S-NC				4.5		
19	3L2T-50S-NH	3		1.09 %	0	2-U6@50	
20	3L2T-50S-NC				3.8		

Table 4-3 Test results of bond strength for the present experiment and Morita et al.[37]

No.	Specimen	p_w	Corrosion Loss (%)					τ_{max} (N/mm^2)				
			Bar location					Bar location				
			T	CT	CB	B	Ave.	T	CT	CB	B	Ave.
1	4LT-∞S-NH	0 %	0	0	0	0	0	1.75	1.78	1.87	1.83	1.81
2	4LT-∞S-NC		10.6	4.7	3.8	5.6	6.2	2.06	2.13	2.14	2.12	2.11
3	4L2T-200S-NH	0.15%	0	0	0	0	0	2.26	2.45	2.51	2.60	2.45
4	4L2T-200S-NC		8.9	4.9	4.4	4.9	5.8	1.93	1.85	1.88	1.93	1.90
5	4L2T-100S-NH	0.29%	0	0	0	0	0	2.55	2.71	2.68	2.77	2.68
6	4L2T-100S-NC		8.2	4.4	5.4	6.3	6.1	2.32	2.18	2.31	2.24	2.26
7	4L4T-200S-NH		0	0	0	0	0	2.60	2.26	2.65	2.55	2.51
8	4L4T-200S-NC		7.4	4.5	4.6	5.2	5.4	2.47	2.60	2.67	2.62	2.59
9	3L2T-100S-NH		0	0		0	0	2.72	2.79		3.21	2.91
10	3L2T-100S-NC		7.4	3.9		6.3	5.8	2.41	2.55		2.50	2.49
11	4L2T-100S-HH		0	0	0	0	0	4.00	4.15	4.06	4.37	4.14
12	4L2T-100S-HC		6.6	4.0	6.0	6.1	5.7	3.04	3.21	3.20	3.25	3.18
13	4L2T-50S-NH	0.58%	0	0	0	0	0	2.24	2.29	1.87	2.23	2.15
14	4L2T-50S-NC1		0.9	0	0.30	0.60	0.5	3.45	3.31	2.84	2.49	2.93
15	4L2T-50S-NC2		5.5	3.6	4.5	6.3	5.0	2.88	2.29	2.52	2.69	2.59
16	4L2T-50S-NC3		6.5	5.5	5.3	6.0	5.8	3.20	2.70	3.44	2.57	2.97
17	4L4T-100S-NH		0	0	0	0	0	4.30	3.38	3.21	3.07	3.49
18	4L4T-100S-NC		5.1	4.5	3.3	5.0	4.5	2.43	2.72	2.48	3.13	2.59
19	3L2T-50S-NH		0	0		0	0	4.14	4.19		4.69	4.20
20	3L2T-50S-NC		5.3	1.9		4.1	3.8	5.01	3.31		2.89	3.72

4.4 MODELING OF BOND-SLIP RELATIONS OF CORRODED STEEL BAR

4.4.1 The suggested bond stress-slip relationship for corroded steel bar

In order to develop bond stress-slip relationship for corroded steel bar, the shape of bond stress-slip curve as well as the bond strength is assumed depending on the corrosion level. As observed from the experimental test described in Chapter 4.3, corrosion influences the bond stress–slip curve in the following manners:

(1) Maximum bonds stress decreases with an increasing corrosion level except in low level corrosion

(2) Slip at maximum bond stress decreases as increase of corrosion level

(3) At early stage of bond stress-slip curve approximately up to 2 N/mm2 or at slip = 0.02 mm, corrosion seems not change the bond stress-slip curve

The bilinear ascending curve as developed by Hayashi et al. [33] has been chosen to model bond slip relationship with additional descending curve representing the damage caused by concrete crushing in front of bar ribs[31]. Hence, the τ-s relationship of corroded reinforcement is developed from uncorroded (healthy) reinforcement considering the influence of corrosion on the bond stress–slip curve as mentioned before.

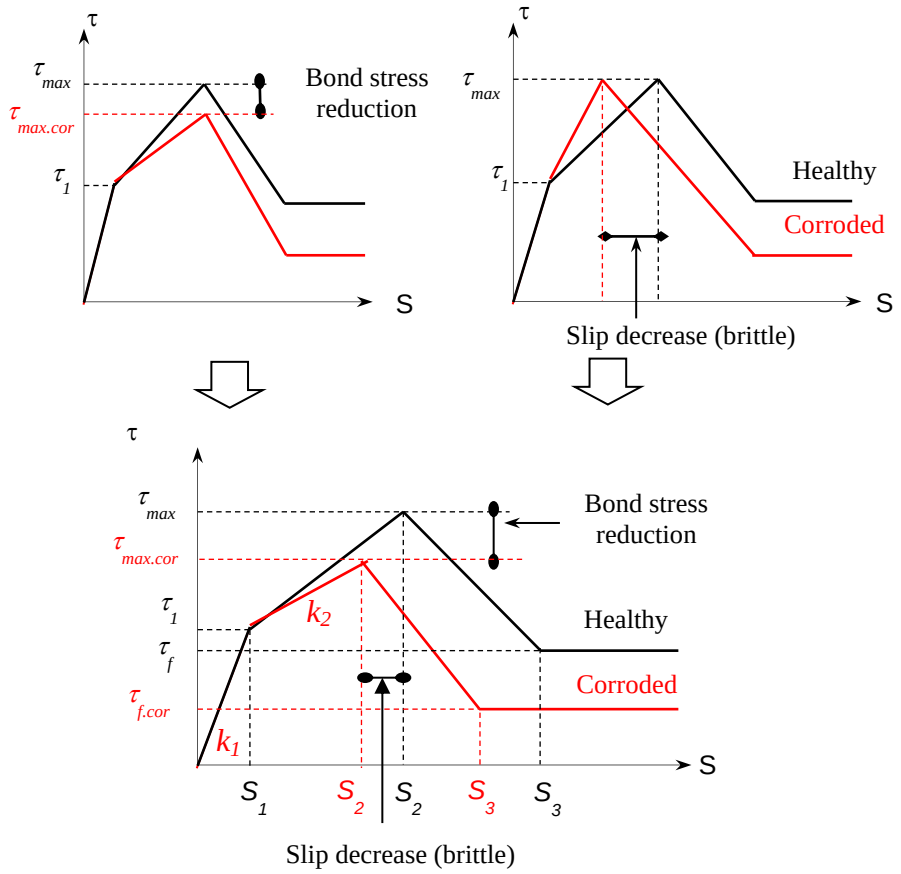

Fig. 4-8 Schematic view of bond-slip relationship for corroded reinforcement

The suggested methods to obtain the bond stress-slip curve for corroded reinforcement can be developed in three stages as follows:

First ascending curve

The first ascending curve is formulated based on the bond stress at slip = 0.02 mm corresponding to the slip due to chemical adhesion and radial micro cracking or the starting point of slip for further of radial cracking and local crushing as shown in Fig. 4-9. This indicates that the bond stress is mostly depending on mechanical properties of concrete while the transverse bar confinement does not govern due to small cracking. As shown in Fig. 4-10(a) the average of bond stiffness is almost constant around k_1=100 N/mm^3 for different corrosion level. This also indicates that corrosion not significantly influenced at small slip. The same behavior was seen for different transverse bar ratio (Fig. 4-10(a)). As a result, here, the first ascending curve is fixed at τ_1 = 2 N/mm^2 and S_1 = 0.02 mm.

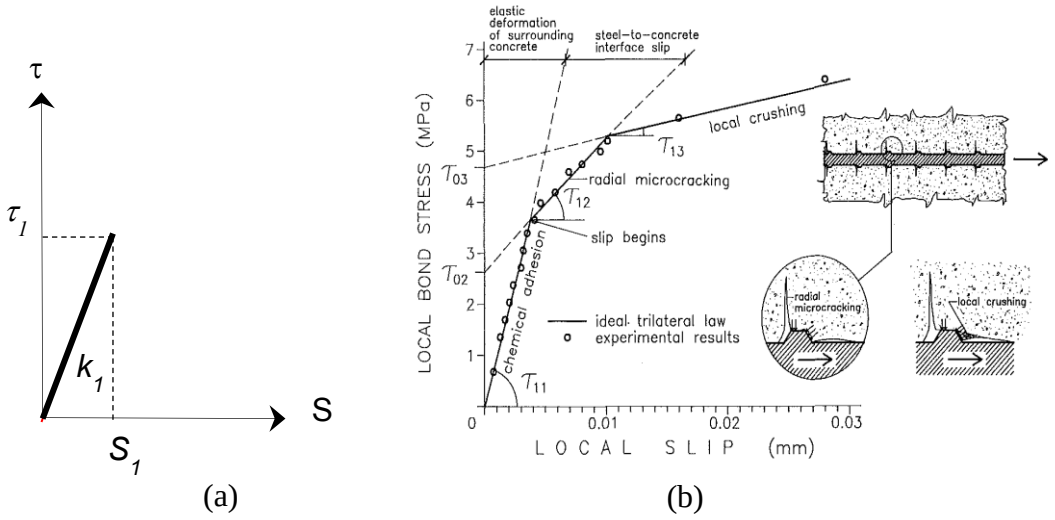

Fig. 4-9 (a) First ascending curve (b) Bond stress-slip at small slip[59]

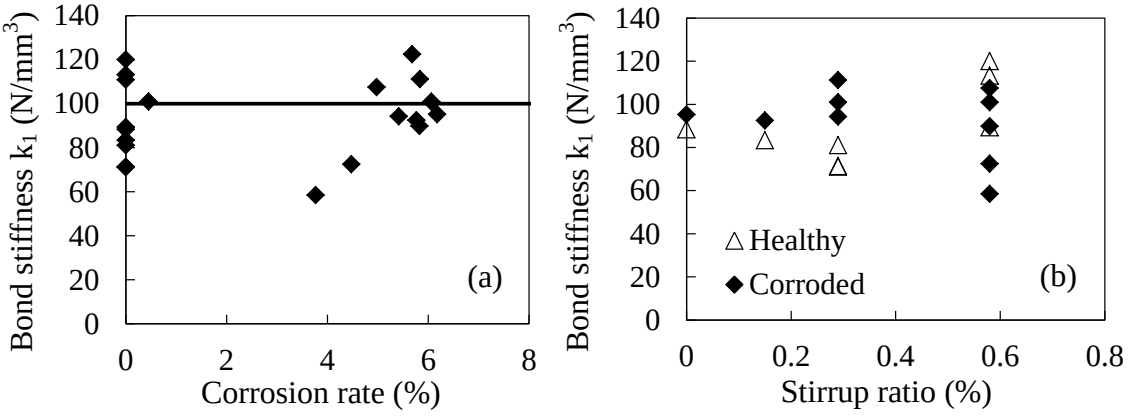

Fig. 4-10 Bond stiffness at slip at τ_1, k_1 vs. (a) corrosion rate (b) transverse bar ratio

Second ascending curve

The second ascending curve of the bond stress-slip curve, Fig. 4-11(a), corresponds to the influence of splitting crack on surrounding concrete with an increasing radial pressure. At the beginning, the confining action from the surrounding concrete plays an important role to balance the radial pressure come from the tensile strength of the uncracked part of concrete and residual tensile strength of the cracked part. When the splitting crack becomes larger and propagates, another confining action from the transverse bars are taking apart as shown in Fig. 4-11(b). In case of corrosion which introduces splitting crack on the surrounding concrete the contribution of confining action from concrete are reduced. However, it is difficult to separate the contribution of surrounding concrete and transverse reinforcement especially when effects of corrosion and corrosion cracking are involved.

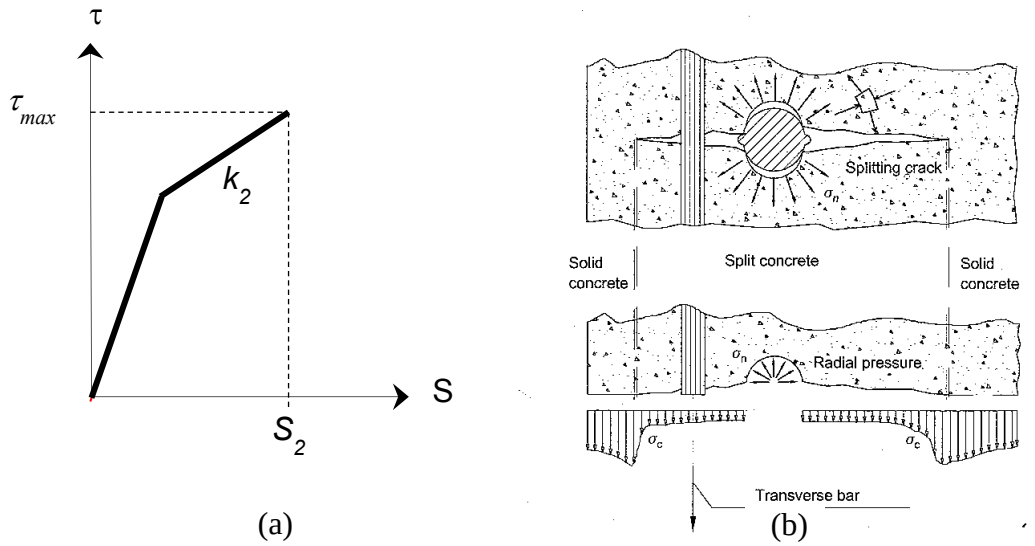

Fig. 4-11 (a) Second ascending curve (b) Splitting crack and confining action [60]

To determine the peak point of ascending curve it requires the maximum bond stress (bond strength) τ_{max} and the slip at maximum bond stress S_2. The bond strength τ_{max} of uncorroded reinforcement can be estimated using the available formula proposed by AIJ code [26] (See Appendix E) which was developed based on empirical data involving significant numbers of specimens and influencing parameters such as concrete cover, concrete strength, bar diameter, and transverse bar ratio on bond splitting behavior. The comparison between bond strength from experimental test and calculated by AIJ formula can be shown in Appendix B.

As illustrated in Fig. 4-12, there is reduction of bond strength with increasing of corrosion levels. To determine the reduction in bond strength as the corrosion increase, a reduction factor of bond strength is introduced to the bond strength of uncorroded reinforcement τ_{max} corresponding to the transverse bars ratio as shown in Fig. 4-12. Thus, the maximum bond stress of corroded reinforcement can be described as

$$\tau_{\max.cor} = (1 - 0.02\Delta w)\tau_{\max} \quad \text{for } p_w = 0.3\text{- } 0.6\ \% \tag{4-1}$$

$$\tau_{\max.cor} = (1 - 0.04\Delta w)\tau_{\max} \quad \text{for } p_w = 0.15\% \tag{4-2}$$

where Δw is corrosion loss in percentage.

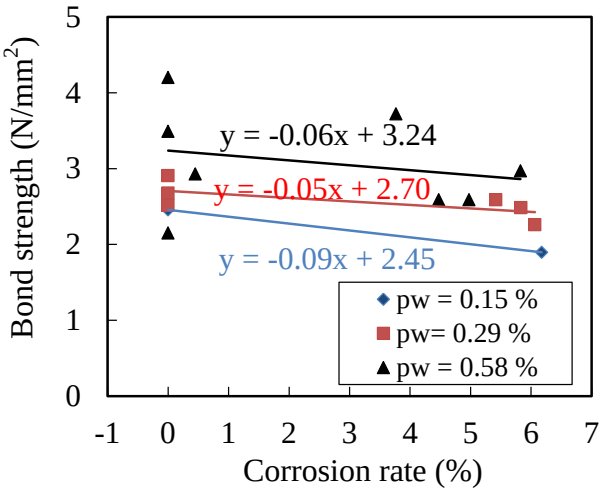

Fig. 4-12 Test results of average bond strength

Fig. 4-13 shows the stiffness at τ_{max} or second bond stiffness k_2 corresponding to different of corrosion loss and transverse bar ratio. The second bond stiffness as shown in Fig. 4-13 was obtained from

$$k_2 = \frac{(\tau_{\max} - 2)}{(S_2 - 0.02)} \tag{4-3}$$

The figure shows also that in term of corrosion loss and transverse bars the different of bond stiffness between uncorroded and corroded reinforcement is relatively wide scatter, although an increase of second bond stiffness with an increase of transverse bars ratio was identified.

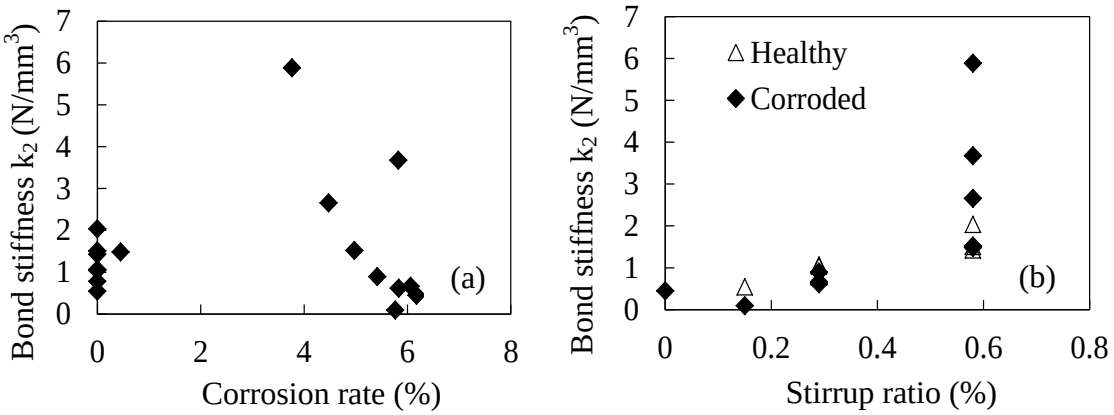

Fig. 4-13 Bond stiffness at τ_{max}, k_2 vs.(a) corrosion rate (b) transverse bar ratio

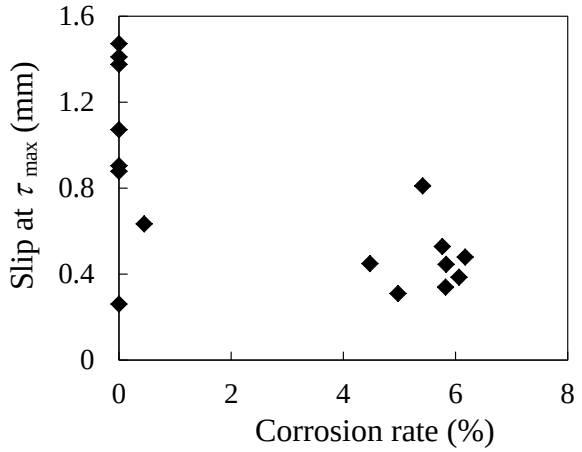

Fig. 4-14 Test results of slip at τ_{max}

Fig. 4-14 shows the slip at τ_{max} from the experimental test it show that with an increase of corrosion level the slip is decreased represent the increasing brittleness in bond-slip behavior as the corrosion process evolves. Due to a wide scatter data and limited number of data, therefore to obtained the slip τ_{max}, $S_{2,}$ for uncorroded and corroded reinforcement. Here, S_2 for uncorroded reinforcement was fixed at 1 mm and for corroded reinforcement the bond stiffness is assumed the same with uncorroded one and S_2 decrease proportionally to the decrease of bond strength τ_{max}. Thus, the second bond stiffness k_2 in N/mm^3 for uncorroded and corroded bars and slip τ_{max}, S_2 in mm for corroded reinforcement can be described as

$$k_2 = \frac{(\tau_{\max} - 2)}{(1 - 0.02)} \tag{4-4}$$

$$S_2 = \frac{(\tau_{\max .cor} - 2)}{k_2} + 0.02 \tag{4-5}$$

From these two parameters of bond stress and slip, the combined action of bond strength reduction and slip reduction varying along with the corrosion level may simulate the influence of corrosion in the bond stress-slip behavior. However, further investigation are required due to limited number of data in order to increase the accuracy.

Descending curve

The bond softening or descending curve in the bond slip relationship was reported by Eligehausen et al. [31] and Harajli et al. [38] from their experimental tests and adopted in CEB-FIP [8]. The descending curve is linearly decreasing to the minimum bond value, τ_f, which is known as minimum bond stress resistance that can be provided only by friction (Fig. 4-15). The descending curve representing the damage caused by concrete crushing in front of bar ribs[31]. Usually it is occurred after maximum bond stress was reached if the splitting failure was occurred. In some case, when the confining action of

surrounding concrete and transverse bar is very large, so, the shearing failure of the concrete between the steel ribs or pullout failure may occur. In that case it is possible to have constant maximum bond stress in large slip as described in CEB-FIP [8]. In this study, all specimens fail in splitting failure as described in Chapter 4.3.2. Therefore, after reaching maximum bond stress the bond gradually decreased.

To determine τ_f and S_3 from the experiment shows that the presence of transverse bars enables to maintain its bond stress after reaching maximum bond stress at least one third of maximum bond stress and slip at τ_f around 2-3 times of S_2. Therefore, τ_f and S_3 is assumed to be described as follows

$\tau_f = 0.5\,\tau_{max}$ for uncorrded reinforcement (4-6)

$\tau_{f.cor} = 0.25\,\tau_{max}$ for uncorrded reinforcement (4-7)

$S_3 = 3\ S_2$ for uncorrded and corroded reinforcement (4-8)

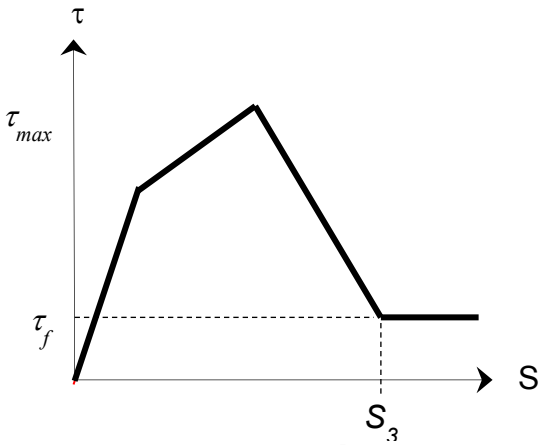

Fig. 4-15 Descending curve

Comparison with experimental test

Fig. 4-16 shows the proposed bond-slip relationship for healthy and corroded reinforcement based on the procedure that developed aforementioned. Fig. 4-16 also shows the comparison between experimental data and suggested bond stress-slip relationship. It demonstrates that a reasonable agreement with the experimental evidence. In the Chapter 5, in order to evaluate the reliability of the proposed bond stress-slip relationship, some experimental tests of RC members are numerically simulated.

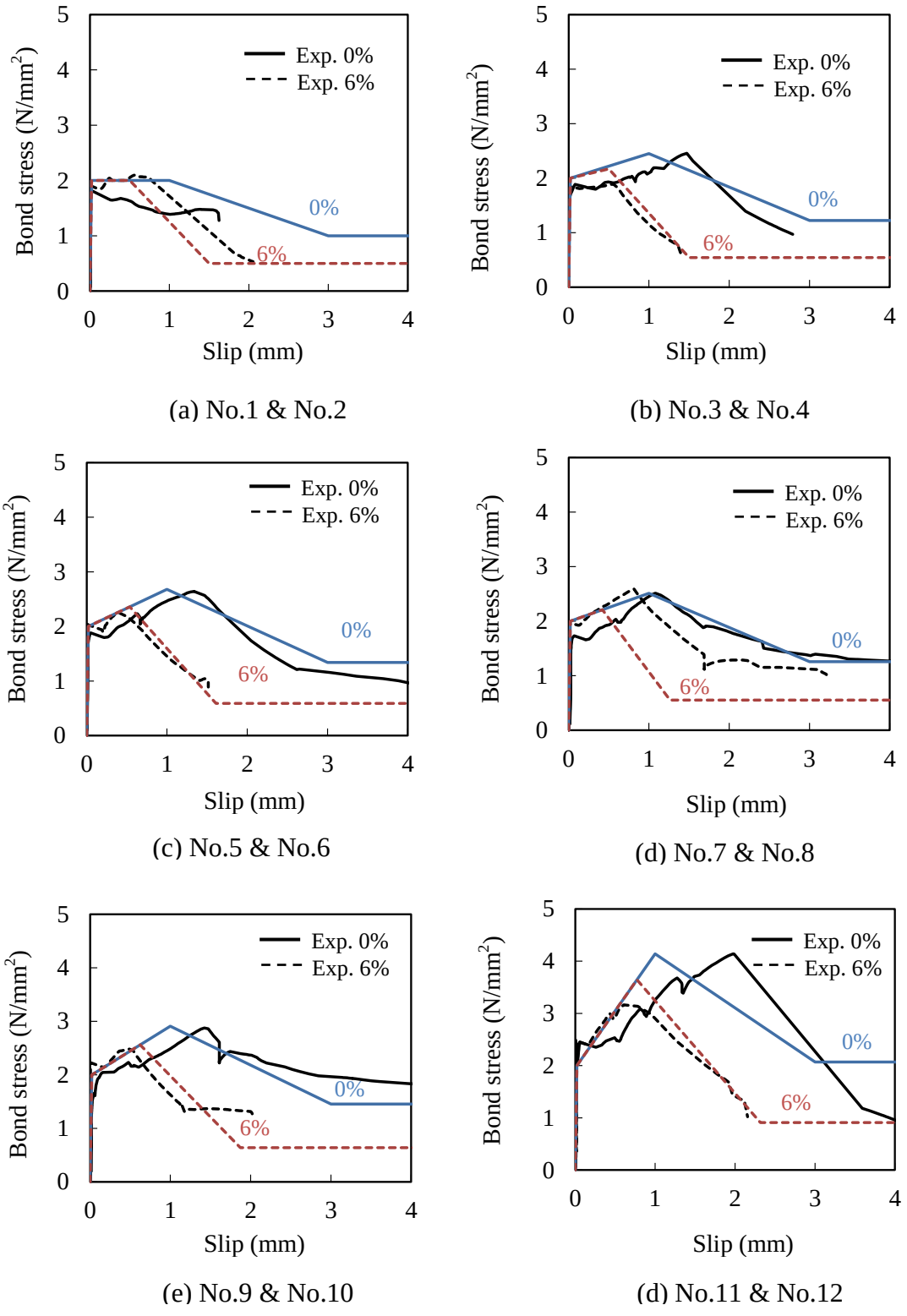

Fig. 4-16 Comparison of bond stress- slip relationship between proposed model and experimental tests

4.4.2 Limitations

The previously described method is only valid if splitting failure governs the bond stress development of the uncorroded (healthy) and corroded reinforcement. This only occurs when smaller cover to bar diameter ratios and transverse bar ratios are used. For larger concrete covers or under high transverse pressure, the maximum radial deformations do not cause cover cracking and the failure is mobilized by shearing failure of the concrete between the steel ribs instead of cracking of the cover.

The proposed methods were basically developed based on the limited corrosion level mostly in low to medium corrosion levels in which corrosion of cover cracking was generated. For very high corrosion level, it has to be assumed that the development of a weak corrosion layer and a degradation of the rib area of the reinforcement steel have an influence on the bond properties [28]. For very severe corrosion, the spalling of concrete cover may be observed in the natural environment that may completely diminish the bond properties. This behavior in the bond interaction between the reinforcement steel and concrete is not considered by the method.

The current bond-slip relationship is also developed based on the limited number of specimens and parameters influencing bond behavior such as cover depth ratio and concrete strength. Therefore, further investigations in both experimental and analytical study are required in order to have better accuracy.

4.5 SUMMARY OF CHAPTER FOUR

The pullout test on corroded RC tensile members was performed to evaluate effect corrosion on bond behavior of corroded RC members. The parameter study of the different of confinement by means of transverse bars was investigated. The following conclusions can be drawn according to experimental results that discussed in this chapter.

a) Different behavior of bond stress-slip relationship between uncorroded and corroded reinforcement was observed from the experimental tests. Compared to uncorroded reinforcement, lower maximum bond stress and smaller slip at maximum bond stress was shown for corroded reinforcement and after reaching maximum bond stress, the bond rapidly deteriorated for corroded reinforcement.
b) An important contribution of transverse bars to maintain residual bond splitting capacity for corroded specimens was observed. The more transverse bar is provided, the higher residual bond splitting strength is generated.
c) A small effect of bar location in casting direction on the bond stress-slip relationships was observed for both corroded and healthy specimens. A high contribution of concrete strength on the confinement of bar was also identified.

d) The crack pattern at failure for corroded specimens was mainly governed by splitting cracks parallel to longitudinal bar as an extension from the existing corrosion cracks and combined with a low slope of inclined splitting cracks. For healthy specimens, it was dominated by inclined splitting cracks and the distribution of the inclined cracks was governed by the presence of stirrups.
e) Based on the experimental test of corroded reinforcement using two parameters that influence the bond-slip behavior due to corrosion i.e. the reduction of bond strength and slip, the simple bond stress-slip curve for corroded reinforcement was proposed which may useful for structural assessment and design.

Next chapter deals with the evaluation of structural performance of corroded RC members using a non-linear finite element analysis. The important parameters of material and mechanical properties of corroded reinforcement that was obtained from the experimental test as described in Chapter 3 and 4 were adopted in the analysis.

Chapter Five

EVALUATION OF STRUCTURAL PERFORMANCE OF CORRODED RC MEMBERS

Chapter 5
EVALUATION OF STRUCTURAL PERFORMANCE OF CORRODED REINFORCED CONCRETE MEMBERS

5.1 INTRODUCTION

For simulating the influence of corrosion on the structural performance of RC members in a reliable numerical analysis, the changes in the material properties and the elements geometry caused by corrosion damage are essential to be formulated. Thus, the deterioration model should be able to capture the following aspects:

1. loss of cross-sectional area of reinforcement, in the longitudinal bars and in the transverse bars, including the transverse bars stress generate by corrosion expansion
2. reduction of concrete section and the changes in the strength and ductility of concrete due to cover cracking or cover spalling,
3. bond deterioration between concrete and reinforcement corresponding to the corrosion level of reinforcement and confinement conditions or reduction of transverse bar area.

In this chapter, the methodology for evaluation the mechanical behavior and residual load-carrying capacity of corroded reinforced concrete members is discussed based on the assumption that the effect of corrosion can be modeled as a change in the geometry and material properties of concrete, reinforcement and bond between reinforcement and concrete. A relatively similar methodology has been proposed by Coronelli et al.[39] and Saether [40]. The difference between approaches is in the selecting of material models for reinforcement and concrete as well as bond-stress slip relationship. The effect of transverse bar stress induced by expansion pressure obtained from experimental test as described in Chapter 2 was also implemented in the assessment of corroded RC members in the main frame of numerical analysis through finite element model.

Moreover, for assessment requirement of corroded RC members, firstly, it is necessary to define the deterioration model of material and mechanical properties of reinforcement, concrete and bond between concrete and reinforcement as a result of effect of corrosion of reinforcement.

5.2 DETERIORATION MODEL

5.2.1 Deterioration model for reinforcement

Corrosion of reinforcement produces the rust formation which has two to six times the volume of original steel and low mechanical properties. Corrosion also produces pits or holes in the surfaces of reinforcement, reducing strength capacity as a result of the cross-sectional area reduction. Due to the low mechanical properties of corrosion product, only the residual cross-sectional area of reinforcements is considered in the analysis. Corrosion may form reinforcement in different types of damage from a localized corrosion or pitting corrosion to more widespread corrosion known as uniform corrosion depending on the corrosion process such as chloride attack and carbonation[41,42].

The loss of sectional area of reinforcement accurately can be obtained by direct measurements. When concrete cover has spalled off by large corrosion, the residual bar diameter can be measured directly on the exposed bars after removing the corrosion rust. For small corrosion level where cover has cracked but has not yet spalled off, an indirect measurement to estimate corrosion penetration from cracked width as mentioned in Chapter 2can be adopted. The residual area of reinforcement due to uniform corrosion can be easily calculated as

$$A_{sc} = \pi/4 (d - 2x)^2 \tag{5-1}$$

where d is original bar diameter and x is depth of corrosion penetration. For localized corrosion based on experimental test conducted by Gonzalez et al. [43] the maximum penetration of pitting corrosion is approximately 4 to 8 times the average corrosion penetration of uniform corrosion. To calculate the residual area of locally corroded bar, the pit configuration proposed by Val et al[44] is used.

The mechanical properties of corroded reinforcement has been investigated by several researchers [45–49]. From their experimental investigation the mechanical properties of steel reinforcements i.e. yield, ultimate and elastic modulus is not significantly influenced by corrosion when calculated using the actual area of steel crosssection. Therefore, the corresponding mechanical properties of uncorroded reinforcement practically can be used for corroded reinforcement. However, the uniform corrosion shows a significant influence on the ductility of steel reinforcement [47,50]. In a pitting corrosion of reinforcement the ultimate strain of locally corroded reinforcement is reduced more significant because the notch effect induced higher localized strain in the bar and show brittle behavior [39,47,51].

In the numerical analysis using the finite element analysis, sometimes it is much easier to model reduction of mechanical properties of materials than reduction of geometrical properties i.e. crosssectional area of corroded reinforcement. Noguchi et al. [52] has been

proposed the constitutive law for corroded steel bar for numerical analysis as shown in Fig. 5-1(a). The constitutive law for steel bar can be obtained by determining the yield point and the elastic modulus of steel bar using the degree of corrosion as parameter (expressed as the mass loss rate). In this case, the cross-sectional area of corroded bar is assumed to be the same as the uncorroded steel reinforcement, while apparent mechanical properties of the corroded steel reinforcement is reduced. Noguchi et al. [52] also divided the steel reinforcement properties for uniform and pitting corrosion depending on the corrosion process. The formula for mechanical properties of corroded steel bar are as follows

For uniform corrosion

$$\sigma_{yc} = (1 - 1.24(\Delta w/100))\sigma_y \tag{5-2}$$

$$E_{cs} = (1 - 0.75(\Delta w/100))E_s \tag{5-3}$$

For pitting corrosion

$$\sigma_{yc} = (1 - 1.98(\Delta w/100))\sigma_y \tag{5-4}$$

$$E_{cs} = (1 - 1.13(\Delta w/100))E_{ss} \tag{5-5}$$

where σ_{sy} and σ_{cy} are yield strength of un-corroded and corroded steel bar, respectively. E_{sy} and E_{cy} are elastic modulus of un-corroded and corroded steel bar, respectively. Δ_w is corrosion percentage by weigh (%).

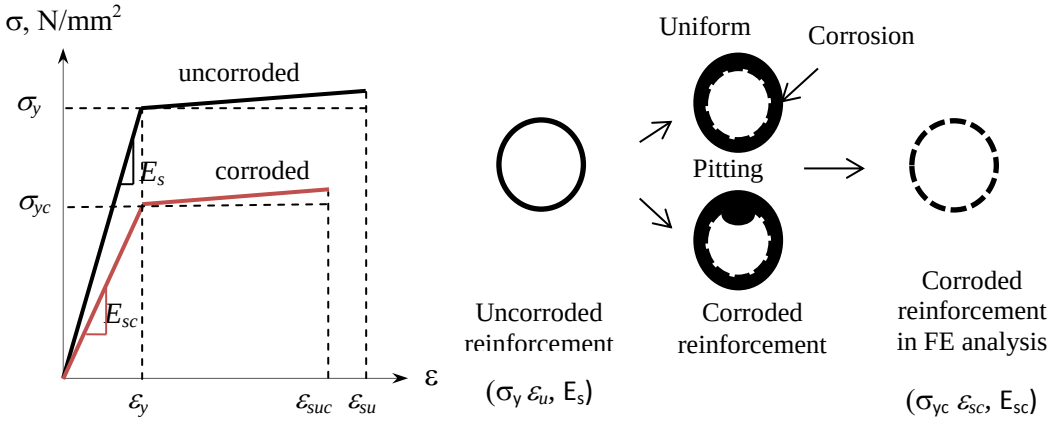

Fig. 5-1 Constitutive law for corroded reinforcement corrosion

For determining the ultimate strain or elongation of corroded reinforcement the empirical formula developed by Du et al[47] for embedded bar in concrete can be used as follows

$$\varepsilon_{suc} = (1 - 0.05\Delta w)\varepsilon_{su} \tag{5-6}$$

where ε_{su} and ε_{suc} are ultimate strain of uncorroded and corroded steel reinforcement, respectively. Δ_w is corrosion percentage of reinforcement.

For transverse reinforcement, not only the decrease of reinforcement strength due to loss crosssection area should be taken into account, but also the reduction of strength induced by stress on the transverse bar due to corrosion cracking. As mentioned in Chapter 2, there is an increasing transverse bar stress with a growing of crack width corresponding with increasing of corrosion level. The stress on transverse bar may reach half of yield stress of transverse bar if using a normal strength of transverse reinforcement. Therefore, this stress needs to be taken into account so, the apparent strength becomes smaller (Fig. 5-2). Combined with the constitutive laws derived by Noguchi, the apparent yield strength of transverse bars in N/mm^2 can be expressed in equation (5-7) to (5-10). The reduction part was obtained from experimental test data based on the regression of transverse bar stress induced by corrosion expansion as described in Chapter 2.

For uniform corrosion

$$\sigma_{ycw} = (1 - 1.24(\Delta w/100))\sigma_{yw} - (19.2\Delta w + 5.28), \text{ for high strength concrete} \quad (5\text{-}7)$$

$$\sigma_{ycw} = (1 - 1.24(\Delta w/100))\sigma_{yw} - (2.77\Delta w + 6.15), \text{ for normal concrete} \quad (5\text{-}8)$$

For pitting corrosion

$$\sigma_{ycw} = (1 - 1.98(\Delta w/100))\sigma_{yw} - (19.2\Delta w + 5.28), \text{ for high strength concrete} \quad (5\text{-}9)$$

$$\sigma_{ycw} = (1 - 1.98(\Delta w/100))\sigma_{yw} - (2.77\Delta w + 6.15), \text{ for normal concrete} \quad (5\text{-}10)$$

where σ_{yw} and σ_{ycw} are yield strength of uncorroded and corroded steel reinforcement, respectively. Δ_w is corrosion percentage of reinforcement.

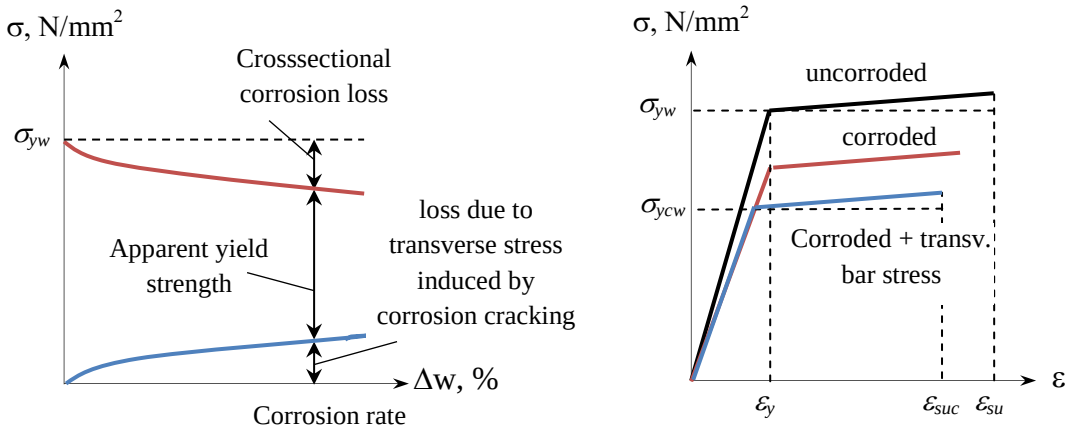

Fig. 5-2 (a) Apparent yield strength of transverse bar (b) Constitutive law for reinforcement

5.2.2 Deterioration model for concrete

Concrete damage induced by corrosion in the form of diffusion of corrosion product or aggressive agent into concrete pores and cracking of surrounding concrete due to expansion of corrosion products need to be considered. The diffusion process of aggressive agents within the concrete matrix is very complex and available knowledge is insufficient. Herein, the concrete damage by corrosion is only corresponding to cracking or spalling of concrete cover. If the surrounding concrete around corroded reinforcement has been cracked, it indicates that the tensile strength of concrete has been reached. Thus, any further tensile stress generated by mechanical loading provoked larger cracking. Depending on the position and direction, cracked concrete will affect to load carrying capacity, stiffness and force distribution in the structure.

For concrete in tension, the cracking damage of concrete induced by expansion of corrosion product is introduced by reducing the tensile strength from its tensile strength of sound concrete (Fig. 5-3(a)). The reduction rate is determined based on the relation of average concrete tensile strength and corrosion rate as obtained from the experimental tension test described in Chapter 3. Thus, the tensile strength of cracked concrete can be described as follows

$$\sigma_{t.cracked} = (1 - 0.1125\Delta w)\sigma_t \geq 0.55\sigma_t \tag{5-11}$$

where $\sigma_{t.cracked}$ and σ_t are tensile strength of cracked and sound concrete, respectively. Δ_w is corrosion percentage of reinforcement.

For cracking of concrete in the compression region, lower concrete strength also should be considered than the sound concrete strength (Fig. 5-3(b)). Here, the reduction in compressive strength is assumed to be proportional to the reduction of the tensile strength. Thus, the tensile strength of cracked concrete is as follows

$$\sigma_{Bcracked} = \frac{\sigma_{tcracked}}{\sigma_t}\sigma_B \tag{5-12}$$

where $\sigma_{B.cracked}$ and σ_B are compressive strength of cracked and sound concrete, respectively.

In finite element analysis, the cracked concrete can be modeled as same geometry with the sound concrete, but the material properties was modified (Fig. 5-4). If corrosion caused spalling of concrete cover, the effect of cover loss can be considered by modifying the geometry of element in the analysis[53].

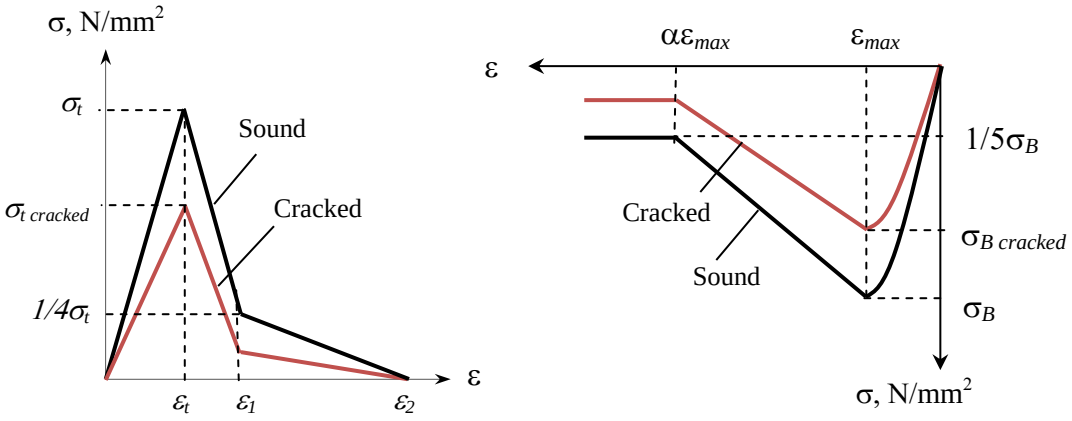

(a) Tensile stress-strain curve (b) Compressive stress-strain curve

Fig. 5-3 Constitutive laws for concrete (a) in compression (b) in tension

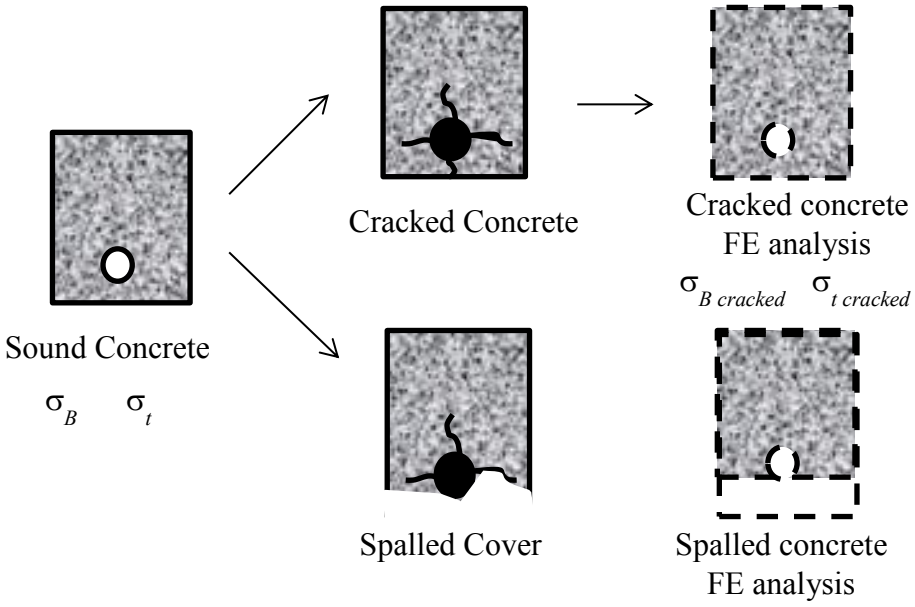

Fig. 5-4 Modeling of cracked or spalled concrete

5.2.3 Deterioration model for bond between concrete and reinforcement

The interaction between reinforcement and surrounding concrete is governed by bond stress and normal splitting stress. The present of corrosion of reinforcement may weaken the bond between concrete and reinforcement and reduce the bond capacity caused by splitting stress induced by corrosion product expansion and corrosion layer between both materials. Several influencing factors such as corrosion penetration, confinement of concrete cover and transverse reinforcement, bar position, and current density have been identified affecting the bond strength of corroded reinforcement[25,28].

The presence of transverse bar has a significant influence on the bond splitting capacity of corroded reinforcement[54,55]. The influence of transverse bar ratio on bond splitting deterioration of corroded reinforcement has been experimentally investigated and discussed in Chapter 4. The formula to determine bond strength from various

One dimensional model of bond-slip relationship for uncorroded reinforcement has been used to analyze the structural performance of RC structures and adopted in the code[8]. As illustrated in Fig. 4-8, the bond-slip response of corroded reinforcement is a combined action of bond strength deterioration and slip decrease at peak bond stress with increasing corrosion levels representing the brittle behavior of bond-slip response. A simple bond-slip model as shown in Fig.5-5 has been proposed which developed from Hayashi's bond-slip model. The formulation of the bond stress-slip relations for corroded reinforcement was described in Chapter 4.4.

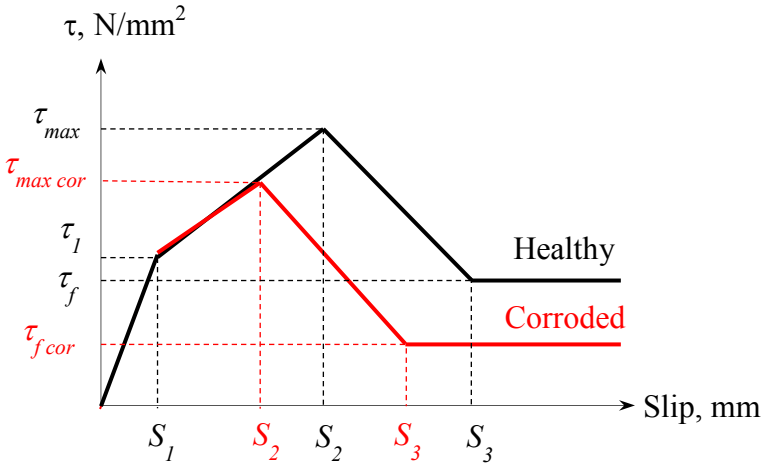

Fig. 5-5 Proposed bond-slip model

5.3 NUMERICAL SIMULATIONS FOR ASSESSMENT OF CORRODED RC BEAMS

5.3.1 Model Parameters

Some of RC beams tested by El Maaddawy[56] have been modeled with an emphasis to evaluate the interaction between degree of corrosion and the load carrying capacity of RC beams having corroded longitudinal bars. Table 5-1 shows the specimen categories based on time exposure and corrosion loss. Table 5-2 and Table 5-3 show concrete and reinforcement properties of specimens. The typical bar arrangement of beams is shown in Fig. 5-6. From the figure the corroded region is in the bottom longitudinal bars in the middle of beams with exposed length of 1400 mm. The transverse bars at corroded region are protected from corrosion by anti-corrosion epoxy resin and plastic tape. The loading system applied four-point bending having constant moment in the middle third

of beam and the longitudinal reinforcements were well-anchored in the support because no corrosion applied at the end third of beam.

Table 5-1 Specimen conditions

Specimen	Time corrosion exposure days	Measured Corrosion loss %	Max. Crack width mm
Virgin	0	0	0
CN-50	50	8.9	0.9
CN-110	110	14.2	1.2

Table 5-2 Concrete properties of beams

Compresive strength N/mm^2	Splitting strength N/mm^2	Elastic modulus N/mm^2
40	2.5	29725

Table 5-3 Reinforcement properties of beams

	Yield stress σ_y (N/mm^2)	Yield strain ε_y (μ)	Tensile strength σ_{max} (N/mm^2)
D15	450	2250	585
ϕ8	340	1700	500

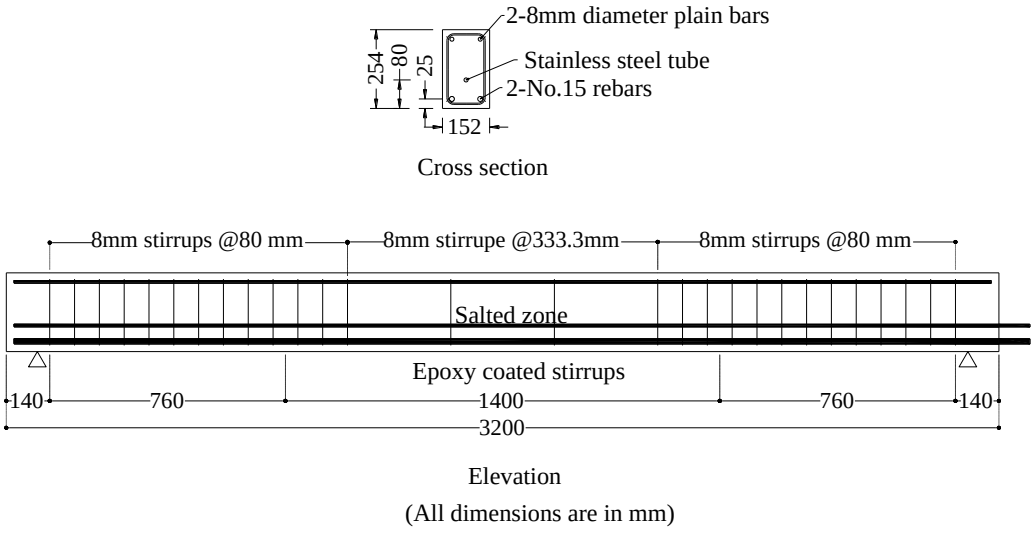

Fig. 5-6 Typical test specimens[56]

The beams were studied in the plane stress analysis as shown in Fig. 5-7. The concrete is modeled by eight-node quadrilateral plane stress element with a thickness equal to width of beam section. The longitudinal bars were represented by two-node truss elements with interface element having bond-slip relations while the transverse bars are modeled as embedded reinforcement with perfect bond. The nonlinear constitutive models for each component were taking into account as shown in Fig. 5-8.

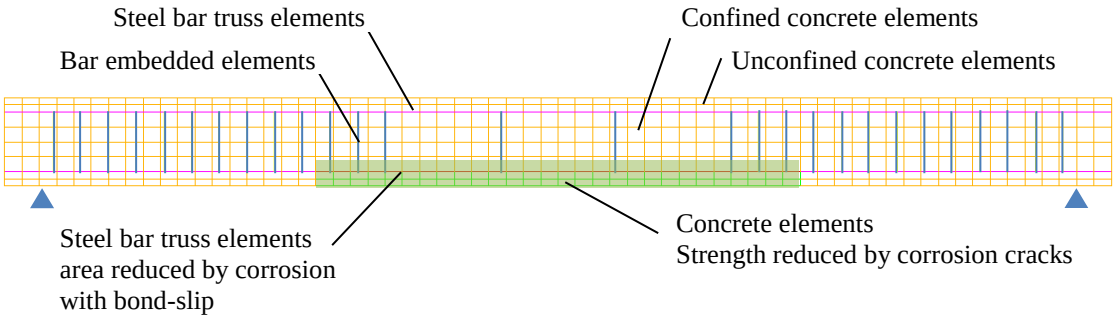

Fig. 5-7 FE model of corroded RC beam

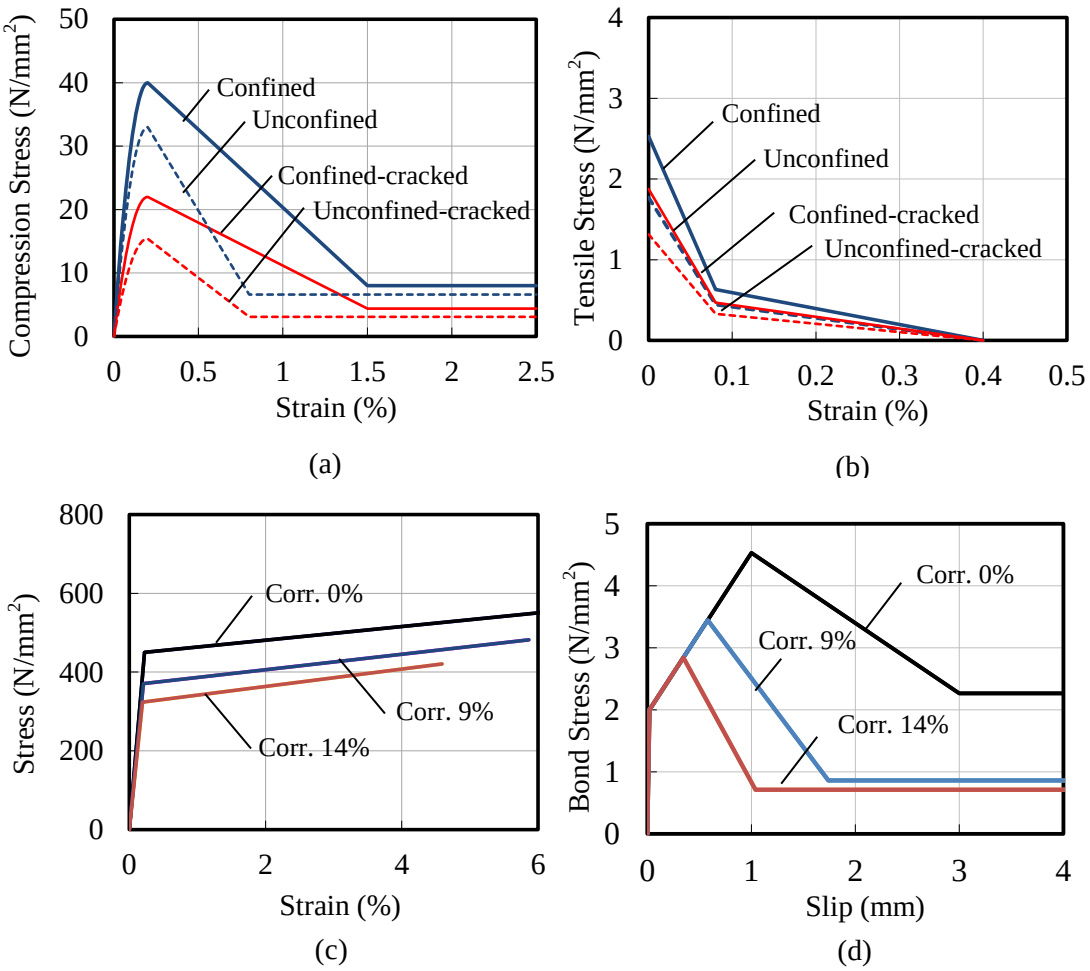

Fig. 5-8 Mechanical properties of corroded RC beam

5.3.2 Numerical results

Fig. 5-9 shows load and mid-span deflection relationships of beams under vertical monotonic loading. The experimental and analytical results show that corrosion of longitudinal reinforcement decrease the load carrying capacity of corroded beams due to sectional loss of reinforcement. The effect of corrosion also influenced the deflection capacity which is the deflection at beam failure. As shown in Fig. 5-9, the experimental test showed that the deflection capacity of corroded beam having 9% and 14% of weight loss of bottom longitudinal reinforcement increased the deflection. This could be attributed to (a) the deflection increase as decrease of tensile reinforcement area because the same concrete and compression steel area in the compression region, and (b) the bond deterioration due to corrosion caused an increase in beam deflection. However, for higher corrosion level the decrease of deflection capacity was also due to reduction of maximum steel elongation as result of formation of pitting corrosion[39,57].

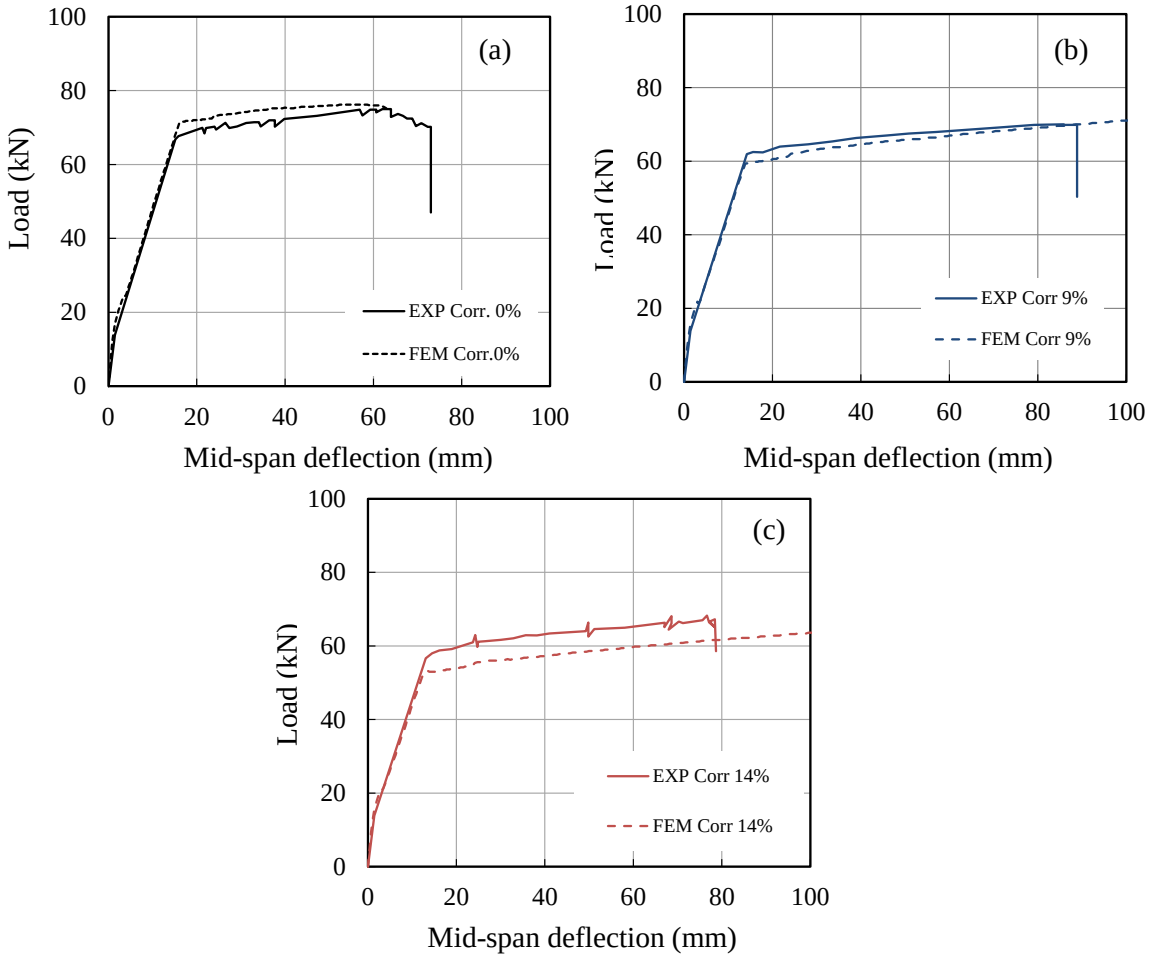

Fig. 5-9 Load – midspan deflection relationships

As shown in Fig. 5-9 the predicted load-deflection curve from current numerical analysis shows a good agreement with the experimental test data on determining the yielding strength and ultimate deflection of corroded RC beams. Some differences on the results between experiment and analysis can be attributed to variation in the prediction of yield strength and concrete crushing.

5.4 NUMERICAL SIMULATIONS FOR ASSESSMENT OF CORRODED RC COLUMNS

5.3.3 Model parameters

To simulate the effect of corrosion on structural performance of corroded reinforced concrete columns, some RC columns were modeled with special attention in transformation of material and geometrical properties of reinforcements, concrete and bond properties due to corrosion. The geometry of column and the reinforcement arrangement are described in Fig. 5-10. The configuration of column is based on the experimental test conducted by Shinohara et al.[58]. Some modification was made by changing the longitudinal bar diameter and the steel strength of longitudinal and transverse bars to make the column failed in flexure for uncorroded columns. The mechanical properties of current concrete and steel reinforcement are summarized in Table 5-4 and Table 5-5.

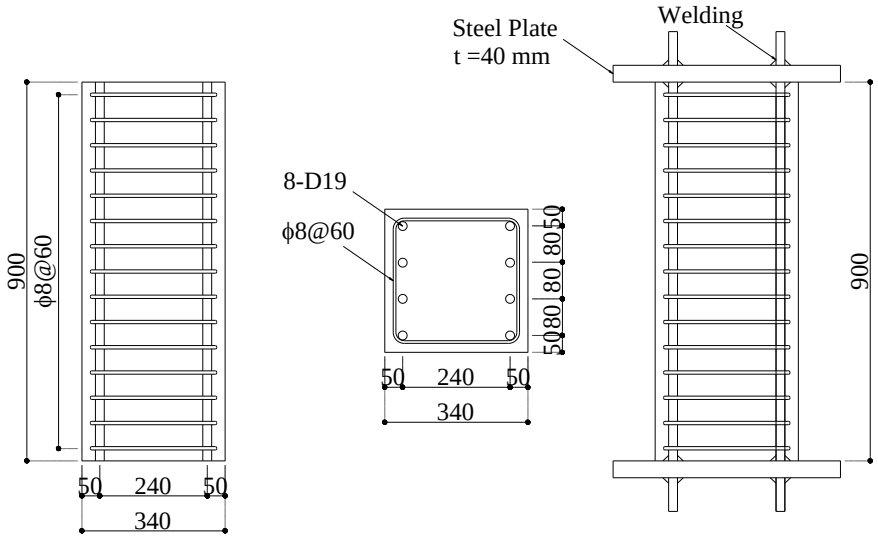

Fig. 5-10 Geometry and bar arrangement of column test

Table 5-4 Concrete properties of column

Concrete	σ_B (N/mm^2)	ε_{max}	E_c (N/mm2)	α	σ_t (N/mm^2)	W_1 (mm)	W_2 (mm)	v
Core	48	0.002	3.43E+04	10 - 40	2.8	0.032	0.16	0.2
Cover	34	0.002	2.74E+04	4	1.8	0.032	0.16	0.2

Table 5-5 Reinforcement properties of column

Type	σ_y (N/mm^2)	E_s (N/mm^2)	v
D19	345	2.00×10^5	0.3
ϕ8	295	2.00×10^5	0.3

To simulate the corrosion effect, three different corrosion levels are considered i.e. 3%, 6% and 10% including the uncorroded columns as reference. Both longitudinal and transverse bars are assumed to have the same of corrosion levels. The stress generated on transverse bars due to expansion of corrosion product is considered to be taken into account in the analysis using the apparent yield strength of transverse bar as mentioned in section 5.2.3. The constant axial load ratio of 0 and 0.1 are given in the columns. The material and bond properties corresponding to corrosion level are summarized in Table 5-6 and Table 5-7.

Table 5-6 Material properties corresponding to corrosion level

Test	Corr. level %	Concrete		Longitudinal bar		Transverse bar		Axial Load ratio σ_0/σ_B
		σ_B N/mm^2	E_c N/mm^2	σ_y N/mm^2	E_s N/mm^2	σ_{yw} N/mm^2	E_{sw} N/mm^2	
N 00-C 00	0	48	3.43E+04	345	2.00E+05	295	2.05E+05	0
N 00- C 03	3	32	2.67E+04	325	1.93E+05	215	1.98E+05	0
N 00- C 06	6	26	2.41E+04	304	1.86E+05	140	1.91E+05	0
N 00- C 10	10	26	2.41E+04	277	1.71E+05	39	1.82E+05	0
N 10- C 00	0	48	3.43E+04	345	2.00E+05	295	2.05E+05	0.1
N 10- C 03	3	32	2.67E+04	325	1.93E+05	215	1.98E+05	0.1
N 10- C 06	6	26	2.41E+04	304	1.86E+05	140	1.91E+05	0.1
N 10- C 10	10	26	2.41E+04	277	1.71E+05	39	1.82E+05	0.1

Table 5-7 Bond properties corresponding to corrosion level

Corrosion level	τ_1 N/mm^2	τ_{max} N/mm^2	Slip at τ_1 mm	Slip at τ_{max} mm
0%	2	5.6	0.02	1.00
3%	2	5.26	0.02	0.91
6%	2	4.93	0.02	0.82
10%	2	4.48	0.02	0.70

A nonlinear finite element model using DIANA program was used here to analysis the corroded column behavior. The mesh generate on the column model is shown in Fig. 5-11. The concrete is modeled by eight-node quadrilateral plane stress element with a thickness equal to the width of column section. The longitudinal bars are represented by two-node truss elements with interface element connecting the concrete element and

rebar element exhibiting a relative slip between both materials, while the transverse bars are modeled as embedded reinforcement with perfect bond. The nonlinear constitutive models for each component are taking into account. The elastoplastic stress-strain relation for reinforcement, the incremental stress-strain relationship for concrete with smeared cracks and bond stress slip relationship as proposed in Chapter 4 were adopted. The parameters such as material strength, stiffness and softening are specified on the basis of the corrosion level as described in Chapter 5.2 and summarized in Table 5-6 and Table 5-7. The numerical analysis was performed on the basis of displacement control up to top deflection of 20 mm which the specimens reach the maximum capacity.

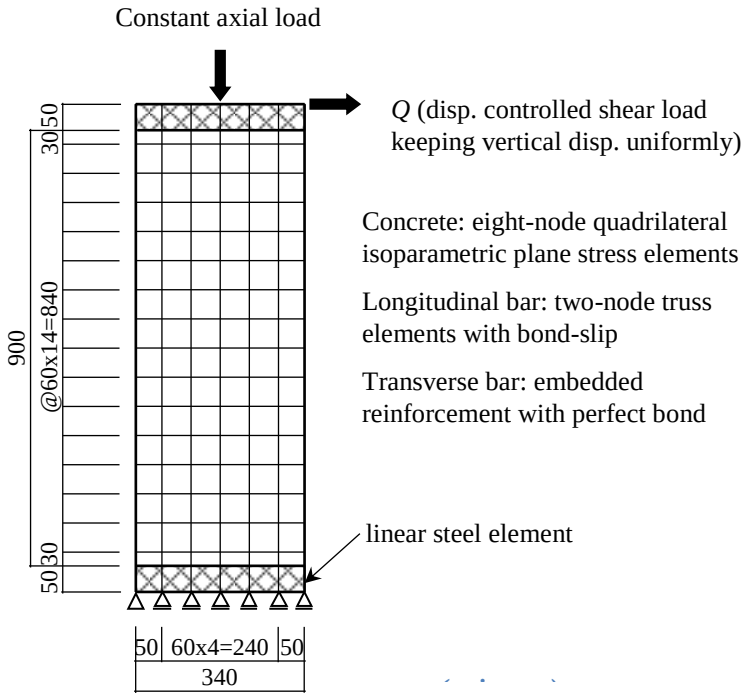

Fig. 5-11 Finite element mesh of reinforced concrete column

5.3.4 Numerical results

Fig. 5-12 shows the shear force and rotation response of columns under lateral monotonic loading. The analysis result indicates the stiffness deterioration of corroded column as shown in the shear force and rotation response presented in Fig. 5-12 for both pre-cracking and post-cracking stages. The stiffness decay can be explained from the chain of events corresponding to the formation of bending cracks, bending shear cracks, crushing of concrete cover, yielding of longitudinal bars or partial failure of bond. In general a decreasing load levels with an increasing of corrosion levels are identified corresponding to the different crack events.

The shear force-rotation response of healthy column is firstly specified by formation of bending crack mostly located at top and bottom of column, followed by bending shear cracks and then yielding of longitudinal bar until reaching the maximum force as shown

in Fig. 5-12. Compared to the corroded columns, the cracking events is almost the same with the healthy column except for specimen N10-C06 and N10-C10. It shows that larger corrosion level increases the possibility to have shear cracking at low load level or to have shear failure before yielding of longitudinal bars for column with corroded bars having 6% (N10-C06) and 10% (N10-C10) of corrosion level as shown in Fig. 5-12(b). This can be attributed to the lower apparent yield strength of transverse bar induced by corrosion cracking due to corrosion expansion. Moreover, the presence of axial load generates much more shear stress in the concrete.

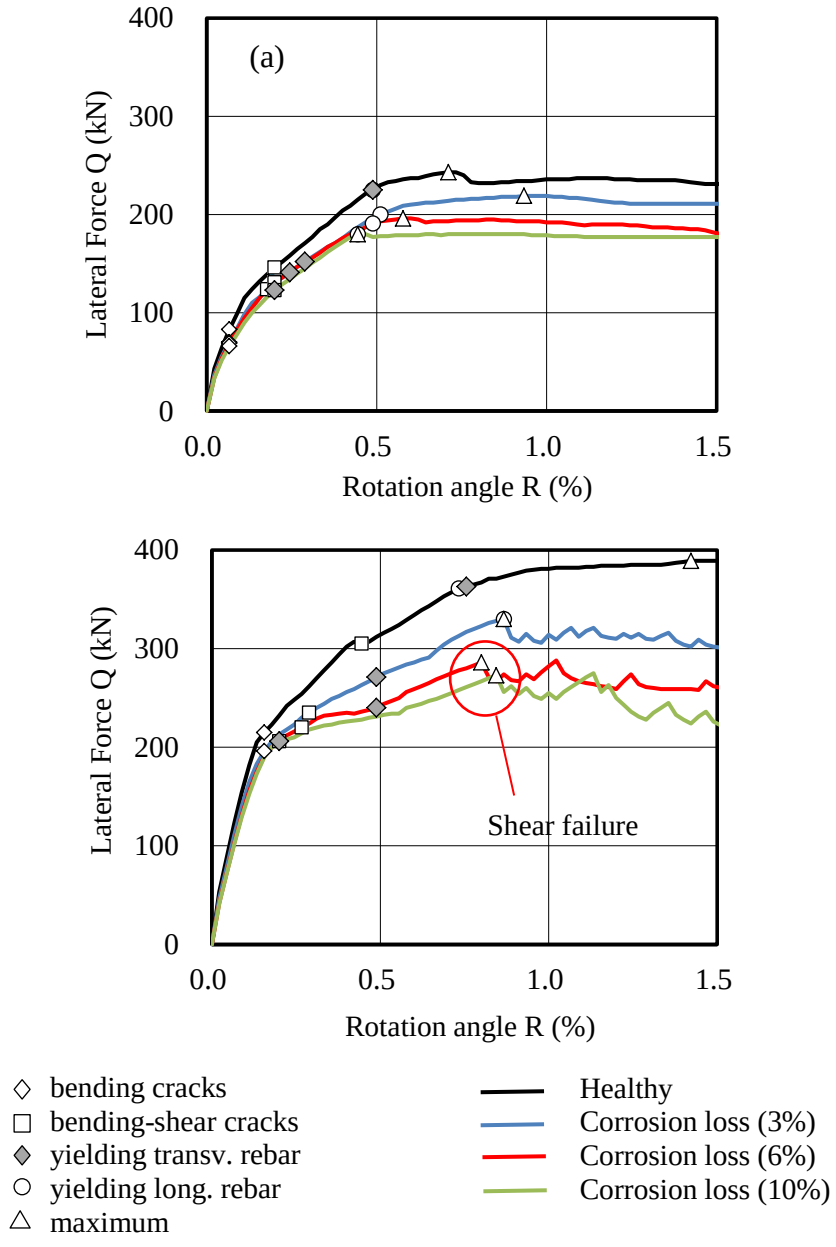

Fig. 5-12 Numerical results of lateral force-rotation responses:
(a) axial load ratio $\sigma_0/\sigma_B = 0$ (b) axial load ratio $\sigma_0/\sigma_B = 0.1$

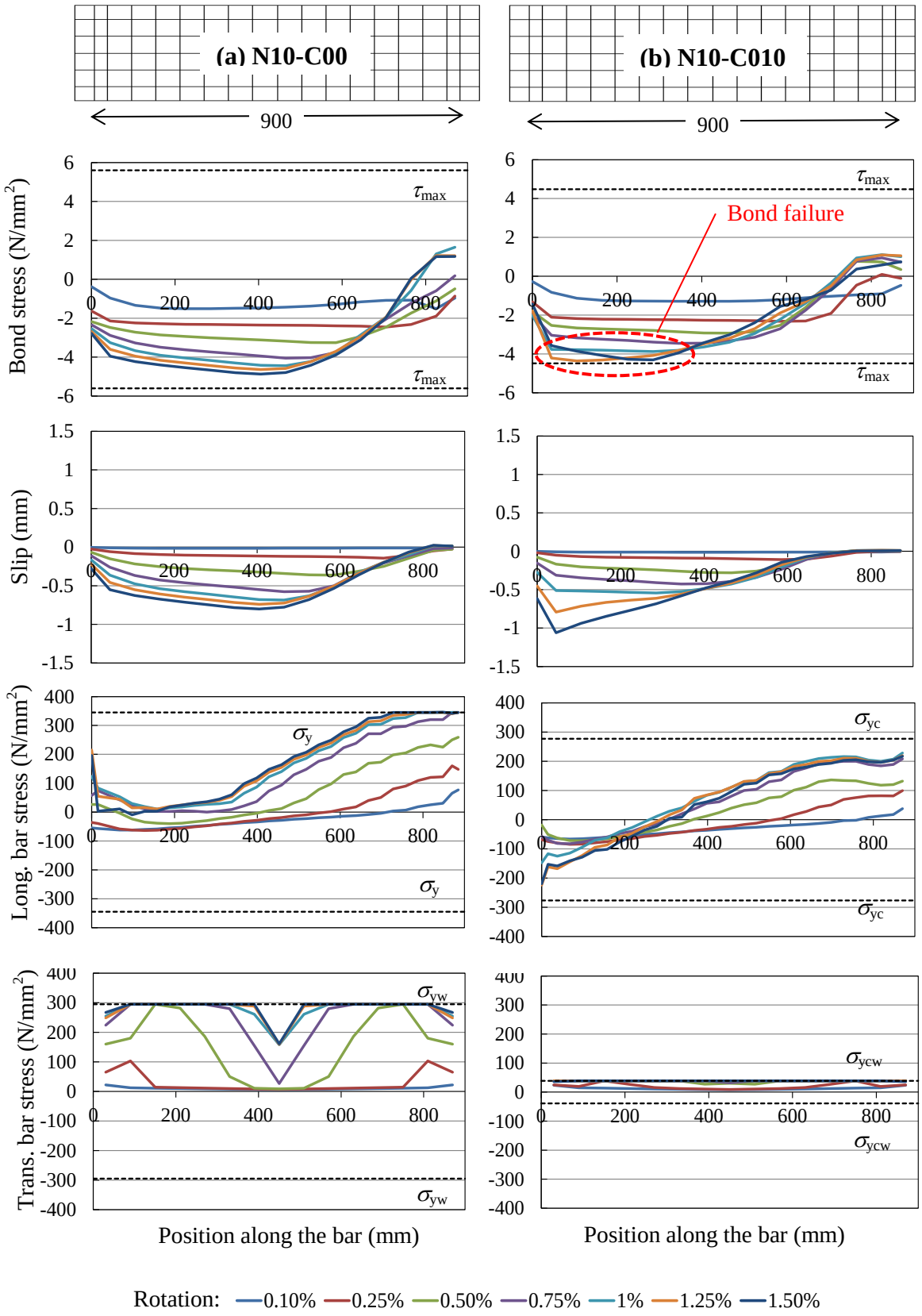

Fig. 5-13 Numerical results of bond stress, slip, longitudinal and transverse bar stress along the bar (a) N10-C00 (b) N10-C10

The effect of corrosion does not only affect to the loss of steel reinforcement and concrete section, but also bond deterioration. Therefore, to consider the effect of bond deterioration on column member particularly on the column N10-C10 who is indicated by shear failure before the yielding of longitudinal reinforcement (Fig. 5-12(b)), the bond stress and slip of longitudinal bar including the longitudinal bar stress and maximum transverse bar stress along the length of column with different rotation levels are presented in Fig. 5-13. As a comparison, the healthy type of column was also analyzed here considering good bond condition as shown in Fig. 5-13(a). The results of bond stress and slip of longitudinal bar including the longitudinal bar stress and maximum transverse bar stress for N10-C03 and N10-C06 is presented in Appendix F.

From the analysis results of the corroded column of N10-C10 it shows that some part of bar reach the maximum bond stress when rotation R was larger than 1.25%. This is also indicated by the large slip along the longitudinal bar after 1.25% of rotation. When the bond is completely lost along the column span different stress distribution took place and the truss mechanism became impaired and the arch action is activated. This analysis also leads to the recognition of the different mode of failure of corroded RC columns from flexural failure preceded by yielding of longitudinal bars to shear (N10-C00 and N10-C03) and shear failure before bar yielding (N10-C06 and N10-C10) which indicate a brittle behavior.

Another possibile critical event for bond loss is the anchorage failures, but in this case the reinforcement anchorages are assumed to be perfectly anchored. In addition, once cover of column cracks because of corrosion or cover spalling in compression region, the compressed reinforcement tends to buckle. However, the buckling of reinforcement is not taken into consideration in this study.

Cracking behaviors

Fig. 5-14 and Fig. 5-15 show distribution of crack strain obtained from FE analysis at R = 0.5% and at maximum lateral force (Q_{max}) for the healthy and the corroded columns i.e. 3%, 6% and 10% of corrosion loss. As shown in Fig. 5-14, there were no so much different of maximum crack strain at rotation R=0.5%, however with an increasing corrosion level the crack region became wider indicated by larger area of higher crack strain. Meanwhile, the maximum crack strain at maximum lateral force (Q_{max}) tended to decrease with increasing corrosion level reflecting the bond deterioration.

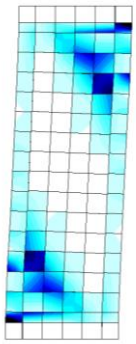

$Cr_{max.}$=0.0152
N00-C00 (Q=225 kN)

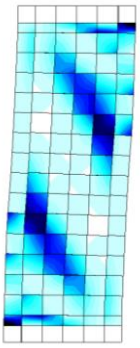

$Cr_{max.}$=0.0134
N00-C03 (Q=199 kN)

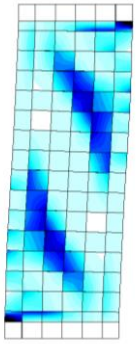

$Cr_{max.}$=0.0141
N00-C06 Q=194 kN

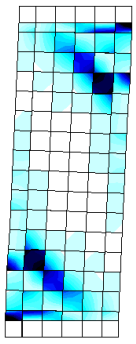

$Cr_{max.}$=0.0166
N00-C10 Q=172 kN

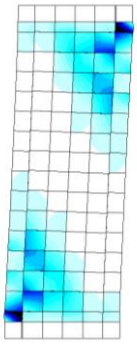

$Cr_{max.}$=0.0124
N10-C00 Q=312 kN

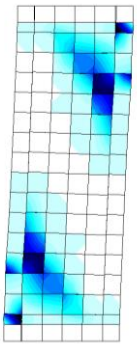

$Cr_{max.}$=0.0113
N10-C03 Q=277 kN

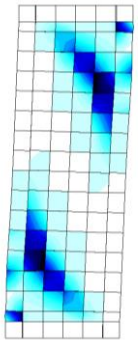

$Cr_{max.}$=0.0115
N10-C06 Q=252 kN

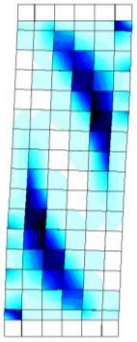

$Cr_{max.}$=0.0108
N10-C10 Q=249 kN

Crack strain level (%)

Fig. 5-14 Crack strain level of columns when R=0.5%

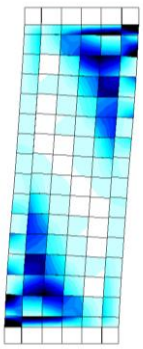

$Cr_{max.}$=0.0228
N00-C00 (R=0.71%)
Q_{max}=243 kN

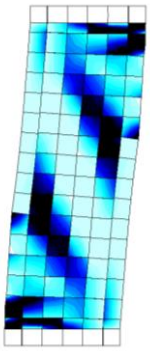

$Cr_{max.}$=0.0225
N00-C03 (R=0.89%)
Q_{max}=219 kN

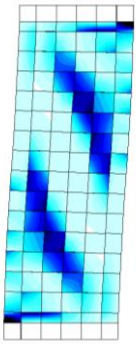

$Cr_{max.}$=0.0172
N00-C06 (R=0.58%)
Q_{max}=196 kN

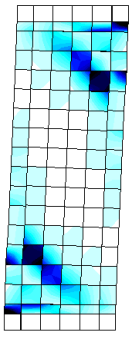

$Cr_{max.}$=0.0166
N00-C10 (R=0.44%)
Q_{max}=180 kN

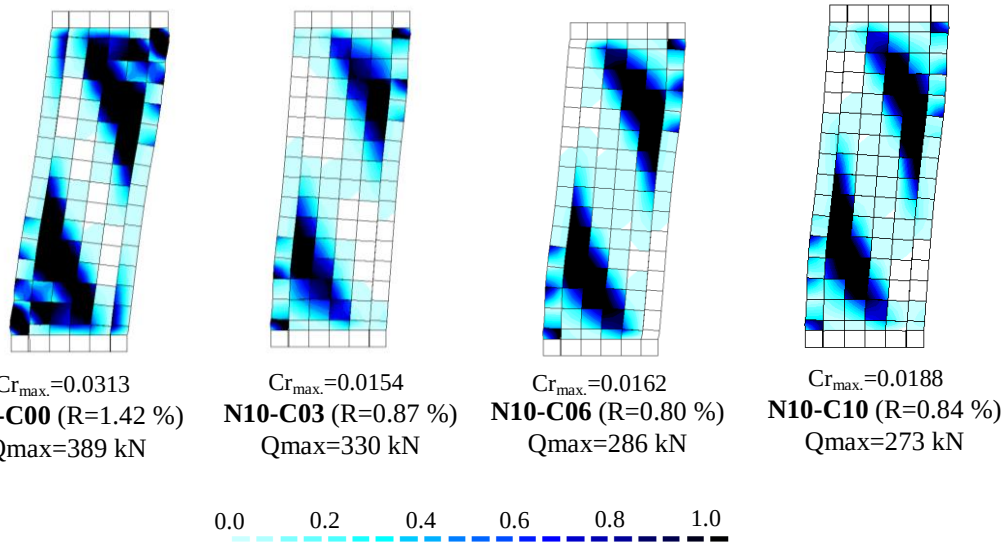

Fig. 5-15 Crack strain level of columns when Qmax

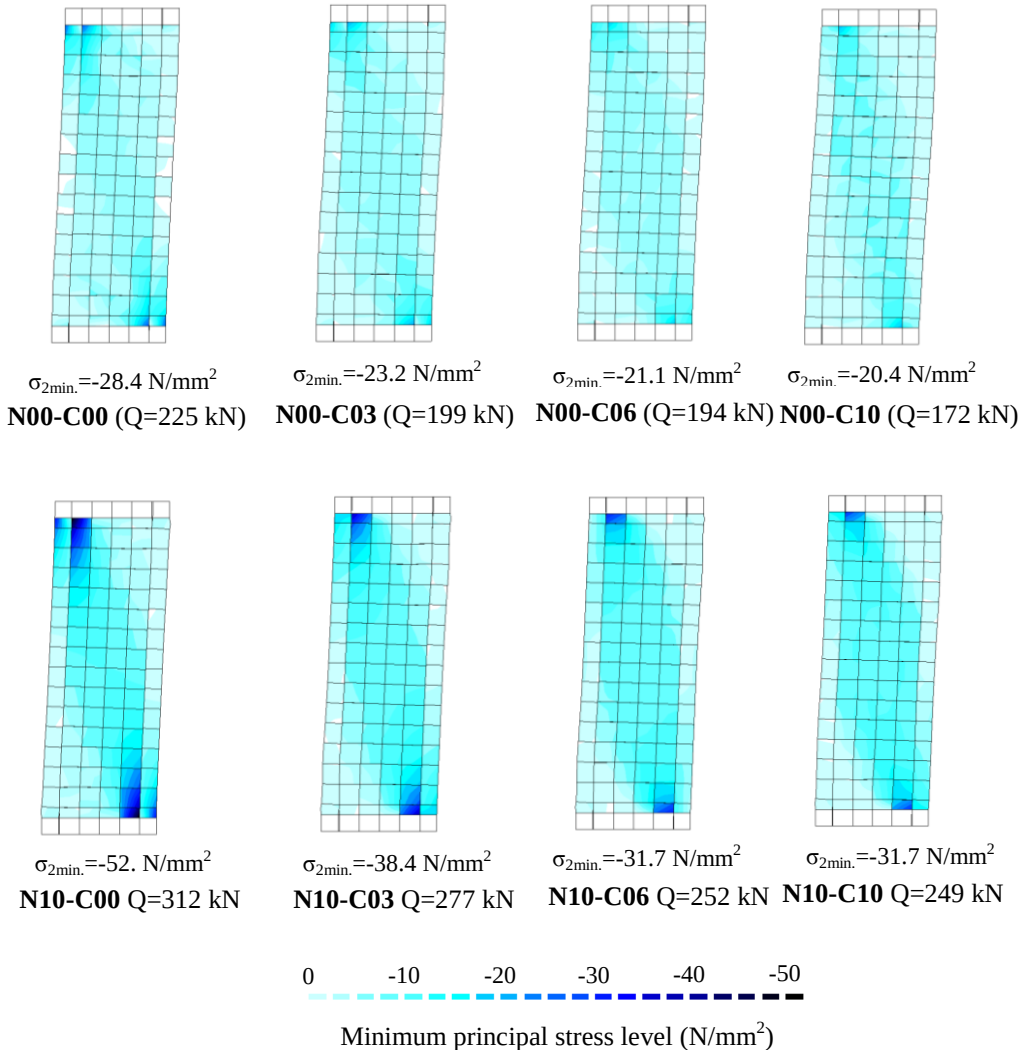

Fig. 5-16 Minimum principal stress of columns when R=0.5%

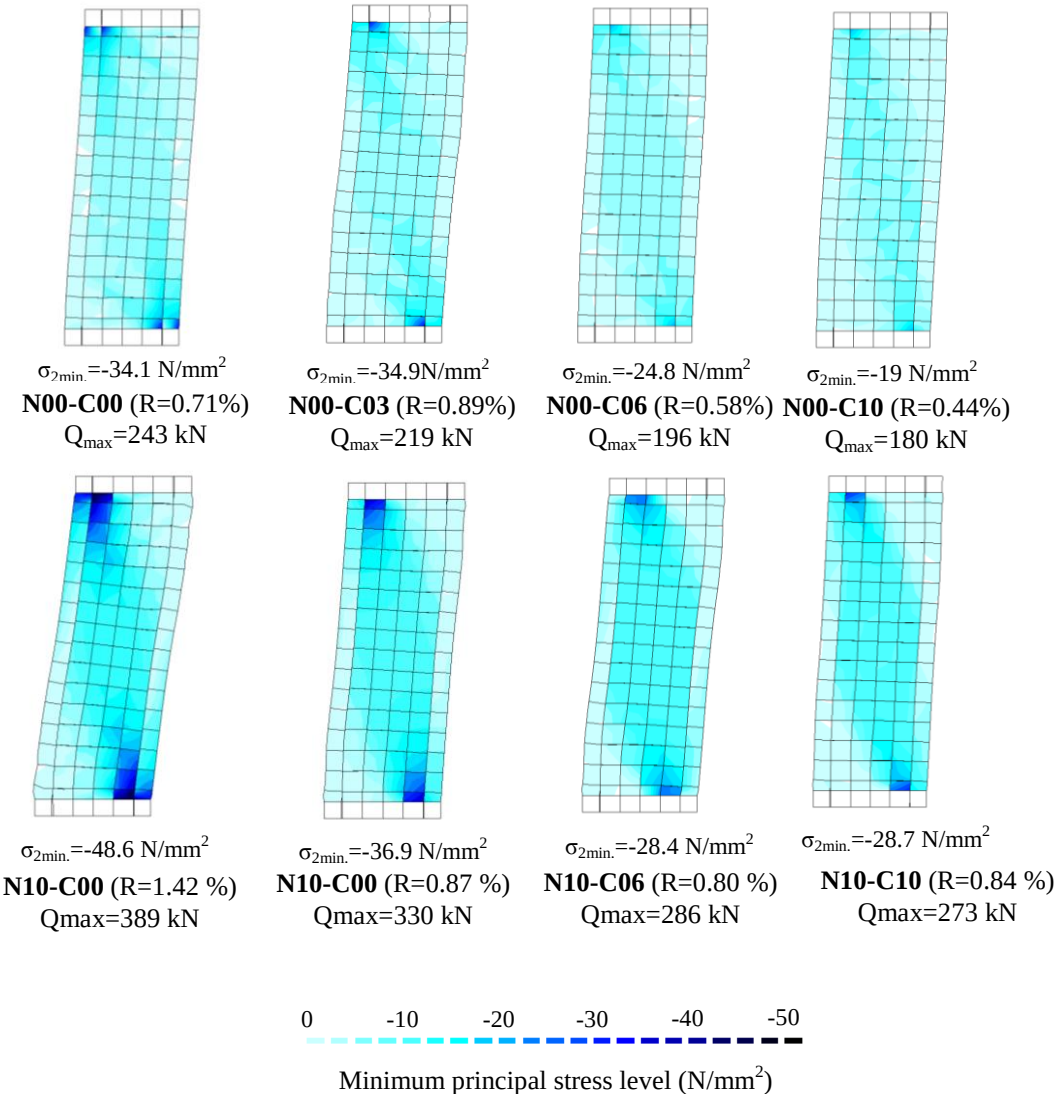

Fig. 5-17 Minimum principal stress of columns when Qmax

The minimum principal stress at R = 0.5% and at maximum lateral force (Q_{max}) are also presented in Fig. 5-16 and Fig. 5-17. Moreover, the minimum principal strains of concrete tended to decrease with an increasing corrosion level corresponding to the deterioration of concrete material properties. As shown in Fig. 5-17 the presence of axial load also increase the minimum principal strains. The effect axial load showed an extensive shear cracking at failure since larger axial load produces larger shear stresses in the concrete.

5.5 SUMMARY OF CHAPTER FIVE

In order to assess the structural performance of corroded reinforced members on the prediction the serviceability and the safety performance, the numerical analysis through finite element modeling can be used as useful instrument. In this chapter, the key parameters of geometrical and material properties of structural element such as concrete, reinforcement and their bond links on the basis of corrosion deterioration which obtained from the previous experimental test described in Chapter 2 to Chapter 4 are integrated to simulate the behavior of corroded RC beams and columns using finite element analysis.

The deterioration of reinforcement, concrete and bond properties in the numerical analysis may be recognized in the difference of chain of event i.e. bending crack, bending shear cracks, and yielding of longitudinal, bond failure and shear cracking which is characterized from the structural responses for different corrosion levels. The stiffness and strength deterioration due to corrosion of reinforcement are identified from the analysis which reflected by a decreasing load levels with an increasing of corrosion levels corresponding to different events, i.e. bending crack, bending shear cracks, yielding of longitudinal and shear cracking.

From the analysis results, several phenomena should be considered when assessing the corroded RC elements. Not only reduction of reinforcement cross sectional area of reinforcement and the bond deteriorations should be taken into account, but also the reduction of concrete strength due to corrosion cracking and the apparent strength of transverse bars. These aspects contribute to the stiffness deterioration as well as the strength and ductility of structures when corrosion is involved. The analysis showed that shear became a critical point in the presence of axial load and lower apparent strength of transverse bars since the larger axial loads produce larger shear stresses in the concrete.

Moreover, further research is required in the assessment of shear strength of corroded column including detail experimental data since the number of studies on the structural response of corroded RC columns is still limited.

- blank page -

Chapter Six

CONCLUSIONS

Chapter 6
CONCLUSIONS

6.1 SUMMARY AND CONCLUSIONS

This research aimed to improve the knowledge of the structural behavior of deteriorated reinforced concrete members with focus on evaluating the effect of corrosion on cracking behavior and bond behavior between reinforcement and concrete. The research program encompassed both laboratory experiments and numerical simulations to study the structural performance of deteriorated RC members. The major conclusions of this research are summarized in this chapter.

The influence of corrosion on the cracking behavior in term of crack initiation and crack propagation due to corrosion product expansion were investigated through experiment of accelerated corrosion test. Based on this experiment combined with the non-linear finite element analysis, the relations between corrosion loss and cover crack width and corrosion loss and stress on transverse bar were obtained. The important conclusions of this work are listed here

- The test results show that corrosion loss among longitudinal bars in a beam is not uniformly distributed. This is caused by the different positions in casting direction and chloride diffusion direction and the different of water and oxygen availability. The different in corrosion distribution among longitudinal bars influence the distribution of internal pressure (loading pattern) due to corrosion product expansion. Based on numerical simulations, the uneven corrosion distribution among longitudinal bars, influence the cracking pattern but it does not influence the crack width so much if the average corrosion rate is considered.
- The test carried out in this thesis showed a significant influence of concrete strength on the crack width growth due to corrosion product expansion. Larger crack width was generated on cover for high strength concrete compared to normal concrete. This can be due to lower porosity of high strength concrete which prevent corrosion product to penetrate to the surrounding concrete and generate larger expansion. Meanwhile, the presence of confinement up to 0.3% of transverse bar ratio showed an insignificant effect on the crack width growth.

- Larger stress in transverse bars was identified for high strength concrete specimen corresponding to larger crack opening. This stress on transverse bar may reduce the residual shear capacity of RC structures, particularly when using normal strength of transverse bars.
- The numerical approach through non-linear finite element analysis of corrosion-induced cover cracking showed a reasonable agreement with the experimental results. However, a larger volume increase ratio of corrosion product is required in the model when evaluating member with high strength concrete since the diffusion of corrosion products into concrete pores and cracks was not considered in the present analysis.

The influences of corrosion on bond behavior of reinforcement steel in concrete were studied through the experiments from tensile and pullout test with special attention to the effect of corrosion and different of confinement by mean of transverse bars. The main conclusions of this work are summarized here

- From the experimental test of tension member, the average crack spacing decreased with increasing of corrosion level up to 4% of corrosion level. This is mainly due to the increasing of bond stress for small corrosion level up to 1% and to the decreasing of concrete tensile strength induced by cracks around corroded bar for higher corrosion levels. Based on the analysis of experimental results, the relation between the reduction of concrete tensile strength and corrosion level was formulated.
- From the numerical analysis of tension member, it was shown that the maximum bond stress and bond stiffness are important parameters of bond-slip relationship on predicting overall tension stiffening and cracking behavior. The bi-linear ascending curve of bond stress-slip relation produced a good agreement with the experimental results on predicting tension stiffening and cracking behavior, because it had higher initial bond stiffness and followed by lower bond stiffness for further loading due to growth in splitting cracks and presence of the soft layer of corrosion rust.
- From the pullout test results the different behavior of bond stress-slip relationship between uncorroded and corroded reinforcement was observed from the experimental tests. Compared to uncorroded reinforcement, lower maximum bond stress and smaller slip at maximum bond stress was shown for corroded reinforcement and after reaching maximum bond stress, the bond rapidly deteriorated for corroded reinforcement. Using the available test data, the simple bond stress-slip relationship for corroded reinforcement was developed. The bond-slip model was then applied to the analysis of corroded columns using non-linear finite element simulations.
- The significant contribution of transverse bars to maintain residual bond splitting strength for corroded specimens was identified. The more transverse bar is

provided, the higher residual bond splitting strength is generated. As long as adequate amount of transverse reinforcement took in place in the section, the bond must not completely impair whether corrosion cracks occur on the concrete cover. The test results showed minor influence of bar location in casting direction on the bond splitting capacity and bond stress-slip relationships were observed for both corroded and healthy RC members.

The knowledge obtained through accelerated corrosion and bond test was implemented in the finite element method which can be used for the assessment of corroded RC structures. The application in analysis considering the changes of geometry and material properties of concrete and reinforcement and bond properties on the basis of corrosion deterioration.

From the numerical analysis results of corroded RC columns, some phenomena of change in the events of structural response were identified. Several aspects should be considered when assessing the corroded RC elements which contribute to the stiffness deterioration as well as the strength and ductility of structures when corrosion effects involved. Not only reduction of reinforcement cross sectional area of reinforcement and the bond deteriorations should be taken into account, but also the reduction of concrete strength due to corrosion cracking and the apparent strength of transverse bars. The analysis showed that shear became a critical point in the presence of axial load since the larger axial load produces larger shear stresses in the concrete and lower apparent strength of transverse bars which reduced the contribution of transverse bars on shear capacity.

6.2 SUGGESTIONS FOR FUTURE RESEARCH

The research on corrosion induced cover cracking in term of mechanical properties of corrosion rust and deformability of corrosion product in the surrounding concrete need to be improved. The corrosion model which takes into account the effect of rust diffusion into concrete pores and rust flowing through crack opening needs to be further developed since it would be useful for further verification and calibration of model on prediction of corrosion rate through observed crack width.

Little experimental data is available for the bond behavior with corroded transverse bar and its effect on the cracking behavior and structural response of RC structures. The present study was limited to the evaluation of corroded longitudinal bar with different and low transverse bar ratio to simulate the reduction of cross-sectional area of transverse bars. Effect of transverse bar stress due to corrosion expansion on structural element need to be more detail investigated considering significant influence on structural performance as shown in simulations. Therefore, further experimental

investigation of the bond of corroded reinforcement considering the effect of corroded transverse bar and stress generated on transverse bar is suggested.

REFERENCES

1. CAESAR. *CAESAR Structural Assessment Report*, Public Work Research Institute (PWRI), Japan. 1–30 (2013).

2. Molina, F. J., Alonso, C. & Andrade, C. Cover cracking as a function of rebar corrosion: Part 2—Numerical model. *Mater. Struct.* **26,** 532–548 (1993).

3. Liu, Y. & Weyers, R. E. Modeling the time-to-corrosion cracking in chloride contaminated reinforced concrete structures. *ACI Mater. J.* **95,** 675–681 (1998).

4. Vu, K., Stewart, M. G. & Mullard, J. Corrosion-Induced Cracking : Experimental Data and Predictive Models. *ACI Struct. J.* **102,** 719–726 (2005).

5. Mullard, J. A. & Stewart, M. G. Corrosion-Induced Cover Cracking : New Test Data and Predictive Models. *ACI Struct. J.* **108,** 71–79 (2011).

6. Andrade, C.; Aloso, C; Molina, F. J. Cover cracking as a function of bar corrosion : Part I-Experimental test. *Mater. Struct.* **26,** 453–464 (1993).

7. ACI Committee 224. *ACI-224R Control of Cracking in Concrete Structures*. (American Concrete Institute, 2001).

8. Committee Euro-International du Béton. *CEB-FIP model code 1990*. (Thomas Telfold, 1993).

9. Sakai, K. ; Shimomura, T. ; Sugiyama, T. in *Concr. Durab. Repair Technol.* 28–44 (1999).

10. Alonso, C., Andrade, C. & Diez, J. M. Factors controlling cracking of concrete affected by reinforcement corrosion. *Mater. Struct.* **31,** 435–441 (1998).

11. Maruyama, K. Cracking behavior of Concrete due to corrosion of reinforcing bars. *Trans. Japan Concr. Inst.* **10,** 505–510 (1988).

12. Morinaga, S. Prediction of service life of reinforced concrete buildings based on the corrosion rate of the reinforcing steel. in *Proceeding 5th Int. Conf. Durab. Build. Mater. components* 5–16 (1990).

13. Rodriguez, J.; Ortega, L. M.; Casal, J. Corrosion of reinforcement and service life of concrete structures. in *Proceeding 7th Int. Conf. Durab. Build. Mater. components* 117–126 (1996).

14. Vidal, T., Castel, a & François, R. Analyzing crack width to predict corrosion in reinforced concrete. *Cem. Concr. Res.* **34,** 165–174 (2004).

15. JCI-SC Committe. *Corrosion of Concrete structures - Standards Test Method for Corrosion Protection*. (Japan Concrete Institute, 1991).

16. Kurumisawa, Kiyofumi; Tanaka, K. Difference in the void structure of each driving height of the cement paste. *Proceeding Japan Concr. Inst. Res.* **23,** 781–786 (2001).

17. Tanaka, K. & Kurumisawa, K. Development of technique for observing pores in hardened cement paste. *Cem. Concr. Res.* **32,** 1435–1441 (2002).

18. Caré, S., Nguyen, Q. T., L'Hostis, V. & Berthaud, Y. Mechanical properties of the rust layer induced by impressed current method in reinforced mortar. *Cem. Concr. Res.* **38,** 1079–1091 (2008).

19. Lundgren, K. Bond between ribbed bars and concrete. Part 2: The effect of corrosion. *Mag. Concr. Res.* **57,** 383–395 (2005).

20. Shinohara, Y. Effect of Axial Load on The Shear-Transfer Mechanism during Shear Damage Progress in R/C Columns. in *3rd fib Int. Congr.* (2010).

21. Diana, T. DIANA Finite Element Analysis. User's Manual Release 9.4.4. (2011).

22. Aryanto, A. & Shinohara, Y. Influence of Bond-Slip Relationship and Tensile Strength on Bond Behavior between Corroded Steel Bar and Concrete. *J. Struc. Const. Eng. AIJ* **78,** 559–567 (2013).

23. Shinohara, Y. Effect of Confinement upon Crack Behaviors caused by Corrosion-Product Expansion around Corroding Bars. in *Proceeding 12th Int. Conf. Durab. Build. Mater. Components* 1577–1584 (2011).

24. Amleh, L. & Mirza, S. Corrosion influence on bond between steel and concrete. *ACI Struct. J.* **96,** 415–423 (1999).

25. Auyeung, Y., Balaguru, P. & Chung, L. Bond Behavior of Corroded Reinforcement Bars. *ACI Mater. J.* **97,** 214–221 (2001).

26. Architectural Institute of Japan. *Design Guidelines for Earthquake Resistant Reinforced Concrete Buildings Based on Inelastic Displacement Concept*. (1999).

27. Almusallam, A. a., Al-Gahtani, A. S., Aziz, A. R. & Rasheeduzzafar. Effect of reinforcement strength corrosion on bond strength. *Constr. Build. Mater.* **10,** 123–129 (1996).

28. Al-Sulaimani, G. J., Kaleemullah, M. & Basunbul, I. A. Influence of Corrosion and Cracking on Bond Behavior and Strength of Reinforced Concrete Members. *ACI Mater. J.* **87,** (1990).

29. Dai, J. & Kato, E. *Cracking and Tension Stiffening Behavior of Corroded RC Members*. 24 (2007).

30. Hayashi, S. & Kokusho, S. Bond Behavior in the Neighborhood of the Crack. *Finite Elem. Anal. Reinf. Concr. Struct. ASCE* 364–373 (1985).

31. Eligehausen, R., Popov, E. & Bertero, V. *Local bond stress-slip relationships of deformed bars under generalized excitations Technical Rep. UCB/EERC-83/23*. (1983).

32. Harajli, M. H., Hout, M. & Jalkh, W. Local Bond Stress-Slip Behavior of Reinforcing Bars Embedded in Plain and Fiber Concrete. *ACI Mater. J.* **92,** 343–354 (1995).

33. Hayashi, S. & Kokusho, S. Bond Behavior in the Neighborhood of the Crack. *Finite Elem. Anal. Reinf. Concr. Struct. ASCE* 364–373 (1985).

34. Mangat, P. S. & Elgarf, M. S. Bond characteristics of corroding reinforcement in concrete beams. *Mater. Corros.* **32,** 89–97 (1999).

35. Berra, M., Castellani, Ã. A., Coronelli, D., Zanni, S. & Zhang, G. Steel – concrete bond deterioration due to corrosion : finite-element analysis for different confinement levels. *Mag. Concr. Res.* **55,** 237–247 (2003).

36. Hanjari, K. Z., Coronelli, D. & Lundgren, K. Bond capacity of severely corroded bars with corroded stirrups. *Mag. Concr. Res.* **63,** 953–968 (2011).

37. Morita, Shinohara, Y. & Hayashi, S. Bond Behavior of RC Members with Corroded Longitudinal Reinforcement. in *Proceeding Ann. Meet. Arch. Inst. Japan, AIJ* 411–414 (2011).

38. Harajli, M. H., Hout, M. & Jalkh, W. Local Bond Stress-Slip Behavior of Reinforcing Bars Embedded in Plain and Fiber Concrete. *ACI Mater. J.* **92,** 343–354 (1995).

39. Coronelli, D. & Gambarova, P. Structural Assessment of Corroded Reinforced Concrete Beams : Modeling Guidelines. **130,** 1214–1224 (2004).

40. Saether, I. Finite element simulation of reinforced concrete beams attacked by corrosion. *Nord. Concr. Res.* **39,** 15–32 (2009).

41. Böhni, H. *Corrosion in Reinforced Concrete Structures*. 248 (Woodhead Publishing Limited, 2005).

42. Broomfield, J. P. *Corrosion of Steel in Concrete*. 240 (Taylor & Francis, 2003).

43. Gonzalez, J. A. *et al.* Some questions on the corrosion of steel in concrete - Part I: When, how and how much steel corrodes. *Mater. Struct.* **29,** 40–46 (1996).

44. Val, D. V, Stewart, M. G. & Melchers, R. E. Effect of reinforcement corrosion on reliability of highway bridges. *Eng. Struct.* **20,** 1010–1019 (1998).

45. Almusallam, A. A. Effect of degree of corrosion on the properties of reinforcing steel bars. *Constr. Build. Mater.* **15,** 361–368 (2001).

46. Cairns, J., Plizzari, G. A., Du, Y., Law, D. W. & Franzoni, C. Mechanical Properties of Corrosion-Damaged Reinforcement. *ACI Mater. J.* **102,** 256–264 (2005).

47. Du, Y. G., Chan, a. H. C. & Clark, L. a. Effect of corrosion on ductility of reinforcing bars. *Mag. Concr. Res.* **57,** 407–419 (2005).

48. Du, Y. G., Clark, L. a. & Chan, a. H. C. Residual capacity of corroded reinforcing bars. *Mag. Concr. Res.* **57,** 135–147 (2005).

49. Apostolopoulos, C. a. & Papadakis, V. G. Consequences of steel corrosion on the ductility properties of reinforcement bar. *Constr. Build. Mater.* **22,** 2316–2324 (2008).

50. Apostolopoulos, C. A. & Michalopoulos, D. The impact of corrosion on the mechanical behavior of steel undergoing plastic deformation. *Mater. Corros.* **58,** 5–12 (2007).

51. Zhang, W., Dai, H., Gu, X. & Wu, S. Effects of Corrosion Pits on Mechanical Properties of Corroded Steel Bars. in *Earth Sp. 2010* 3504–3511 (2010).

52. Lee, H. S., Noguchi, T. & Tomosawa, F. Fundamental study on evaluation of structural performance of reinforced concrete beam damaged by corrosion of longitudinal tensile main rebar by finite element method. *J. Struc. Const. Eng. AIJ* 43–50 (1998).

53. Hanjari, Z., Kettil, P. & Lundgren, K. Analysis of Mechanical Behavior of Corroded Reinforced Concrete Structures. *ACI Mater. J.* **108,** 532–541 (2012).

54. Coronelli, D. Corrosion Cracking and Bond Strength Modeling for Corroded Bars in Reinforced Concrete. *ACI Struct. J.* **99,** 267–276 (2003).

55. Aryanto, A. & Shinohara, Y. Bond splitting capacity of corroded bars confined by various stirrups ratio. in *6th Civ. Eng. Conf. Asian Reg.* (2013).

56. El-Maaddawy, T., Soudki, K. & Topper, T. Long-Term Performance of Corrosion-Damaged Reinforced Concrete Beams. *ACI Mater. J.* **102,** 649–656 (2006).

57. El-Maaddawy, T., Soudki, K. & Topper, T. Analytical model to predict nonlinear flexural behavior of corroded reinforced concrete beams. *ACI Struct. J.* **102,** 550–559 (2005).

58. Shinohara, Y. & Hayashi, S. Effect of axial load on the shear transfer mechanism during shear damage progress in R/C Columns. *J. Struc. Const. Eng. AIJ* **74,** 897–905 (2009).

59. Giuriani, E., Plizzari, G. & Schumm, C. Role of Stirrups and residual tensile strength of cracked concrete on bond. *J. Struct. Eng.* **117,** 1–18 (1991).

60. Plizzari, G. A., Deldossi, M. A. & Massimo, S. Transverse Reinforcement Effects on Anchored deformed Bars. *Mag. Concr.* **50,** 161–177 (2002).

Appendix A

EMPIRICAL CRACK WIDTH CALCULATION

Table. A-1 Empirical crack width calculation for normal concrete

depth penetration	tensile strength	Rodriguez et al.		Vidal et al. v=2			Vu et al					
	N/mm^2	w initial	w prop	ΔAsteel	ΔAsteel.crack	w	r crack	wcp	w	wi	w-wi	x
55	1.9	0.053	**0.08**	3.27	1.97	**0.075**	1.90.E-04	0.84	**0.05**	0.05	0	52.7
60	1.9	0.053	**0.14**	3.57	1.97	**0.092**	1.90.E-04	0.84	**0.10**	0.05	0.05	57.7
70	1.9	0.053	**0.27**	4.16	1.97	**0.126**	1.90.E-04	0.84	**0.15**	0.05	0.1	62.6
80	1.9	0.053	**0.39**	4.75	1.97	**0.160**	1.90.E-04	0.84	**0.20**	0.05	0.15	67.5
90	1.9	0.053	**0.52**	5.34	1.97	**0.194**	1.90.E-04	0.84	**0.25**	0.05	0.2	72.5
100	1.9	0.053	**0.64**	5.93	1.97	**0.228**	1.90.E-04	0.84	**0.30**	0.05	0.25	77.4
110	1.9	0.053	**0.77**	6.52	1.97	**0.262**	1.90.E-04	0.84	**0.35**	0.05	0.3	82.3
120	1.9	0.053	**0.89**	7.11	1.97	**0.296**	1.90.E-04	0.84	**0.40**	0.05	0.35	87.2
130	1.9	0.053	**1.02**	7.70	1.97	**0.330**	1.90.E-04	0.84	**0.45**	0.05	0.4	92.1
140	1.9	0.053	**1.14**	8.29	1.97	**0.363**	1.90.E-04	0.84	**0.50**	0.05	0.45	97.1
150	1.9	0.053	**1.27**	8.88	1.97	**0.397**	1.90.E-04	0.84	**0.55**	0.05	0.5	102.0
160	1.9	0.053	**1.39**	9.47	1.97	**0.431**	1.90.E-04	0.84	**0.60**	0.05	0.55	106.9
170	1.9	0.053	**1.52**	10.05	1.97	**0.465**	1.90.E-04	0.84	**0.65**	0.05	0.6	111.8
180	1.9	0.053	**1.64**	10.64	1.97	**0.498**	1.90.E-04	0.84	**0.70**	0.05	0.65	116.7
190	1.9	0.053	**1.77**	11.22	1.97	**0.532**	1.90.E-04	0.84	**0.75**	0.05	0.7	121.7
200	1.9	0.053	**1.89**	11.81	1.97	**0.566**	1.90.E-04	0.84	**0.80**	0.05	0.75	126.6
210	1.9	0.053	**2.02**	12.39	1.97	**0.599**	1.90.E-04	0.84	**0.85**	0.05	0.8	131.5
220	1.9	0.053	**2.14**	12.97	1.97	**0.633**	1.90.E-04	0.84	**0.90**	0.05	0.85	136.4
230	1.9	0.053	**2.27**	13.56	1.97	**0.666**	1.90.E-04	0.84	**0.95**	0.05	0.9	141.3
240	1.9	0.053	**2.39**	14.14	1.97	**0.700**	1.90.E-04	0.84	**1.00**	0.05	0.95	146.3
250	1.9	0.053	**2.52**	14.72	1.97	**0.733**	1.90.E-04	0.84	**1.05**	0.05	1	151.2
260	1.9	0.053	**2.64**	15.30	1.97	**0.766**	1.90.E-04	0.84	**1.10**	0.05	1.05	156.1
270	1.9	0.053	**2.77**	15.88	1.97	**0.800**	1.90.E-04	0.84	**1.15**	0.05	1.1	161.0
280	1.9	0.053	**2.89**	16.46	1.97	**0.833**	1.90.E-04	0.84	**1.20**	0.05	1.15	165.9
290	1.9	0.053	**3.02**	17.04	1.97	**0.866**	1.90.E-04	0.84	**1.25**	0.05	1.2	170.9
300	1.9	0.053	**3.14**	17.62	1.97	**0.900**	1.90.E-04	0.84	**1.30**	0.05	1.25	175.8

Table. A-2 Empirical crack width calculation for High strength concrete

depth penetration	tensile strength	Rodriguez et al.		Vidal et al. v=2			Vu et al					
	N/mm^2	crack init	crack prop	ΔAsteel	ΔAsteel.crack	width	r crack	wcp	w	wi	w-wi	x
35	2.8	0.032	**0.06**	2.08	0.49	**0.092**	3.02.E-04	0.10	**0.05**	0.05	0	32.4
40	2.8	0.032	**0.13**	2.38	0.49	**0.109**	3.02.E-04	0.10	**0.10**	0.05	0.05	40.2
50	2.8	0.032	**0.25**	2.98	0.49	**0.143**	3.02.E-04	0.10	**0.15**	0.05	0.1	48.0
60	2.8	0.032	**0.38**	3.57	0.49	**0.177**	3.02.E-04	0.11	**0.20**	0.05	0.15	55.8
70	2.8	0.032	**0.50**	4.16	0.49	**0.211**	3.02.E-04	0.12	**0.25**	0.05	0.2	63.6
80	2.8	0.032	**0.63**	4.75	0.49	**0.245**	3.02.E-04	0.13	**0.30**	0.05	0.25	71.4
90	2.8	0.032	**0.75**	5.34	0.49	**0.279**	3.02.E-04	0.14	**0.35**	0.05	0.3	79.2
100	2.8	0.032	**0.88**	5.93	0.49	**0.313**	3.02.E-04	0.15	**0.40**	0.05	0.35	87.0
110	2.8	0.032	**1.00**	6.52	0.49	**0.347**	3.02.E-04	0.15	**0.45**	0.05	0.4	94.9
120	2.8	0.032	**1.13**	7.11	0.49	**0.381**	3.02.E-04	0.16	**0.50**	0.05	0.45	102.7
130	2.8	0.032	**1.25**	7.70	0.49	**0.415**	3.02.E-04	0.16	**0.55**	0.05	0.5	110.5
140	2.8	0.032	**1.38**	8.29	0.49	**0.448**	3.02.E-04	0.17	**0.60**	0.05	0.55	118.3
150	2.8	0.032	**1.50**	8.88	0.49	**0.482**	3.02.E-04	0.17	**0.65**	0.05	0.6	126.1
160	2.8	0.032	**1.63**	9.47	0.49	**0.516**	3.02.E-04	0.17	**0.70**	0.05	0.65	133.9
170	2.8	0.032	**1.75**	10.05	0.49	**0.550**	3.02.E-04	0.17	**0.75**	0.05	0.7	141.7
180	2.8	0.032	**1.88**	10.64	0.49	**0.583**	3.02.E-04	0.18	**0.80**	0.05	0.75	149.5
190	2.8	0.032	**2.00**	11.22	0.49	**0.617**	3.02.E-04	0.18	**0.85**	0.05	0.8	157.3
200	2.8	0.032	**2.13**	11.81	0.49	**0.651**	3.02.E-04	0.18	**0.90**	0.05	0.85	165.1
210	2.8	0.032	**2.25**	12.39	0.49	**0.684**	3.02.E-04	0.18	**0.95**	0.05	0.9	172.9
220	2.8	0.032	**2.38**	12.97	0.49	**0.718**	3.02.E-04	0.18	**1.00**	0.05	0.95	180.7
230	2.8	0.032	**2.50**	13.56	0.49	**0.751**	3.02.E-04	0.18	**1.05**	0.05	1	188.5
240	2.8	0.032	**2.63**	14.14	0.49	**0.785**	3.02.E-04	0.19	**1.10**	0.05	1.05	196.4
250	2.8	0.032	**2.75**	14.72	0.49	**0.818**	3.02.E-04	0.19	**1.15**	0.05	1.1	204.2
260	2.8	0.032	**2.88**	15.30	0.49	**0.851**	3.02.E-04	0.19	**1.20**	0.05	1.15	212.0
270	2.8	0.032	**3.00**	15.88	0.49	**0.885**	3.02.E-04	0.19	**1.25**	0.05	1.2	219.8
280	2.8	0.032	**3.13**	16.46	0.49	**0.918**	3.02.E-04	0.19	**1.30**	0.05	1.25	227.6
290	2.8	0.032	**3.25**	17.04	0.49	**0.951**	3.02.E-04	0.19	**1.35**	0.05	1.3	235.4
300	2.8	0.032	**3.38**	17.62	0.49	**0.985**	3.02.E-04	0.19	**1.40**	0.05	1.35	243.2

Appendix B

EXPERIMENTAL RESULTS: BOND STRENGTH AND BOND STIFFNESS

Table. B-1 Experimental results of corrosion and maximum bond stress

No.	Specimen	p_w	Corrosion Loss (%)					Exp τ_{max} (N/mm^2)				
			Bar location					Bar location				
			T	CT	CB	B	Ave.	T	CT	CB	B	Ave.
1	4LT-∞S-NH	0.00%	0	0	0	0	0	1.75	1.78	1.87	1.83	1.81
2	4LT-∞S-NC		10.6	4.7	3.8	5.6	6.2	2.06	2.13	2.14	2.12	2.11
3	4L2T-200S-NH	0.15%	0	0	0	0	0	2.26	2.45	2.51	2.60	2.45
4	4L2T-200S-NC		8.9	4.9	4.4	4.9	5.8	1.93	1.85	1.88	1.93	1.90
5	4L2T-100S-NH	0.29%	0	0	0	0	0	2.55	2.71	2.68	2.77	2.68
6	4L2T-100S-NC		8.2	4.4	5.4	6.3	6.1	2.32	2.18	2.31	2.24	2.26
7	4L4T-200S-NH		0	0	0	0	0	2.60	2.26	2.65	2.55	2.51
8	4L4T-200S-NC		7.4	4.5	4.6	5.2	5.4	2.47	2.60	2.67	2.62	2.59
9	3L2T-100S-NH		0	0		0	0	2.72	2.79		3.21	2.91
10	3L2T-100S-NC		7.4	3.9		6.3	5.8	2.41	2.55		2.50	2.49
11	4L2T-100S-HH		0	0	0	0	0	4.00	4.15	4.06	4.37	4.14
12	4L2T-100S-HC		6.6	4.0	6.0	6.1	5.7	3.04	3.21	3.20	3.25	3.18
13	4L2T-50S-NH	0.58%	0	0	0	0	0	2.24	2.29	1.87	2.23	2.15
14	4L2T-50S-NC1		0.9	0.00	0.30	0.60	0.5	3.45	3.31	2.84	2.49	2.93
15	4L2T-50S-NC2		5.5	3.6	4.5	6.3	5.0	2.88	2.29	2.52	2.69	2.59
16	4L2T-50S-NC3		6.5	5.5	5.3	6.0	5.8	3.20	2.70	3.44	2.57	2.97
17	4L4T-100S-NH		0	0	0	0	0	4.30	3.38	3.21	3.07	3.49
18	4L4T-100S-NC		5.1	4.5	3.3	5.0	4.5	2.43	2.72	2.48	3.13	2.59
19	3L2T-50S-NH		0	0		0	0	4.14	4.19		4.69	4.20
20	3L2T-50S-NC		5.3	1.9		4.1	3.8	5.01	3.31		2.89	3.72

Table B-2 Comparison between experimental results and empirical formula

No.	Specimen	Exp τ_{max} (N/mm^2) Bar location	Calc τ_{max} (N/mm^2)			Exp τ_{max} / Calc τ_{max}		
		Ave.	AIJ	Maeda	Fuji-Morita	AIJ	Maeda	Fuji-Morita
1	4LT-∞S-NH	1.81	1.60	1.95	2.98	1.13	0.93	0.61
2	4LT-∞S-NC	2.11						
3	4L2T-200S-NH	2.45	2.02	2.41	3.29	1.22	1.02	0.75
4	4L2T-200S-NC	1.90						
5	4L2T-100S-NH	2.68	2.44	2.86	3.60	1.10	0.94	0.74
6	4L2T-100S-NC	2.26						
7	4L4T-200S-NH	2.51	2.69	3.13	3.60	0.94	0.80	0.70
8	4L4T-200S-NC	2.59						
9	3L2T-100S-NH	2.91	2.89	3.55	3.26	1.01	0.82	0.89
10	3L2T-100S-NC	2.49						
11	4L2T-100S-HH	4.14	3.10	3.68	5.09	1.34	1.13	0.81
12	4L2T-100S-HC	3.18						
13	4L2T-50S-NH	2.15	3.76	4.22	3.76	0.57	0.51	0.57
14	4L2T-50S-NC1	2.93						
15	4L2T-50S-NC2	2.59						
16	4L2T-50S-NC3	2.97						
17	4L4T-100S-NH	3.49	3.78	4.28	4.22	0.92	0.81	0.83
18	4L4T-100S-NC	2.59						
19	3L2T-50S-NH	4.20	4.57	5.16	3.33	0.92	0.81	1.26
20	3L2T-50S-NC	3.72						

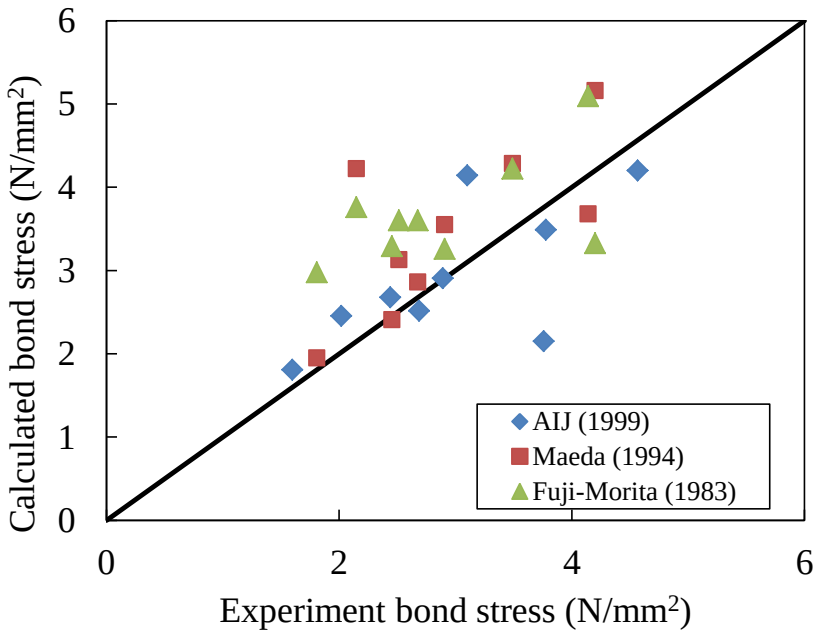

Figure. B-1 Calculated vs. experimental results of bond stress

Table. B-3 Experimental results of bond stiffness

No.	Specimen	Conc. Strength (N/mm^2)	pw (%)	Ave. Corr. Loss (%)	τ_1 (N/mm^2)	Slip at τ_1 (mm)	k_1 (N/mm^3)	τ_{max} (N/mm^2)	Slip at τ_{max} (mm)	k_2 (N/mm^3)
1	4LT-∞S-NH	24	0	0	1.77	0.02	88	1.81	0.03	3.3
2	4LT-∞S-NC	24	0	6.2	1.90	0.02	95	2.11	0.48	0.4
3	4L2T-200S-NH	24	0.15	0	1.67	0.02	83	2.45	1.47	0.5
4	4L2T-200S-NC	24	0.15	5.8	1.85	0.02	93	1.90	0.53	0.1
5	4L2T-100S-NH	24	0.29	0	1.62	0.02	81	2.68	1.38	0.8
6	4L2T-100S-NC	24	0.29	6.1	2.02	0.02	101	2.26	0.39	0.7
7	4L4T-200S-NH	24	0.29	0	1.42	0.02	71	2.51	1.07	1.0
8	4L4T-200S-NC	24	0.29	5.4	1.89	0.02	94	2.59	0.81	0.9
9	3L2T-100S-NH	24	0.29	0	1.43	0.02	71	2.91	1.41	1.1
10	3L2T-100S-NC	24	0.29	5.8	2.22	0.02	111	2.49	0.45	0.6
11	4L2T-100S-HH	48	0.29	0.0	2.22	0.02	111	4.14	1.98	1.0
12	4L2T-100S-HC	48	0.29	5.7	2.45	0.02	122	3.18	0.65	1.2
13	4L2T-50S-NH	24	0.58	0	1.79	0.02	89	2.15	0.26	1.5
14	4L2T-50S-NC1	24	0.58	0.5	2.02	0.02	101	2.93	0.63	1.5
15	4L2T-50S-NC2	24	0.58	5.0	2.15	0.02	108	2.59	0.31	1.5
16	4L2T-50S-NC3	24	0.58	5.8	1.80	0.02	90	2.97	0.34	3.7
17	4L4T-100S-NH	24	0.58	0	2.27	0.02	113	3.49	0.88	1.4
18	4L4T-100S-NC	24	0.58	4.5	1.45	0.02	72	2.59	0.45	2.7
19	3L2T-50S-NH	24	0.58	0	2.40	0.02	120	4.20	0.90	2.0
20	3L2T-50S-NC	24	0.58	3.8	1.17	0.02	58	3.72	0.45	5.9

Appendix C

EXPERIMENTAL RESULTS: CRACK PATTERN AT THE END OF ACCELERATED CORROSION TEST

Specimen No.2 (4LT-∞S-NC) – Corrosion rate 6.2%		
	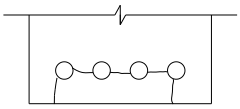	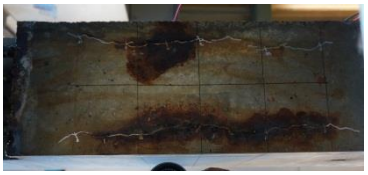
Specimen No.4 (4L2T-200S-NC) – Corrosion rate 5.8%		
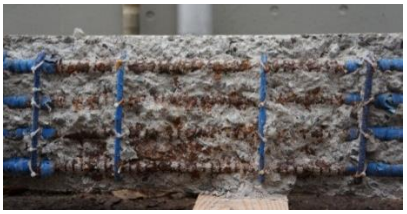	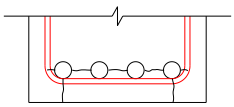	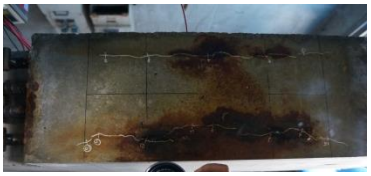
Specimen No.6 (4L2T-100S-NC) – Corrosion rate 6.1%		
	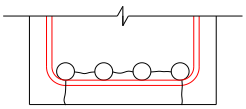	
Specimen No.8 (4L4T-200S-NC) – Corrosion rate 5.4%		
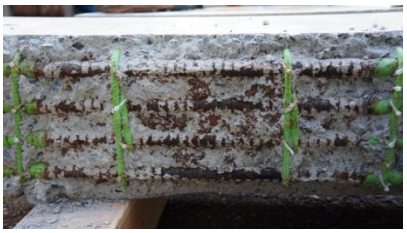	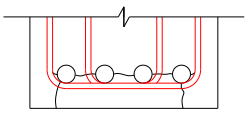	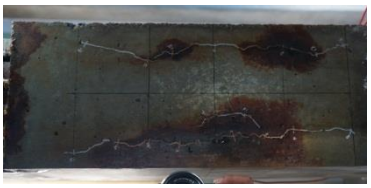
Specimen No.10 (4L4T-200S-NC) – Corrosion rate 5.8%		
	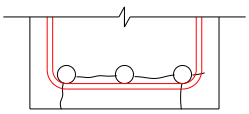	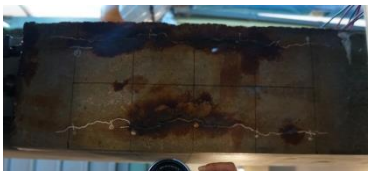
Specimen No.12 (4L2T-100S-HC) – Corrosion rate 5.7%		
	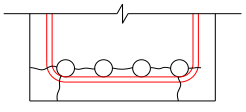	

Figure C-1 Crack pattern at final accelerated corrosion test

Appendix D

EXPERIMENTAL RESULTS: SPECIMEN'S CRACK PATTERN AT PULLOUT TEST

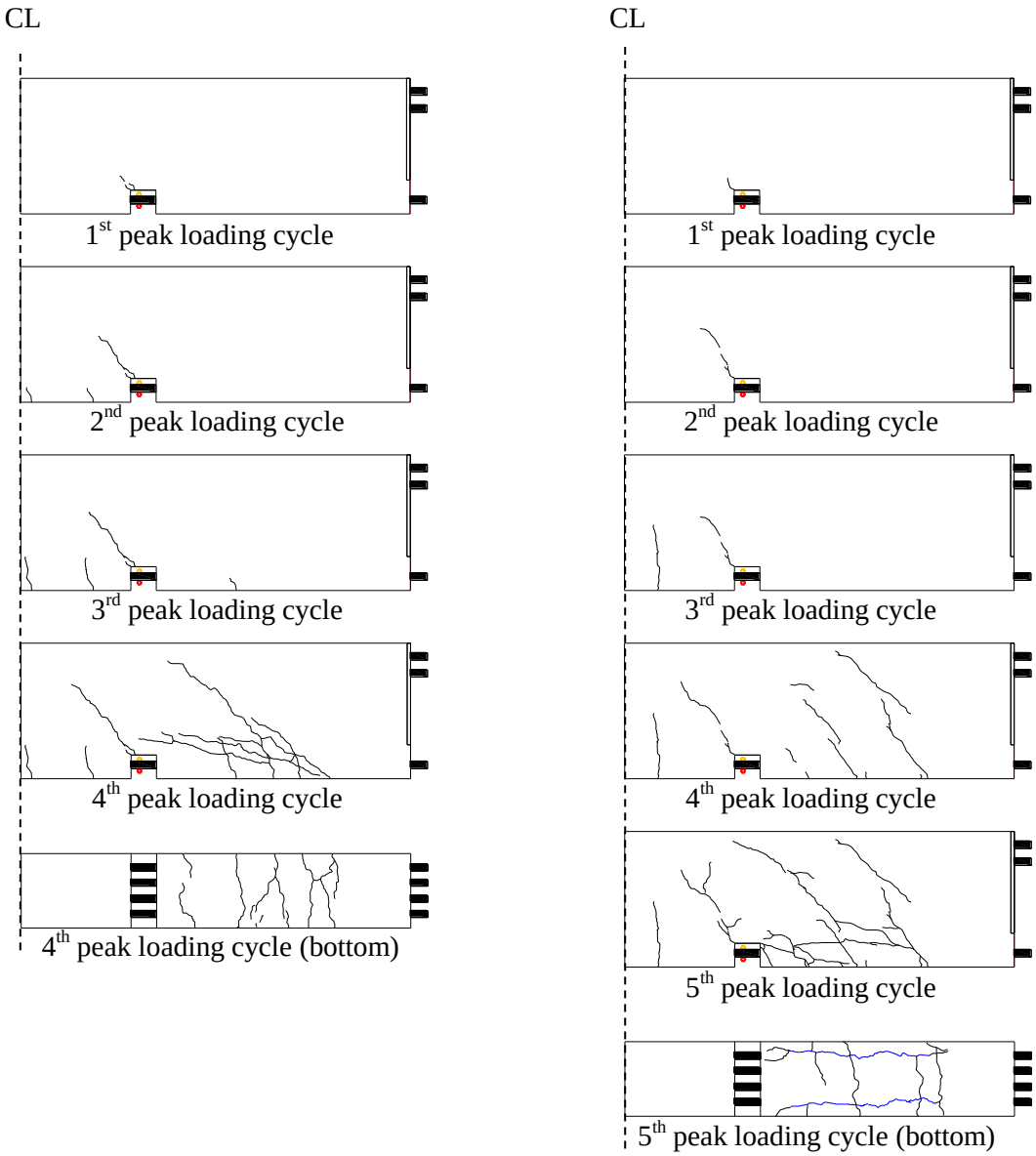

(a) Specimen No.1

(b) Specimen No.2

Figure.D-1 Loading Crack Pattern of Specimen No.1 and No.2

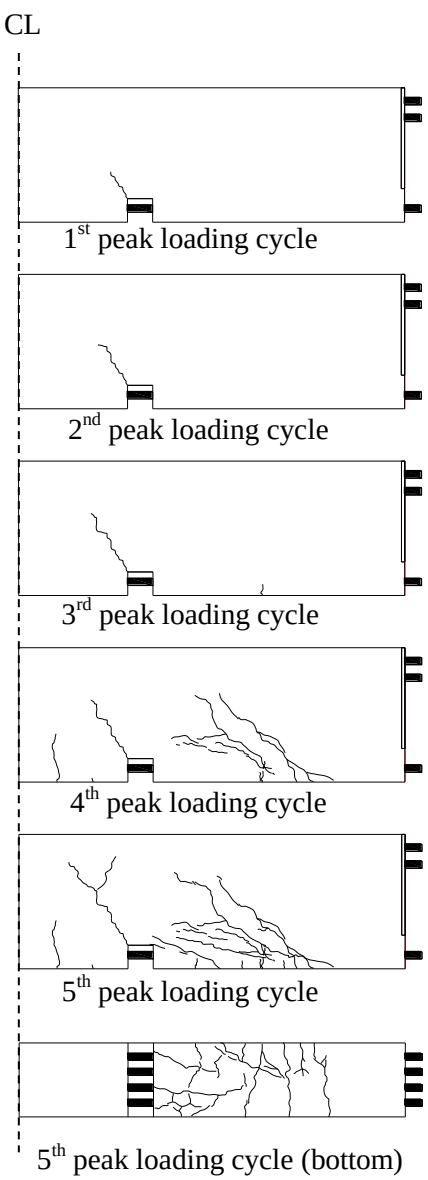

(c) Specimen No.3

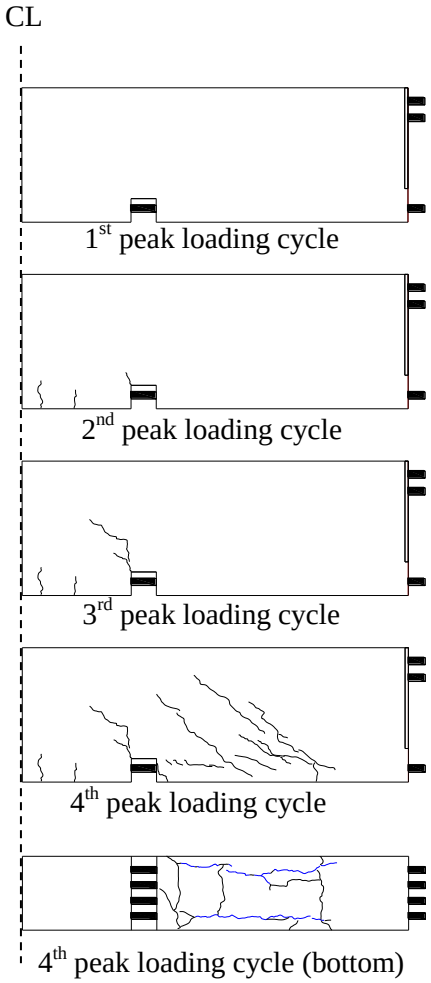

(d) Specimen No.4

Figure.D-2 Loading Crack Pattern of Specimen No.3 and No.4

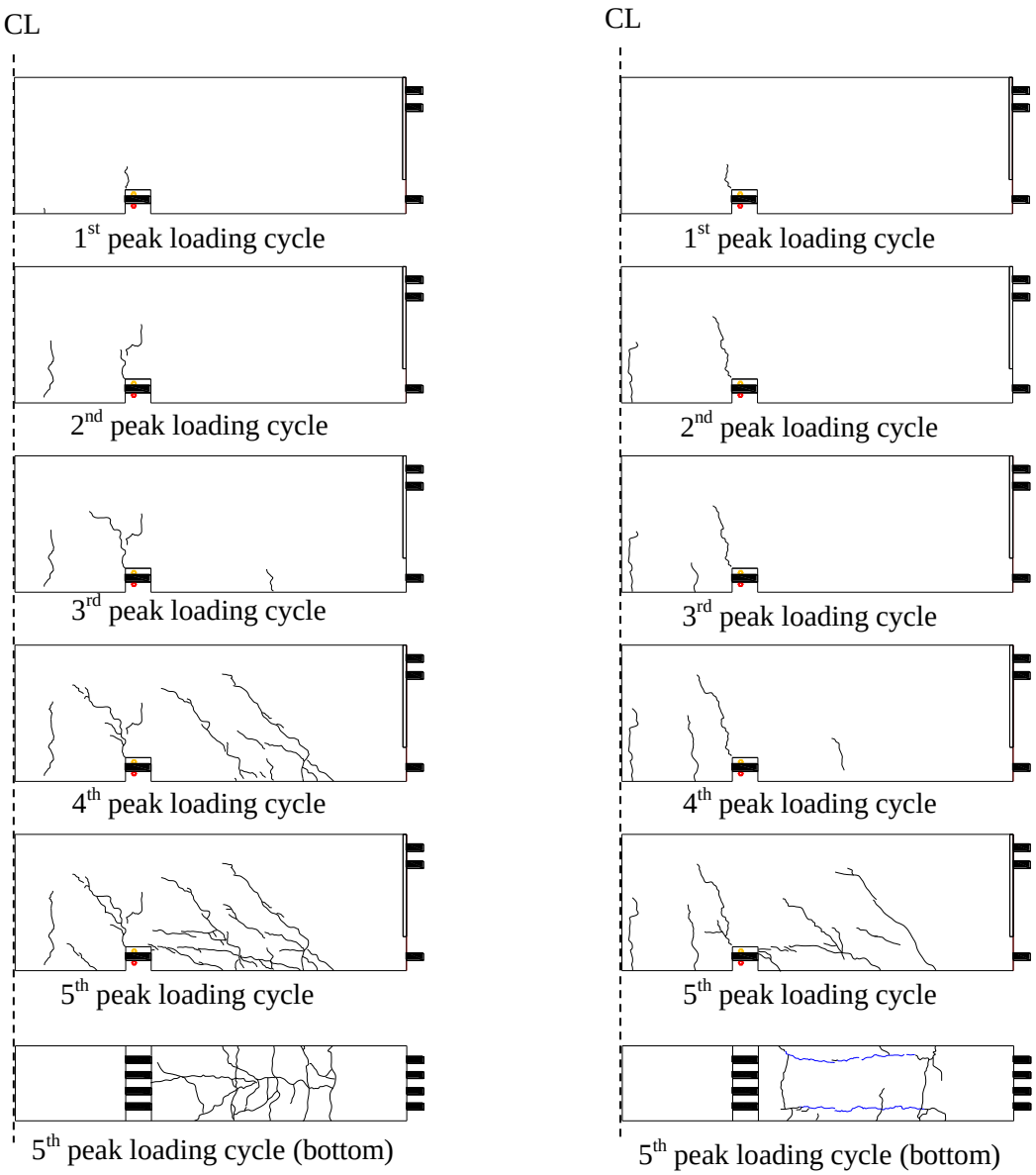

Figure.D-3 Loading Crack Pattern of Specimen No.5 and No.6

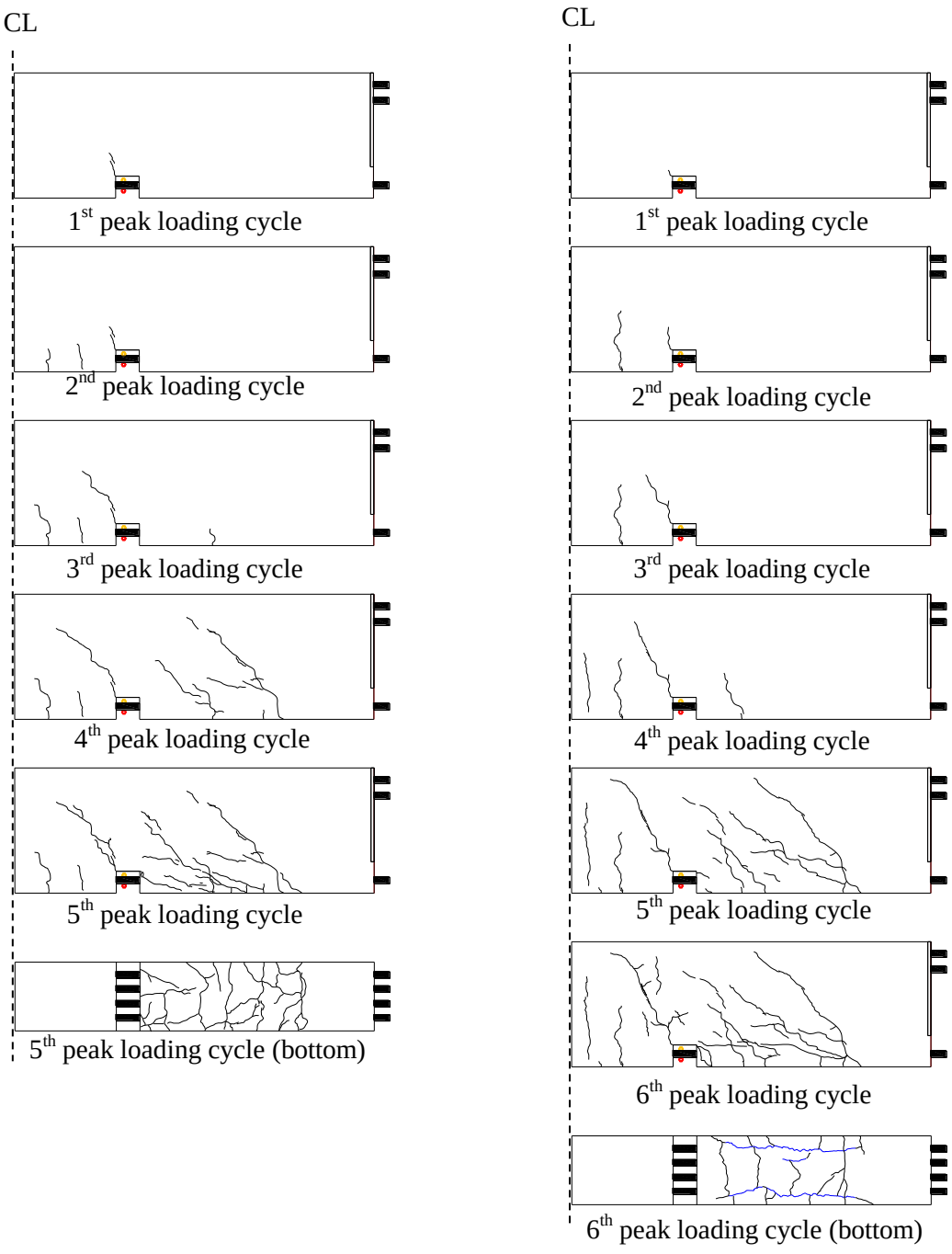

(g) Specimen No.7 (h) Specimen No.8

Figure.D-4 Loading Crack Pattern of Specimen No.7 and No.8

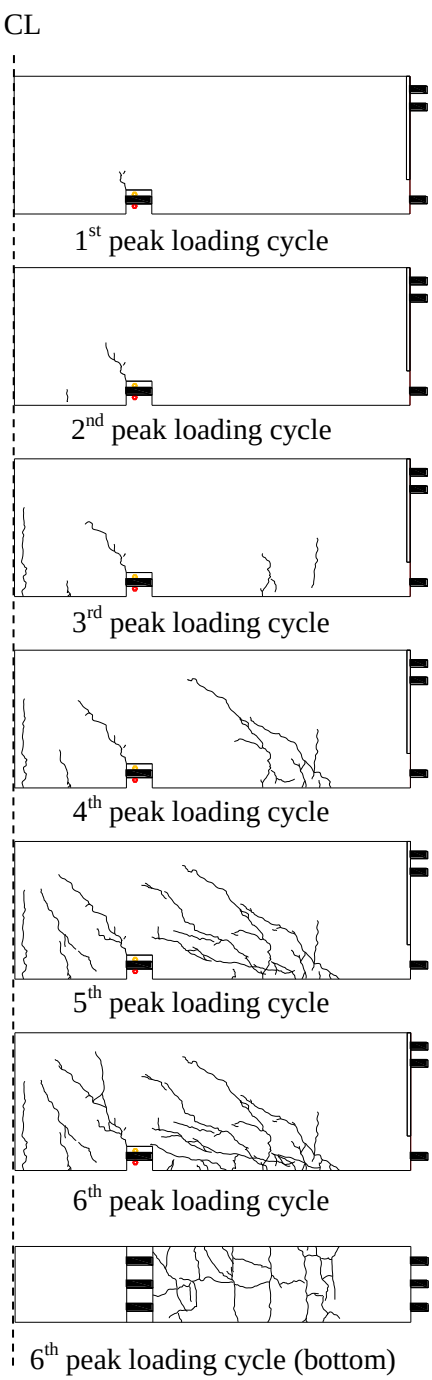

(i) Specimen No.9

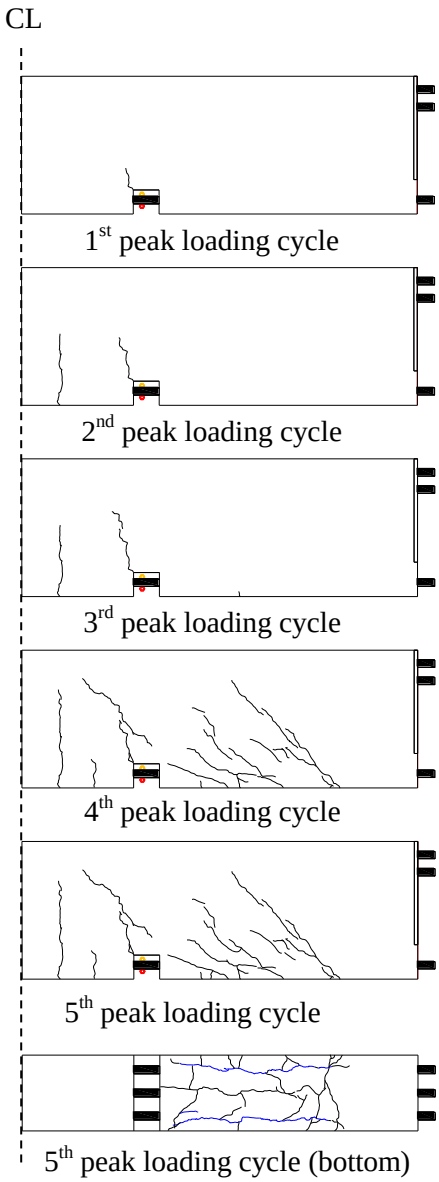

(j) Specimen No.10

Figure.D-5 Loading Crack Pattern of Specimen No.9 and No.10

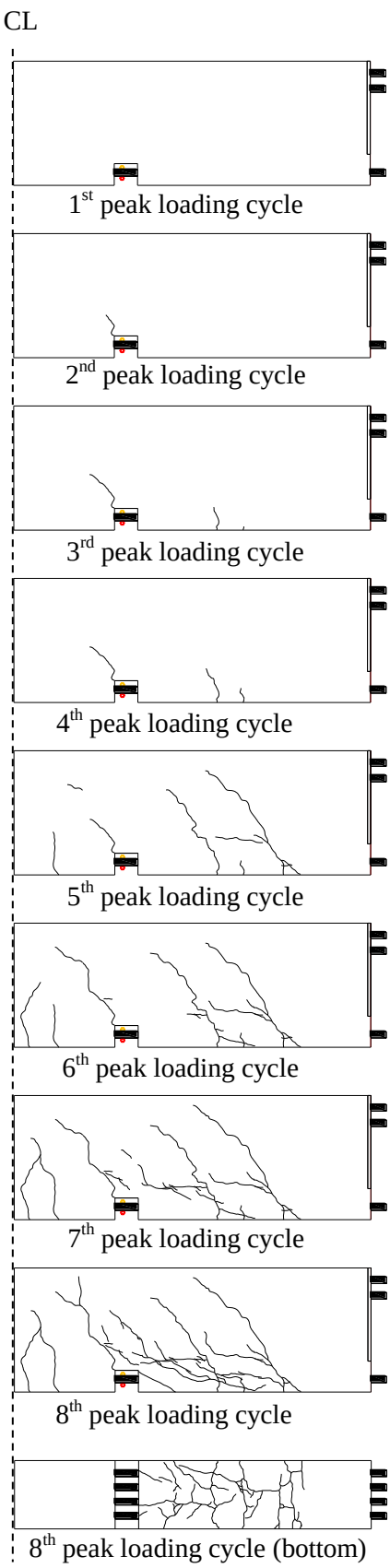

(k) Specimen No.11

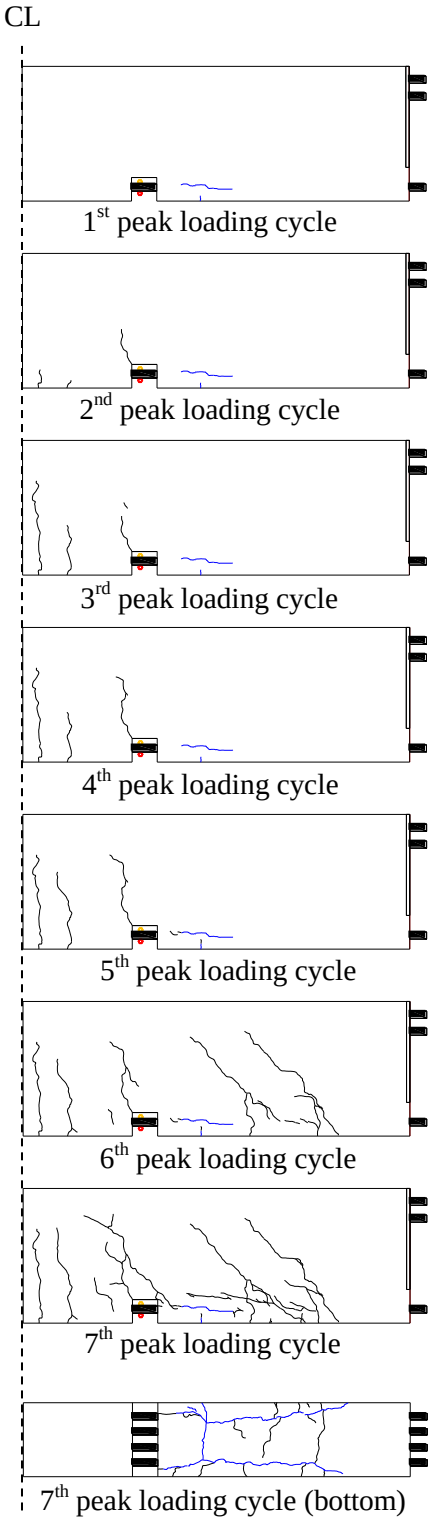

(l) Specimen No.12

Figure D-6 Loading Crack Pattern of Specimen No.11 and No.12

Appendix E

BOND STRENGTH: AIJ GUIDELINES 1999

The calculated bond strength suggested by AIJ guideline (AIJ 1999) which is used in this paper is as follows

The bond strength, τ_{bu}, is computed with the following equation.

$$\tau_{bu} = \alpha_t \left\{ (0.086 b_i + 0.11)\sqrt{\sigma_B} + k_{st} \right\} \quad (\mathrm{N/mm^2}) \qquad \text{(E-1)}$$

where α_t is the strength reduction factor for the top layer reinforcement and expressed as,

α_t = 0.75+σ_B/400 Reinforcement in the top layer of beams
= 1 other reinforcement (Unit: N/mm^2) (E-2)

and bi is the length ratio of the bond splitting failure and expressed as,

$$\begin{aligned} b_i &= \min(b_{si}, b_{ci}) \\ b_{si} &= \frac{b - N_1 d_b}{N_1 d_b} \\ b_{ci} &= \frac{\sqrt{2}(d_{cs} + d_{ct}) - d_b}{d_b} \end{aligned} \qquad \text{(E-3)}$$

and b is the section width, N_1 is the number of reinforcing bars in the first layer, d_{cs} is the thickness of side cover, d_{ct} is the thickness of top/bottom cover. The effect of web reinforcement, k_{st}, is expressed as follows,

$$k_{st} = \begin{cases} \left(56 + \dfrac{47 N_w}{N_1}\right)(b_{si} + 1) p_w & \text{for } b_{ci} \geq b_{si} \\ \dfrac{146 A_w}{d_b s} & \text{for } b_{ci} < b_{si} \end{cases} \quad (\mathrm{N/mm^2}) \qquad \text{(E-4)}$$

where N_w is the number of legs of web reinforcement (=Ns + 2), p_w is web reinforcement ratio, d_b is the diameter of reinforcing bar, A_w is the section area of a single reinforcing bar, s is the spacing of web reinforcing bar.

Appendix F

ANALYSIS RESULTS: ASSESSMENT OF CORRODED COLUMNS

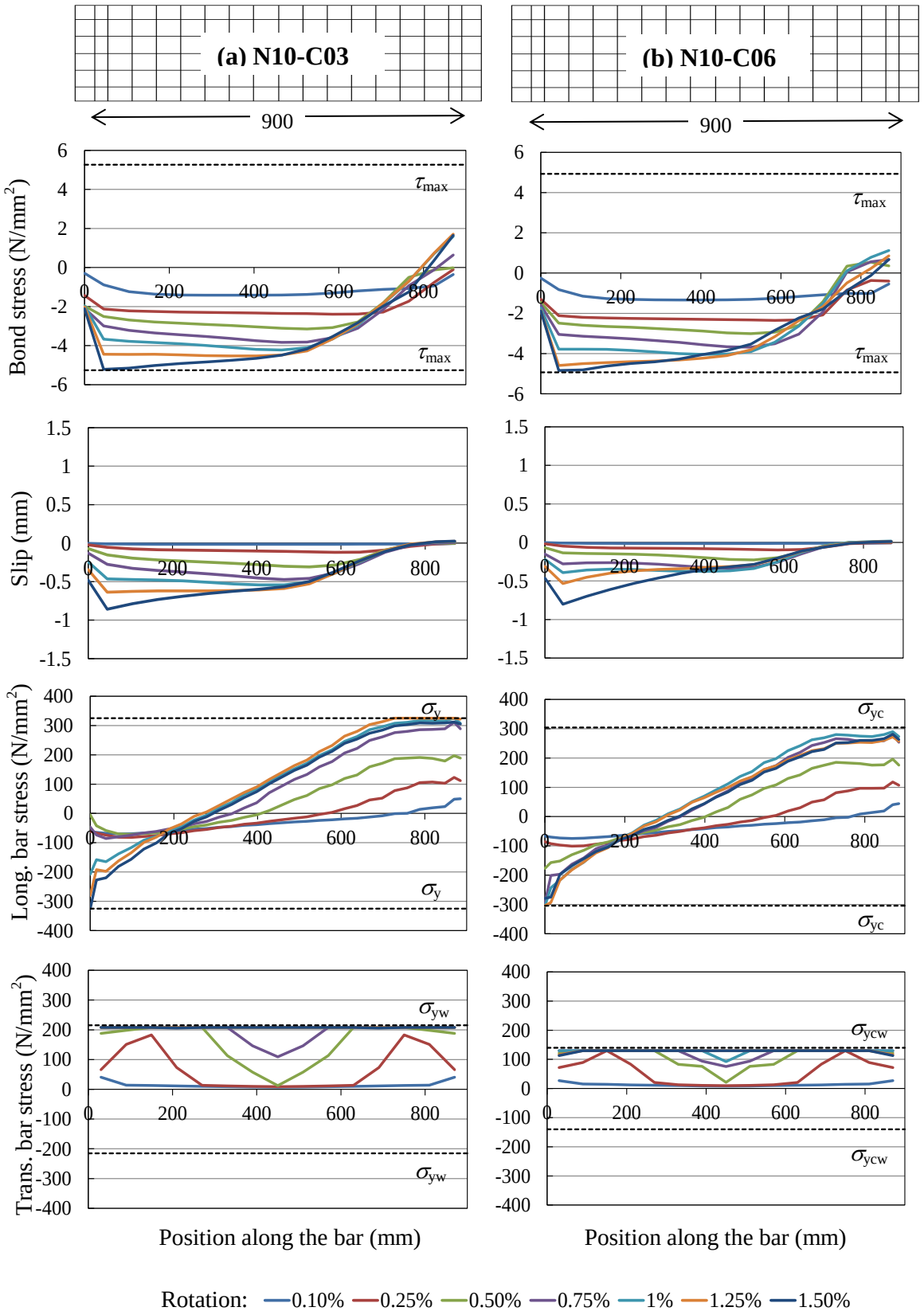

Figure. F-1 Analysis results of bond stress, slip, longitudinal and transverse bar stress along the bar for (a) N10-C03 (b) N10-C06